# Durability of Polymer Impregnated Carbon Textiles as CP Anode for Reinforced Concrete

Von der Fakultät für Bauingenieurwesen der Rheinisch-Westfälischen Technischen Hochschule

Aachen zur Erlangung des akademischen Grades eines Doktors

der Ingenieurwissenschaften

genehmigte Dissertation

vorgelegt von

Amir Asgharzadeh

Berichter: Universitätsprofessor Dr.-Ing. Michael Raupach

Universitätsprofessor Dr.-lng. habil. Brita Daniela Zander

Tag der mündlichen Prüfung: 17.05.2019

# PREFACE

The dissertation is submitted to the RWTH Aachen University in Faculty of Civil Engineering for the degree Philosophiae Doctor.

The research was conducted at the Institute for Building Research of RWTH Aachen University in Aachen, Germany. The main supervisor was University Prof.-Dr.-Ing. Michael Raupach (Chair for Institute for Building Materials Research at RWTH Aachen University) and co-supervisors were Prof.-Dr.-Ing. Bernhard Isecke and University Prof.-Dr.-Ing. Daniela Zander (Chair for Corrosion and Corrosion Protection at RWTH Aachen University).

The dissertation consists of an extended summary, five attached papers (four of them are published or accepted in international scientific journals. One of these is published in international conference proceedings).

The author, Amir Asgharzadeh, attests that the dissertation and the work presented therein are his independent work. The thesis does not contain any material that has previously been submitted for a degree at this university or any other institution.

# ACKNOWLEDGEMENTS

At this point I would like to express my special thanks to the following persons, without whose assistance the production of this doctoral thesis would never have been possible:

My first thanks go to Prof.-Dr.-Ing. Michael Raupach, for the supervision of this work, the friendly help and the numerous ideas that opened up a critical approach to this topic for me. The frequent conversations on an intellectual and personal level will always remain in my memory as an enriching and constructive exchange. I have always found our dialogues to be encouraging and motivating.

I thank Prof. Dr.-rer.-nat. Oliver Weichold for the helpful and scientific discussions. In addition, I would like to thank Christian Helm for the critical discussion with my subject matter. I would also like to thank Dr.-Ing. Joachim Hannawald. For the repeated examination of my publications, his critical observations, his differentiated remarks as well as the relevant discussions, which have given me the strength and courage to write and complete my dissertation.

I would also like to thank Mark Byram for reviewing my dissertation. My extraordinary thanks go to my student assistants. Without their help such a large experimental amount would never have been possible.

I wish to express my gratitude to my family in Iran. I am deeply connected and grateful to my wife, Sharareh, for her unbelievably helpful support and understanding in preparing this dissertation. Especially for her support during my studies, that she encouraged me finish my studies successfully. That's why I dedicate this thesis to her. My very special thanks go to my son Jascha, who gave meaning to my work.

# SUMMARY

Damage to reinforced concrete structures causes immense economic losses every year. Costs due to failure of structures and their repair measures are immense. Much of this damage is due to the corrosive environment of reinforced concrete structures. One option for repairing corrosion-damaged components is cathodic corrosion protection. In cathodic corrosion protection, the reinforcing steel is forced to act cathodically and thus the dissolution of the reinforcing steel is reduced to harmless levels. The cathodic effect can be achieved for example by the attachment of an impressed current anode where the partial oxidation reactions are shifted to the external anode. Widely used in cathodic corrosion protection are mixed metal oxide (MMO) coated titanium meshes.

Currently, the use of anodes made of carbon textile is being developed, which are of particular interest due to their excellent mechanical properties, low weight and crack bridging ability. Additionally, carbon textile is electrically conductive and its functionality as a CP anode has already been validated at the Institute of Building Materials Research (ibac) of the RWTH Aachen University [Paper 5].

Carbon, according to the Pourbaix diagram [1], is not chemically resistant, and can corrode. Therefore, durability studies were required to determine the suitability of carbon as a long term anode material for cathodic protection of steel in concrete. The aim of this thesis is to investigate the durability of carbon textile under anodic polarization. The experiments were carried out using a simulated pore solution and mortar. The influence of anodic polarization on carbon textiles was investigated.

The behavior of unconsumed carbon textile under anodic polarization in alkaline solution was characterized by current density-potential curves through potentiodynamic experiments. SEM images were used to detect decomposition of the sizing of the carbon filaments which was attributed to anodic polarization. Further tests in solution and further SEM images showed that impregnated carbon textiles degraded the epoxy and SBR impregnations. A degradation of the carbon fibers themselves could not be achieved for potentials up to 2200 mV vs. NHE. The decomposition of the sizing and epoxy matrix presumably occurs in the transition region of its current density-potential curves at potentials of about 900 mV vs. NHE and 1050-1150 mV vs. NHE. The SBR impregnation is decomposed at potentials of 490 mV vs. NHE.

After 240 days of potentiostatic polarization, no visible damage has occurred to the mortar test specimens.

However, the bond between carbon textiles and mortar as well as stress corrosion cracking of carbon textiles under anodic polarization was not investigated.

# TABLE OF CONTENT

# LIST OF PAPERS

1. Asgharzadeh, A.; Raupach, M. (2018): Development of a test Method for the Durability of Carbon Textiles under Anodic Polarisation. In: Service Life and Durability of Reinforced Concrete Structures (RILEM Book series), Springer International Publishing, Basel, pp. 143-158.
   (DOI: 10.1007/978-3-319-90236-4_11)

2. Asgharzadeh, A.; Raupach, M. (2018): Durability behavior of polymer impregnated carbon textiles in alkaline solution as CP anode. Materials and Corrosion 2018, pp. 1-12.
   (DOI: 10.1002/maco.201810098)

3. Asgharzadeh, A.; Raupach, M. (2019): Durability of impregnated carbon textiles in mortar as cathodic protection anodes, Magazine of Concrete Research.
   (DOI: 10.1680/jmacr.18.00402)

4. Asgharzadeh, A.; Raupach, M. (2018): Damage mechanisms of polymer impregnated carbon textiles used as Anode Material for Cathodic Protection, Applied Sciences, the special issue of "Textile Reinforced Cement Composites: New Insights in Structural and Material Engineering", 9, 110.
   (DOI: 10.3390/app9010110)

5. Asgharzadeh, A.; Raupach, M.; Koch, D. (2015): Investigations on the Suitability of Technical Textiles for Cathodic Corrosion Protection. Proceedings of the 4th International Conference on Concrete Repair, Rehabilitation and Retrofitting (ICCRRR), Leipzig, 5-7 October 2015.
   ISBN 978-1-138-02843-2

## OTHER PUBLICATION

Asgharzadeh, A.; Raupach, M. (2018): Tensile Strength of Carbon Rovings Impregnated with Different Materials Under Anodic Polarization. Proceedings of the 5th International Conference on Concrete Repair, Rehabilitation and Retrofitting (ICCRRR), Cape Town, South Africa, 19 - 21 Nov. 2018

(https://doi.org/10.1051/matecconf/201819911015)

# SYMBOLS AND ABBREVATIONS

| | | |
|---|---|---|
| $a_{Me\ (ox)}$ | Activity of oxidized species | - |
| $a_{Me\ (red)}$ | Activity of reduced species | - |
| AC | Alternating current | [-] |
| ATME | Activated titanium reference electrode | [-] |
| $A_u$ | Surface of the uncoated roving | |
| c | Mass concentration | |
| CP | Cathodic corrosion protection | [-] |
| DC | Direct current | [-] |
| $d_F$ | Diameter of a filament | |
| E | Potential | [V] |
| E* | Electrochemical equilibrium potential | [V] |
| $E_0$ | Standard potential (for $a_{Me\ (ox)} = a_{Me\ (red)} = 1$) | [V] |
| $E_{comp}$ | Compensated potential | [V] |
| $E_{corr}$ | Rest potential | [V] |
| EDX | Energy dispersive X-ray spectroscopy | |

| | | |
|---|---|---|
| $\eta$ | Overvoltage | [V] |
| $E_{instant,off}$ | Potential immediately after instant –off measurement | [V] |
| EIS | Electrochemical impedance spectroscopy | [-] |
| $E_{measured}$ | Measured potential | [V] |
| $E_{on}$ | Potential immediately before instant –off measurement | [V] |
| $E_{P1}$ | Passivation potential | [V] |
| $E_{P2}$ | Activation potential | [V] |
| $E_t$ | Breakthrough potential | [V] |
| F | Faraday constant | [(A*s)/mol], [C/mol] |
| FTIR | Fourier-transform infrared spectroscopy | [-] |
| I | Current | [A] |
| i | Current density | [A/m²] |
| $i_0$ | Exchange current density | [A/m²] |
| $i_a$ | Anodic partial current density | [A/m²] |
| ICCP | Impressed current cathodic protection | [-] |
| $I_{measured}$ | Measured current voltage | [A] |

| | | |
|---|---|---|
| $I_{on}$ | Current voltage immediately before instant –off measurement | [A] |
| $i_p$ | Passivation current density | [A/m²] |
| $i_{pass}$ | Current density in passive range | [A/m²] |
| $k_A$ | Constant | [-] |
| $l_R$ | Length of a roving | |
| m | Electrochemically converted amount of substance | [g] |
| M | Molar mass | [g/mol] |
| MMO | Mixed metal oxide | [-] |
| n | Number of the electrons of the electrochemical reaction | [equiv. mol-1] |
| $n_F$ | Number of filaments in a roving | |
| NHE | Normal hydrogen electrode | [-] |
| $n_R$ | Number of rovings | |
| OCP | Open circuit potential | [V] |
| p | Pressure | |
| $\phi$ | Electric charge density | C/m² |
| PAN | Polyacrylnitril | [-] |
| R | Molar gas constant | [J/(mol*K)] |

| | | |
|---|---|---|
| R | Electrical resistance | [Ω] |
| SBR | Styrene Butadiene Rubber | [-] |
| SCE | Saturated calomel electrode | [-] |
| SEM | Scanning electron microscopy | [-] |
| T | Absolute Temperature | [K] |
| t | Time | [s] |
| TOC | Total organic carbon | [-] |
| z | Charge number | [-] |
| z | Number of electrons transferred | [-] |
| α | Transfer coefficient | [-] |
| $\eta_D$ | Overpotential | [V] |

# 1 BACKGROUND

Reinforcing steel is covered in concrete by a highly alkaline pore solution with a sub-microscopic thin and non-porous oxide layer. This layer behaves passively and thus prevents anodic dissolution of the reinforcing steel. There are two scenarios that can lead to the loss of this passive layer. First, by carbonation of the concrete down to the depth of reinforcement in which case alkalinity at the steel / concrete interface may be lost. Secondly, penetration of chlorides to the level of the reinforcing steel ad subsequent dissolution of the passive layer. This can result for example from ingress of de-icing salts or seawater. Depassivated areas on the reinforcing steel have a lower electrical potential than the passive areas and form a galvanic cell in which the concrete and its pore water serve as an electrolyte. In this cell the following reactions take place:

$$\mathrm{Fe} \rightarrow \mathrm{Fe}^{2+} + 2\mathrm{e}^{-} \tag{1}$$

$$2\mathrm{e}^{-} + \mathrm{H_2O} + \frac{1}{2}\mathrm{O_2} \rightarrow 2\mathrm{OH}^{-} \tag{2}$$

At the anode, iron is dissolved with the release of electrons (1). The electrons are conducted through the steel to the cathode, where they react with the consumption of water and oxygen to $\mathrm{OH}^{-}$-ions (2). Because of the potential difference, the $\mathrm{OH}^{-}$-ions migrate to the anode and complete the galvanic cell. At the anode, the $\mathrm{OH}^{-}$-ions react with $\mathrm{Fe}^{2+}$ to form iron oxides or iron hydroxides. While carbonation leads to widespread depassivation of the reinforcing steel, the penetration of chlorides often causes a local loss of the passive layer. Consequently, a large cathode to anode area ratio can result with a high driving voltage. This can lead to high corrosion rates and thus rapid cross-sectional loss [2; 3].

Cathodic corrosion protection (CP) is a widely used electrochemical process for the repair of chloride-damaged reinforced concrete structures. Through CP, the steel is forced by the connection of a sacrificial anode or an impressed current anode [4] to act cathodically and thus reduces the anodic dissolution of iron to negligible orders of magnitude. The cathodic effect is synonymous with an inert behavior of the steel. In the field of concrete repair the use of CP systems with impressed current anodes has become common place since it is possible to dispense with removal of the chloride-containing concrete [5].

In addition to the primary effect of the suppression of iron dissolution, the use of impressed current anodes has positive secondary effects. Reduction of the oxygen content at the cathode results in the beneficial secondary effect of realkalization of the concrete in the vicinity of the reinforcing steel [6]. In addition, the current flow in the concrete can lead to a transport of chloride ions from the cathode towards the anode and thus to a reduction of the chloride content in the area of the reinforcement. However, excessive current densities may cause the development of hydrogen at the reinforcement. In the case of prestressing steels, this can cause hydrogen embrittlement. In addition, the concrete can be subjected to internal tensile stresses from the formation of gases causing it to crack. At the anode, oxygen can be evolved and chlorides accumulated, creating harmful conditions for the concrete and anode [7].

Cathodic corrosion protection of steel in concrete in Germany is typically carried out with the utilization of impressed current cathodic protection systems. As an anode material MMO coated titanium is typically used. The suitability of carbon textiles for use as a CP anode has been investigated previously [Paper 5]. Due to its excellent tensile strength and crack bridging ability, carbon can bring other advantages in addition to CP in the repair of reinforced concrete structures Such as crack reduction in overlays.

# 2 INTRODUCTION

In the context of current research and this thesis, the durability of carbon textile as an anode material was investigated.

Initially, the corrosion of steel in reinforced concrete and cathodic corrosion protection of reinforcing steel in is discussed. Subsequently, the electrochemical behavior of carbon is discussed using the Pourbaix diagram and the preparation of carbon materials is presented. Thereafter, previous investigations on carbon textile anodes from literature are presented, followed by a summary of the current state of knowledge.

Additionally, various experiments in saturated calcium hydroxide solutions which simulate the behavior of carbon textile under anodic polarization in concrete are presented and discussed.

Subsequently, the experimental investigations on the anodic permanent polarization of mortar test specimens are presented. The structure of the specimens and the sample matrix are described and the preliminary results of permanent polarization are evaluated. In addition, instant-off measurements were carried out on the specimens and reference specimens were polarized.

Finally, the insights gained in this thesis on the durability of carbon textile under potentiostatic polarization are summarized and an outlook on future research tasks is provided.

The durability of carbon textiles as anode material for CP has previously been investigated [8]. However, there is a lack of experience with the durability of textiles with different impregnations that are currently available on the market. Most of the investigations were concerned with potentials or current densities that were not in line with practical requirements. In this thesis, the investigations in solution were carried out to investigate the dissolution of carbon by anodic polarization after polarization. The surface of the carbon textiles were examined by means of SEM. As a result, the damage mechanisms of the impregnation and sizing were determined. Limit potentials for the operation of CP systems with carbon textile anodes were also determined based on impregnation type.

# 3 OBJECTIVES AND LIMITATIONS

The aim of this work was to investigate the durability of polymer-impregnated carbon textiles as a CP anode in three steps. The three steps were as follows:

1. Determination of parameters which can influence the polarization experiments.
2. Investigation of behavior of carbon textile and possible destruction mechanisms of impregnation material and carbon textile under different potentials and current densities in saturated calcium hydroxide solution.
3. Potentiostatic measurements of polymer-impregnated carbon textile embedded in two different mortars, as well as two different storage conditions over an eight month period.
4. Determination of the limiting potential for damage of the impregnation and sizing under anodic polarization

The experiments for the first step were carried out on SBR-impregnated carbon textiles. The experiments for the second step were carried out on 4 SBR and 4 epoxy impregnated carbon textiles. For the third step, carbon textiles impregnated with selected SBR and epoxy were used. It was hypothesized that the durability behavior of polymer-impregnated carbon textiles could vary depending on the type, material, thickness of the impregnation and also the manufacturing process.

# 4 THEORETICAL BACKGROUND

## 4.1 Cathodic corrosion protection

Cathodic corrosion protection (CP) prevents further development of pitting corrosion and can control the corrosion rate of steel [9; 10]. Therefore, for concrete rehabilitation projects utilizing CP, only concrete in areas that have been affected by reinforcement corrosion where a reduction in cross section and loss of bond has occurred at the reinforcing steel has to be removed. The rehabilitation concept for the installation of CP is normally determined after a potential measurement of the reinforcement from the surface of the concrete. The potential value less than -350mV vs Cu/CuSO4 could assume a possible corrosion of reinforcement [11].

The cathodic corrosion protection of steel in concrete is regulated in DIN EN ISO 12696 [12] and limited to the protection of steel in concrete exposed to the atmosphere. The cathodic corrosion protection system includes an anode system [13] to allow the cathodic protection current to reach the respective surfaces or parts of the concrete and to allow the conversion of electronic to ionic current at the anode-concrete contact surface and its distribution to the surface of the steel embedded in the concrete. The anode system is the most important component of the cathodic protection system and must be able to provide the required protective current density within the projected service life without impairing the bond between anode and concrete or damaging the anode [4].

The main purpose of CP is the reduction of corrosion to an acceptable level. To achieve this, the potential of the reinforcement is shifted in the cathodic direction by the introduction of an external current via embedded or surface-mounted anodes. Figure 1 shows the principle of CP using an impressed current anode [4]. The reinforcement is exposed to an external current via a direct current source using an embedded insoluble anode [14].

Besides the anode, the embedding mortar is probably the most critical component of a CP system. Because it is responsible for an even distribution of the protective current over the surface to be protected. In addition, anode materials embedded in concrete must be able to guarantee permanent current transfer [15]. The currently most widely used anode material is mixed metal oxide (MMO) coated titanium, which is generally selected due to its low weight, insoluble material behavior under anodic polarization, durability and good conductivity [16].

In the context of this research, the suitability of carbon textile as anode material is investigated. Carbon textile shows great promise due to its electrical conductivity, excellent mechanical properties and good processability. In addition, textile concrete with good crack

distribution and small crack widths could offer additional advantages in case of possible static build-up [Paper5].

For the typical operation of a CP system, the current densities are set at a very high level at the beginning of the application and decreased within 2 to 3 months. The current densities are normally 5 mA/m$^2$ or less after decrease and then remain constant [17].

A CP system with an impressed current anode requires the following components as shown in Figure 1: a DC voltage source (rectifier), an anode material, an embedding mortar, connection to the reinforcement, cable connections and monitoring instruments, and embedded reference electrodes. The anode introduces the current into the concrete, it is connected to the positive pole of the rectifier with the reinforcement connected to the negative pole. The potential of the anode is thus shifted in the positive direction and the potential of the reinforcement in the negative direction. To produce an electrical circuit, the anode is usually embedded in mortar. The pore solution in mortar and old concrete fulfills the role of the electrolyte.

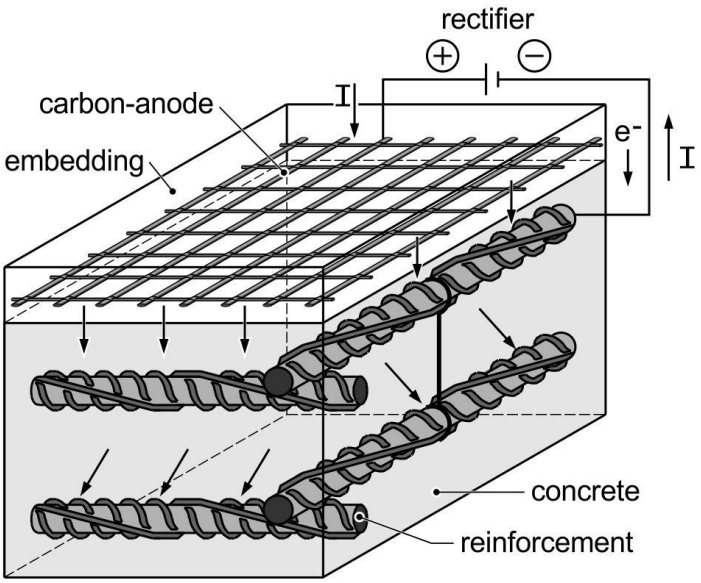


Figure 1: Scheme of an impressed current CP system with embedded carbon textile anode [Paper 1]

The embedding mortar should be easy to install and form a firm bond to the anode material. In addition, it must have sufficient conductivity and good mechanical properties [Paper 5].

The mortar is also used to provide an even distribution of the protective current.

Research is currently underway to determine whether carbon textiles, when used as an anode material, can permanently protect the reinforcing steel in concrete.

For better understanding of the cathodic corrosion protection and associate chemical reactions a short introduction on corrosion is provided here.

**Corrosion of reinforcing Steel in concrete**

In the absence of chlorides, reinforcing steel in concrete is generally protected against corrosion. The formation of a protective film on the steel at the concrete interface leads to the passivation of reinforcing steel [18; 19]. The stability of this film depends essentially on the oxygen content and on the pH-value of the interstitial solution at the steel/concrete interface [1]

The passivity of steel in concrete is a result of the high alkalinity of the concrete. During cement hydration the aqueous phase rapidly reaches high pH-values which are in the order of about pH = 12.5, depending on the type of cement [20; 21]. During the strength development process, further alkalis such as KOH and NaOH dissolve and increase the pH value to values in the range of 13.0 to 13.8. [22]

The protection of the steel in the concrete relies on a passivating oxide layer of $Fe_3O_4$, which oxidizes to $Fe_2O_3$ on the electrolyte side. This thin layer of a few atoms (2 – 20 nm) [14] prevents the further dissolution process of the steel due to its high density. However, the resistance of this passive layer is bound to the alkalinity of the electrolyte. Oxides normally found on reinforcing steel are either ferrous ($Fe^{+2}$) or ferric ($Fe^{+3}$). These are chemically stable within concrete provided that the concrete is not carbonated and free of chlorides at the concrete and steel interface. Ferric oxide is considered to be more stable than ferrous oxide, especially in the presence of chlorides. The iron oxide is converted into the more stable, hydrated Ferric oxide (2FeOOH) over time. This conversion process is never complete and is measured as a continued very low passive corrosion rate, as discussed later. The development of the ferric oxide film proceeds according to the following anodic reactions: [19]

$$2Fe \rightarrow 2Fe^{2+} + 4^{e-} \tag{3}$$

$$2Fe^{2+} + 4OH^{-} \rightarrow 2Fe(OH)_2 \tag{4}$$

$$2Fe(OH)_2 + \frac{1}{2}O_2 \rightarrow 2\gamma - FeOOH + H_2O \tag{5}$$

Corrosion of the steel will occur if the concrete is carbonated as neither oxide is protected at a pH below approximately 11. As noted above, the ferric oxide is more resistant to chlorides than the ferrous oxide. Pitting corrosion can occur if chloride ions come into contact with the

reinforcing bar at a location where the ferrous oxide has not been converted. This reaction competes with the normal passivation process and will only proceed when the chloride content is sufficiently high in comparison to the oxygen and hydroxide content. This is the basis for the underlying theory as to why chloride-to-hydroxide ratios are related to the onset of pitting corrosion. In non-carbonated concrete, this corrosion threshold is approximately 0.9 kg/m$^3$ (1.5 lb/yd$^3$) of concrete. This passivation process can also be described in electrochemical terms [23; 24].

**Electrochemical Fundamentals of Corrosion**

Electrochemical corrosion describes metal dissolution under the action of a liquid medium with electrolytic conductivity and reduction of an oxidizing agent to form an electric circuit consisting of an electron current in the metal and an ion current in the medium [25; 26; 27]. At least two individual electrochemical reactions are involved in electrochemical corrosion reactions as follows [28; 29]:

- anodic process, electron release (oxidation):

$$Me \rightarrow Me^{z+} + ze^- \quad \text{(metal dissolution)} \quad (6)$$

- cathodic process, electron acceptance (reduction):

$$Me^{z+} + ze^- \rightarrow Me \quad \text{(metal deposition)} \quad (7)$$

$$2H^+ + 2e^- \rightarrow H_2 \quad \text{(hydrogen corrosion type)} \quad (8)$$

$$O_2 + 2H_2O + 4e^- \rightarrow 4OH^- \quad \text{(oxygen corrosion type)} \quad (9)$$

The reactions take place at one electrode, in which an electrochemical sub-process can take place. This consists of a metallic conductor in contact with an ion-conducting phase. Through the interaction between metal and electrolyte, metal ions of the metal enter the electrolyte [30]. The corrosion reaction is in most cases of an electrochemical nature. Material and

medium together form the corrosion system. In addition to the suitability of the material, the rate of corrosion depends on temperature, potential level and concentration of the medium or mechanical stress. The corrosion of the metal in the aggressive medium can take the form of an even surface loss or discrete localized dissolution of the surface. The electron release (anode) and the electron acceptance (cathode) each form partial reactions in which the partial currents take place. This current flow leads to the electrochemical turnover which can be described using Faraday's law [31]:

$$m = \frac{M}{z\,F}\,I\,t \tag{10}$$

Here, m is the electrochemically converted amount of substance in g, M the molar mass in g/mol, z the charge number, F the Faraday constant: 96487 As/mol, I the Current in A and t the time in s.

The current I is proportional to the chemical conversion rate dm/dt. This means that the corrosion rate correlates with the corrosion current [32]. The equilibrium potential is the potential at which the oxidation and reduction reactions of the same redox system proceed at the same speed. The free reaction enthalpy is zero at equilibrium potential and the Nernst equation [32, 33] applies to the electrochemical equilibrium potential E*.

$$E^{*} = E_0\,\frac{R\,T}{z\,F}\,\ln\frac{a_{Me\,(ox)}}{a_{Me\,(red)}} \tag{11}$$

Here, $E_0$ is the standard potential (for $a_{Me\,(ox)} = a_{Me\,(red)} = 1$) in V, R the molar gas constant in J/(mol*K), z the charge number, F the Faraday constant in (A*s)/mol, T the absolute temperature in K, $a_{Me\,(ox)}$ the activity of oxidized species and $a_{Me\,(red)}$ the activity of reduced species.

**Corrosion current and polarization (current density potential curve)**

The current density potential curve can be recorded on single electrodes with defined electrode processes, which is appropriately called an overvoltage curve. Figure 2 shows the overvoltage curve of a single electrode.

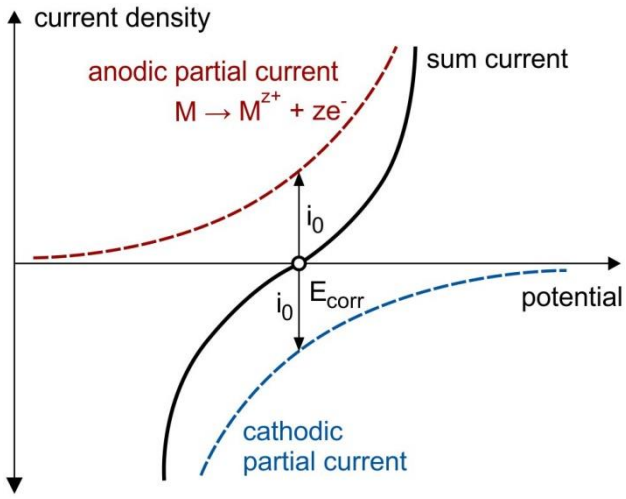


Figure 2 Schematic diagram of an overpotential-current density curve of a metal electrode

The current densities ($i_0$) present at the resting potential ($E_{corr}$) are referred to as the exchange current density, at which there is a correlation between the anodic partial current density $i_a$ and the exchange current density $i_0$ with polarization:

$$i_a = i_0 \exp [k_A \eta] \quad (12)$$

Here, $i_a$ is the anodic partial current density in A/m$^2$, $i_0$ the exchange current density in A/m$^2$, $k_A$ is a constant and η the overvoltage in V.

Using current density potential curves, materials and the stability of their passive film can be characterized electrochemically as described in Figure 3 [34].

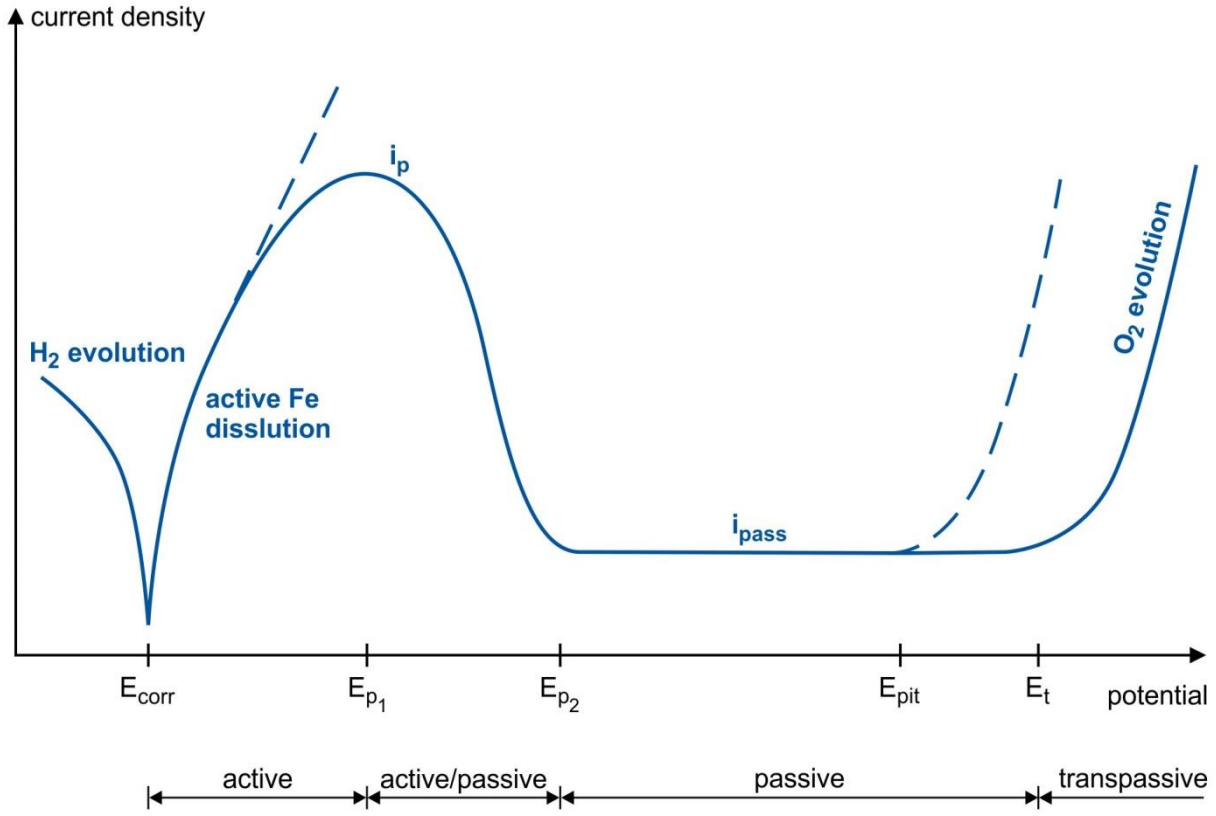


Figure 3 Schematic representation of a current density potential curve

Here, $E_{corr}$ is the rest potential in V, $E_{P1}$ the passivation potential in V, $E_{P2}$ the activation potential in V, $E_t$ the breakthrough potential in V, $i_p$ the passivation current density in A/m$^2$, and $i_{pass}$ the current density in passive range in A/m$^2$.

The potential dependence of the partial currents of the anodic and cathodic partial reactions can be represented in current density potential curves. The current is related to the effective electrode surface. At the resting or corrosion potential ($E_R$ or $E_{cor}$), where the anodic and cathodic partial reactions are equal, the corrosion system is without current (no external current).

**Determination of the corrosion current density (Stern-Geary equation)**

The exchange current density is the current density that can be determined at the point of free corrosion potential in an electrolyte for an electrode due to the corrosion reaction. The exchange current density is determined by semi-logarithmic representation of the E-i- curve, whereby the partial current density lg|i-|=f(ηD) is assigned to the cathodic branch and the partial current density lg|i+|=f(ηD) to the anodic branch with ηD as pass overvoltage. The exchange current density in equilibrium (E=E*) is the measure of the reaction speed at which no current flows outwards. However, in order for an electrochemical reaction to take place,

the equilibrium potential must be exceeded or undershot. This process is called polarization and the deviation from E* is called overvoltage $\eta = E - E^*$. However, the exchange current density only applies to an (through) overvoltage η=0, i.e. for reversible electrode behavior. The Tafel equations apply to the partial current densities of penetration-resistant electrodes:

$$i^+ = +i_0 \exp[+\frac{\propto zF}{RT}\eta_D] \text{ und } i^- = -i_0 \exp[-\frac{(1-\propto)zF}{RT}\eta_D] \quad (13)$$

Here, I is the current density in A/m², $i_0$ the exchange current density in A/m², α the transfer coefficient, z the number of transferred electrons, F the Faraday constant in (A*s)/mol, R the gas constant in J/(mol*K), T the absolute temperature in K and $\eta_D$ the overpotential in V.
For a total current density overvoltage curve of a penetration-resistant reaction, the Tafel line results:

$$i = i_0 \exp[\frac{\propto zF}{RT}\eta_D] - \exp[-\frac{(1-\propto)zF}{RT}\eta_D] \quad (14)$$

Here, I is the current density in A/m², $i_0$ the exchange current density in A/m², α the transfer coefficient, z the number of transferred electrons, F the Faraday constant in (A*s)/mol, R the gas constant in J/(mol*K), T the absolute temperature in K and $\eta_D$ the overpotential in V.

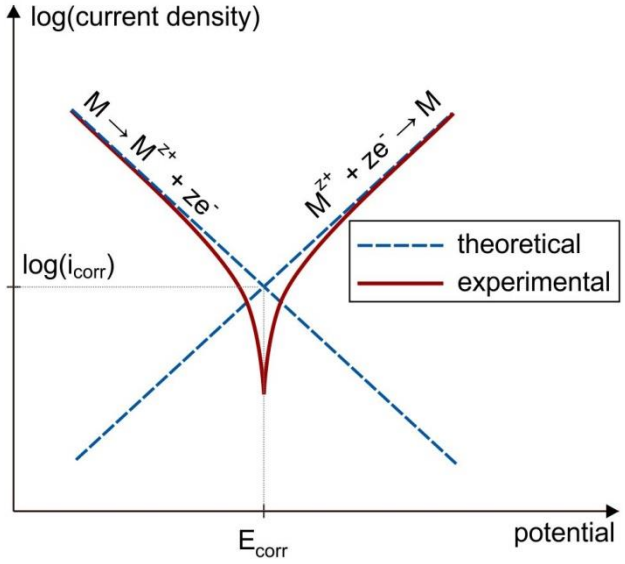


Figure 4: Determination of the corrosion current density from current density potential curves

Under favorable conditions, it is possible to determine the corrosion current (lg I) by extrapolation of both branches in the direction of the free corrosion potential after the cathodic curve has been folded down Figure 4.

**Chloride-induced corrosion**

One of the most severe causes for reinforcing steel corrosion occurs in the presence of chloride ions [35]. The source of chloride ions in concrete can be internal or external [36; 37; 38] such as:

-The use of chloride-contaminated components

-The use of $CaCl_2$ as an accelerator when mixing the concrete

-Diffusion into the concrete from the outside environment

Nowadays the ingress of chlorides from the outside environment is the largest source of chloride-contamination. Intrusion occurs through diffusion or by co-transport with capillary water. In concrete, chlorides can be either dissolved in the pore solution (=free chlorides) or chemically and physically bound to the cement hydrates and their surfaces (=bound chlorides) [39]. Only the free chlorides are responsible for initiating the process of corrosion [118].

After reaching of a critical chloride content near the reinforcement steel, a localized breakdown of the passive film can be induced [40; 41], resulting in the pitting corrosion process. [13; 21; 42]. The phase of chloride-permeation up to the depassivation of reinforcing steel is commonly referred to as the initiation phase. With the onset of corrosion the degradation phase begins. Figure 5 shows that damage to structural elements occur only after the damage or propagation phase has been initiated.

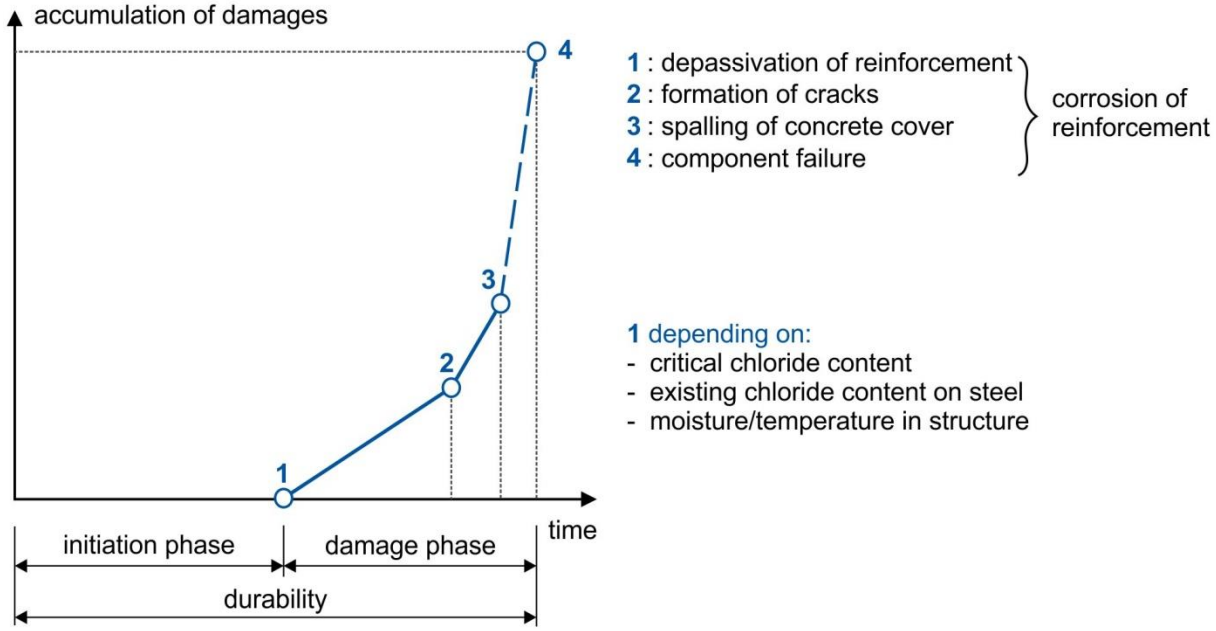


Figure 5: Course of damage in structures suffering chloride-induced corrosion, according to [43]

The current approach to quantifying chloride-induced corrosion of reinforcing steel in concrete follows from defining chloride threshold values [39]. However, there is no

consensus in the scientific community for the specific determination of a critical level of chlorides, above which serious problems occur [44; 39; 45; 46; 47; 48].

## 4.2 Technical Textiles

The term carbon refers to carbon fiber composites that consist of any number of woven or laid carbon fiber rovings which are impregnated with polymers to obtain a more rigid and stronger material. Carbon fiber composites are known, for example, from motor sports and aircraft construction. In the construction industry, mats are increasingly used as reinforcement in textile concrete due to their low weight, chemical resistance and excellent mechanical properties.

The average diameter of a single fiber is around 5-7 µm. If single fibers are bundled together, they are called carbon rovings. Carbon rovings consist of thousands of bonded carbon fibers. [49] To improve adhesion and handling for further application, carbon rovings are impregnated. Figure 6 schematically shows the composition of a carbon roving.

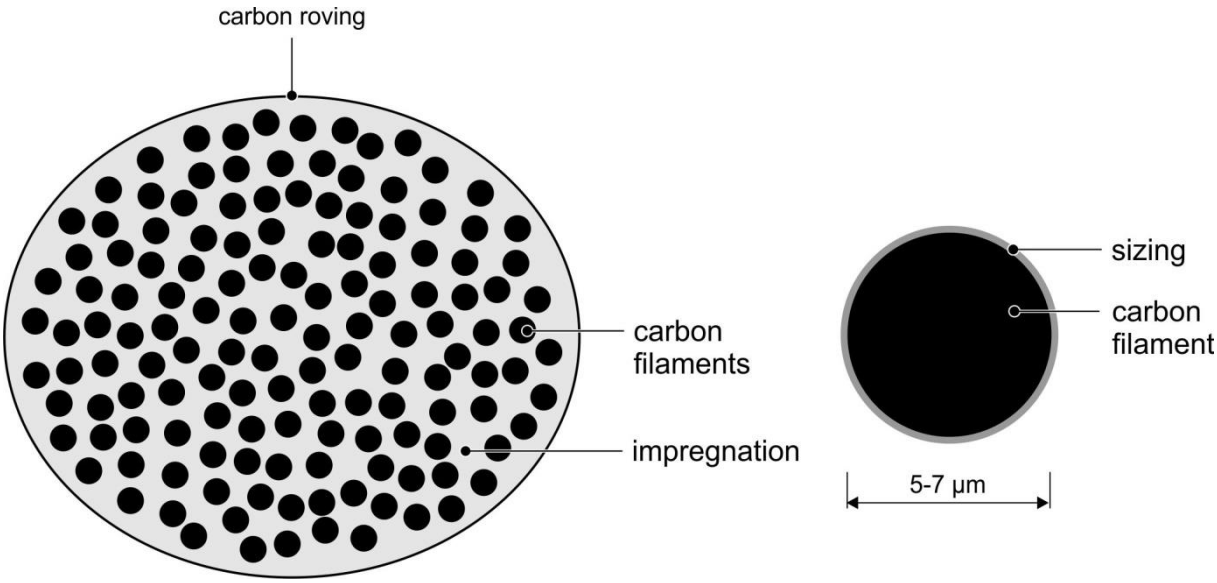


Figure 6: composition of a carbon roving (schematic)

To achieve optimal interaction between the composites of one carbon roving, homogeneous mixing of sizing and impregnation must occur.

During the process of impregnation, the formation of 3 different phases is possible:

1. No mixing of sizing and impregnation: Sizing does not detach from carbon fiber during impregnation. This results in a degradation of mechanical properties [50].
2. Partial mixing of sizing and impregnation: During impregnation a concentration gradient develops. The concentration of sizing decreases with increasing distance

from the carbon fiber. Along the interface no complete inter-linkage of the molecules occurs [51; 52].

3. Homogeneous mixing of sizing and impregnation: According to the chemical reactivity between sizing and carbon fiber two scenarios have to be considered. If there is no covalent binding between sizing and carbon fiber, resin can covalently bind to the carbon fiber during impregnation [49]. If there is covalent binding between sizing and carbon fiber, mixing proceeds as follows. According to [53; 54; 55] the relatively small molecules of the hardener component may mingle with the sizing film, resulting in a homogeneous mixing along the interface.

To achieve good adhesion between different materials, direct contact at the molecular level is paramount [56]. Thus, homogeneous mixing of sizing and impregnation results in enhanced mechanical properties [49]. Figure 7 shows the formation of interfaces during the impregnation of the carbon fibre.

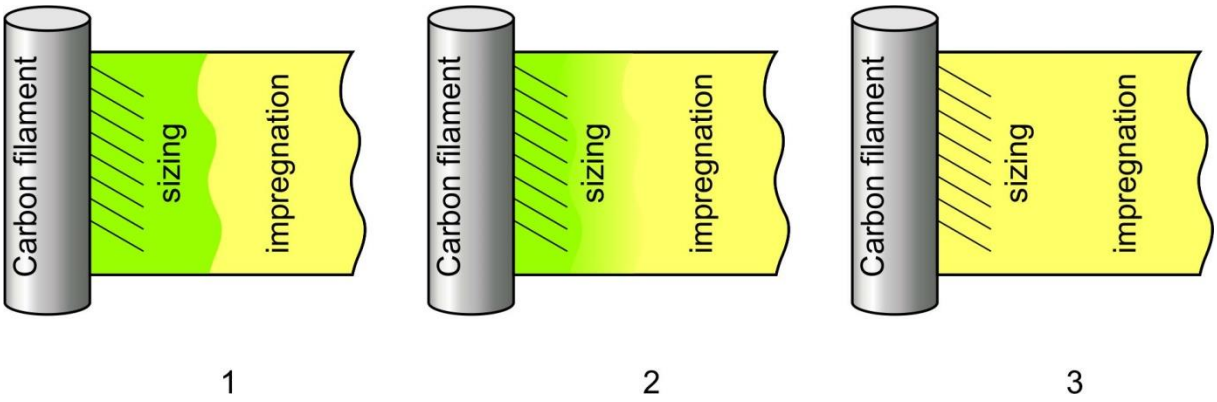


Figure 7: Interphase formation during impregnation of the carbon fiber, according to [55]

In the next chapters the production of carbon fiber, surface activation of fiber, sizing and impregnation with details are explained.

**Carbon fiber production**

Carbon fiber is the term generally applied to fibers containing a mass fraction of carbon > 92 %. Carbon fibers can be produced from different chemical polymers. Most commonly used materials are Polyacrylnitril (PAN), Pech und Cellulose [57; 58]. However, PAN-based

carbon fibers achieve highest strength, which makes them the dominant fiber when it comes to industrial production [59; 49].

Processing of PAN-based carbon fibers consists of several stages:

First, PAN fibers are stabilized in air, which makes them unsusceptible for melting during the following higher temperature treatment. After oxidation, initially white PAN fibers turn black. These black fibers are subsequently heated in an inert atmosphere to 1000-1500 °C. At temperatures around 1300 °C the fibers reach their maximum strength (up to 5000 N/mm$^2$). High-tensile fibers develop, which is the main part of carbon fiber production [60]. Temperature increase must be low to preserve the fiber's high degree of molecular order. For an improved fiber texture (i.e. orientation of the basal planes and thus increase of elastic modulus) fibers are held for a very short duration at temperatures up to 3000 °C.

Figure 8 shows the schematic PAN-based carbon fiber production.

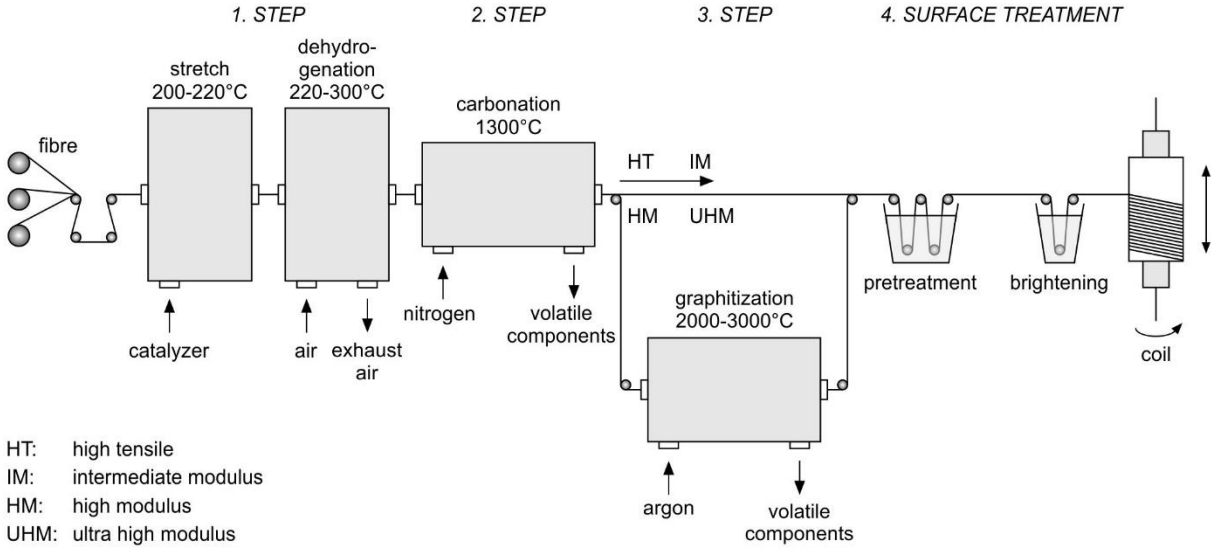


Figure 8: manufacturing process of carbon fibers, according to [61]

Normally carbon fiber yield is approximately 50 %. [62]

**Modification of the carbon fiber surface using anodic polarization**

The next step in the typical production process of carbon fiber is to activate the surface of the produced carbon fiber. The surface is activated electrochemical by anodic oxidation in an electrolytic solution. Surface activation ensures enhanced wettability.

The surface of the carbon is activated after fiber produced by electrochemically oxidizing the surface [63]. To activate the surface, there are also other methods such as plasma treatment [64], wet chemical or thermal oxidation [65] of the carbon fiber. The aim of activating the surface is to generate polar groups on the relatively non-polar carbon fiber surface. This in turn achieves better wettability and thus better adhesion of the coating. The treatment of the surface can influence the oxygen absolute content [66; 67; 68; 69]. Oxygen content on the fiber surface enables covalent bonds between carbon fiber, sizing and impregnation. When the surface is activated, carbon fiber serves as an anode and is polarized against a counter electrode made of graphite block in distilled water [70]. Oxygen-containing groups are produced by the polarization or chemical and electrochemical reactions on the surface of carbon fibers [63; 71]. Possible oxygen-containing groups can be hydroxyl, carbonyl and carboxyl groups. These groups are generated at defect sites or by breaking the graphitic lattice on the surface [72].

Yumitori and Nakanishi [73; 74] have investigated the effect of anodic oxidation in different electrolytes on the adhesion of carbon fibers to epoxy resin. The carbon fibers were polarized up to 60 seconds at a constant current density of 30,000 mA/m². With increasing charge density, an increased formation of surface oxides such as hydroxylene, carbonylene and carboxylene was observed by X-ray photoelectron spectroscopy. Under the SEM, the formation of longitudinal grooves and crevices could be observed. The discoloration of the solutions is therefore due to the dissolution of the carbon fibers. Up to a certain charge density, increased adhesion between the carbon fibers and an epoxy resin embedding produced by casting after polarization could be achieved by polarization, which can be explained by bonds between the epoxy resin and the hydroxyl and carboxyl groups that are increasingly present.

**Sizing material**

After surface activation each fiber is then coated by a mixture of various chemicals (sizing) to protect it from mechanical damage during handling and improve its wetting performance [75], [76; 77]. Furthermore sizing leads to more chemical reactive site as well as an increased surface area for adhesion [78; 79; 80] found that particle size and distribution of sizing agent significantly influence the wetting performance of carbon fibers.
The adhesion promoters for textile materials are called sizing and are applied to the filaments during the production. This coating material performs various functions [60].

Only sized carbon fibers are used in industry [63], so the chemical-physical influence of the sizing is very important. The sizing is made of a polymer that is usually applied to the carbon fiber from a water-based dispersion and then dried. The sizing has three main tasks. Firstly, it serves to protect the carbon fibers from mechanical stress. Secondly, the chemical-physical properties of the sizing are of high importance for the wetting behavior of the resin system. Thirdly, the sizing is to act as a link between the carbon fiber and the matrix. In order to optimize the connection of the systems at the interface, the bonding capacity at the carbon fiber surface as well as the subsequent bonding to the resin system are of particular importance.

Most coatings consist of polymers with good wetting properties of the fibers. They often contain polar groups that facilitate wetting but can absorb moisture. This means that they attract water and soften the boundary layer. This reduces the adhesion between the coating material and the fiber. Since the surface of carbon filaments gives a number of reactive groups, the coating can bind to the filaments. The coatings for different impregnations are not the same. In the production of epoxy impregnated carbon, epoxy based coatings are used to ensure good chemical compatibility of the two components. Other coatings are also applied such as vinyl ester resins, phenolic resins and polyurethane sizing [60]. Electrochemical treatment of the surface also improves adhesion [60].

**Impregnation materials**

As mentioned previously, carbon rovings need to be impregnated. Unimpregnated carbon rovings are characterized by extremely small cavities between the single carbon filaments. Due to the small dimensions of the fiber interstices, intrusion of mortar is not possible. While the outermost filaments are directly connected to the surrounding concrete, the inner filaments are not bonded with the surrounding matrix. Under tensile load these filaments remain unstressed [81]. To improve bonding, textile impregnation turned out to be most effective. The fine matrix of impregnation materials enables the intrusion to the roving's inner core. Thus, load transfer is evenly distributed throughout the roving's cross-section. [82; 83]
In practice, epoxy resin or styrene-butadiene rubber (SBR) based coatings are used for impregnation. [82]
Generally, epoxy resin results from the mixture of a base resin and a hardener component. The base resin consists of epichlorohydrin and phenol. After mixing of resin and hardener the

initial physical state is liquid. The curing occurs at room temperature or under addition of heat, depending on the hardener characteristics. [84; 85]
SBR-based coatings are aqueous dispersions consisting of rubbery butadiene particles and polystyrene. It is a fluid milk-white solution with a solids content of 48 % typically and density of 1.09 g/cm$^3$ [86]. The reaction between butadiene and styrene occurs, in which carbon double bonds are activated by initiating substances or heat supply [87; 88].

## 4.3 Carbon textile as anode material for cathodic protection

### 4.3.1 Thermodynamic stability

The Pourbaix diagram [1] shows the dominant reactants and products of the redox reactions of substances in an aqueous solution as a function of electrochemical potential and pH value. Oxidation is generally a process in which electrons are removed from an atom; during reduction electrons are added to the atom. Since neither oxidation nor reduction can occur on their own, i.e. there is always a coupling of these reactions, which are referred to as redox reactions [89].
The corrosion behaviour of materials can be discussed using Pourbaix diagrams. The diagrams are divided into fields by lines at which equilibrium exists between individual possible redox reactions. The diagrams are based on the potential and pH value. In the Pourbaix diagrams, the pH value at the contact surface between solution and material is taken into account. However, despite strong anodic electrolytes, this can be locally strongly acidic due to acidification as a result of, for example, oxygen or chlorine gas development [112]. Using the equation (15), all possible redox reaction equations for the starting material are derived. The equation shows that a reducing agent B and water are in equilibrium with an oxidizing agent A, hydrogen ions $H^+$ and electrons $e^-$. The number of atoms and electrons on both sides must be stoichiometrically balanced. It should be noted that an atom A cannot formally react to form atom B, since stoichiometry cannot be achieved in this way.

$$bB + xH_2O \rightleftharpoons aA + mH^+ + ne^- \tag{15}$$

The line functions of the Pourbaix diagram are determined using the Nernst equation (16).

$$E = E_0 - \frac{0{,}059}{n}\log\frac{B^b}{A^a} - \frac{0{,}059m}{n}pH \tag{16}$$

The dashed lines show the redox reactions of water. Anodic potentials can lead to oxygen development, which is the upper of the two dashed lines:

$$2H_2O \rightleftharpoons O_2 + 4H^+ + 4e^- \quad (17)$$

In alkaline solutions this is done by dissolving hydroxide ions [90; 91]:

$$4OH^- \rightleftharpoons O_2 + 2H_2O + 4e^- \quad (18)$$

The lower dashed line represents the hydrogen development under cathodic potentials:

$$2H^+ + 2e^- \rightleftharpoons 2H_2 \quad (19)$$

The lines in Pourbaix diagram show the corrosion behaviour of the material. In the area where no active material behavior is present, a distinction can be made between inert behavior on the one hand and passive behavior on the other. Inert means that the material is present as the material, but no corrosion is possible. Passive, however, indicates that the material is typically coated with its corrosion product and separates the contact between the material and the solution. Passivity does not necessarily imply the absence of corrosion [1]. Passive state according to DIN EN ISO 8044 [119] only applies to metals and in the case of carbon no passive layers are formed on the surface and therefore the term passive cannot be used for carbon.
The Pourbaix diagram, the equations behind it and standard chemical formulas show that the predominant potential is the trigger for corrosive processes and thus critical potentials exist [114].

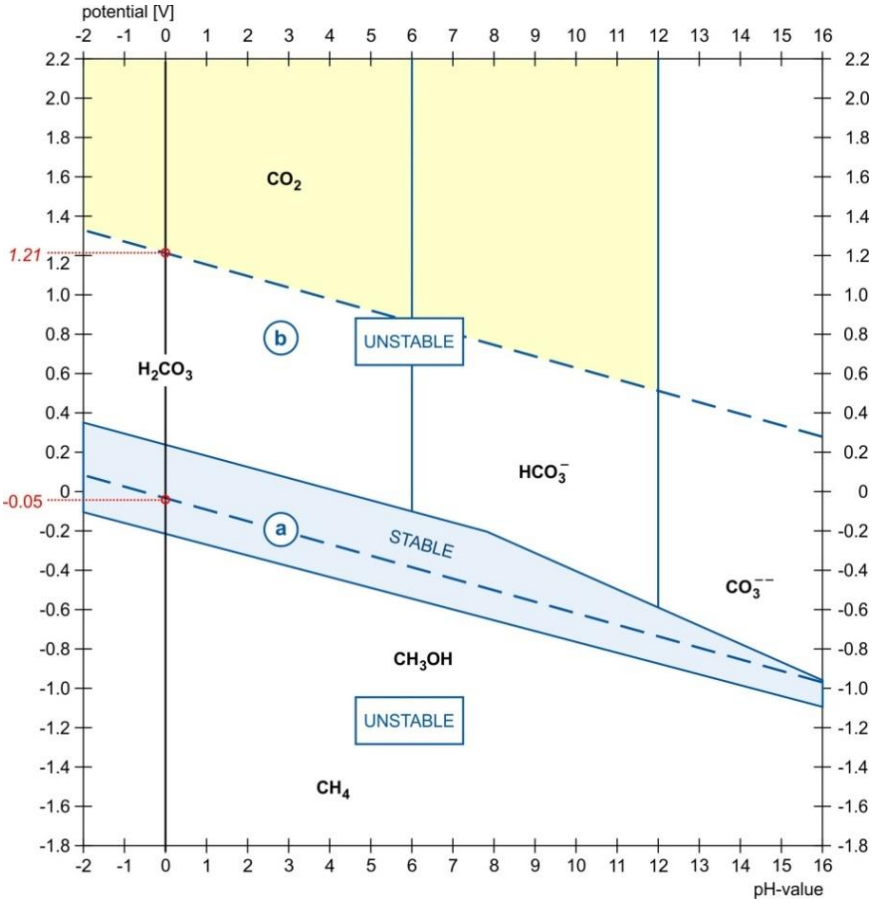


Figure 9: Simplified Pourbaix diagram for carbon in aqueous solution [1]

The simplified Pourbaix diagram for carbon shown in Figure 9 [1] shows the stability range of water within the dashed lines a and b. Above and below the boundary lines water is electrochemically unstable and reacts as described above. The diagram takes into account all useful carbon compounds, such as methane for the group of alkanes, methanol from the group of alcohols or formaldehyde from the group of aldehydes.

Carbon has a small area where it exhibits stable material behaviour. There is no passivity range for carbon in aqueous solution. The stable area is shown in Figure 9 with a blue area. With polarization, carbon can be oxidized to carbonic acid at pH values up to about 6, between pH values of about 6 to 10 to hydrogen carbonates and above pH values of 10 to carbonates. In addition, below a pH of 12, carbon dioxide can be formed from both carbon and its oxidation products. By anodic polarization, the surface of the carbon fiber is oxidized to hydroxyl, carbonyl, carboxyl and lactone functional groups [108]. These groups are oxidized to carbonate, carbon dioxide and carbonic acid under continued anodic polarization [109].

A corrosion of the carbon should already take place at low anodic potentials. For this reason, carbon textile does not appear to be suitable as an anode material for a CP system. However, limitations must also be placed on the meaningfulness of the diagram as it relates

to carbon filaments used in CP as the diagram is only valid for pure carbon in aqueous solutions. First, carbon used in CP is not pure carbon, but rather a carbon fiber composite. These technical textiles are coated and impregnated with SBR or epoxy resin. Furthermore, the Pourbaix diagram makes only conditionally statements about the kinetics of the electrochemical processes of technical carbon textiles.

### 4.3.2 Previous experiments in solution and in mortar

As an anode material for cathodic corrosion protection, carbon is a new material and still little researched. Therefore, there is only a limited number of test and research results and published literature on this topic. The following section presents the experiments and findings that have dealt with the behavior of carbon-based materials in alkaline environments used as CP anode. Much of the research does not focus on technical textiles with polymeric impregnations, which are currently used on construction sites. Some have shown experiments with extremely high potentials or current densities in order to really destroy the carbon and have low suitability with the usual CP applications.

The predecessor of current carbon textiles was the CarboCath System. Mork et al. [92] presented the concept of using CarboCath as an anode material for CP. The CarboCath textiles were flexible mats without impregnation or coating of the fibers. Structures with carbon textile anodes, saturated Calomel reference electrode and a titanium rod as counter electrode were polarized in a simulated pore solution with pH value 13 and over voltages between 1000 and 6000 mV. The carbon textile anodes were weighed before and after polarization. With a polarization of 2000 mV and a current density of 620 mA/m² related to substrate surface, a weight loss of 3 % was determined after 168 hours. However, of 3000 mV and a current density of 8800 mA/m² related to substrate surface, a loss of 44 % was already determined during the same period. Under the scanning electron microscope, the surface of the carbon textile after a polarization of 1800 mV over 168 hours was found to remain intact. At a polarization of 3000 mV, a clear decomposition of the carbon textile could be seen. Therefore, the authors concluded that carbon textile is stable below a polarization of 2000 mV [92]. In addition, three projects were presented where the CarboCath system was used for the repair of corrosion damaged structures. These are two test areas of 5 m² each on a bridge in Öland, Sweden, a parking garage of 3500 m² in Heilbronn, Germany and the underside of a 2000 m² harbor in Honningsvåg, Norway [93]. All structures were shown to meet the 100 mV protection criterion after 24 months respectively.

Chini et al [95] have developed a new anode design. In the design, a carbon roving without impregnation was cast in a non-conductive epoxy resin cylinder and the cylinder was cut off and ground so that only the cross-section of the roving comes into contact with the solution.

This minimized the uncertainty factor of the anode surface when determining the current density. This was repeated for each test and up to 20 tests were carried out with one encapsulated anode. The anode had a cross-sectional area of approximately 10 mm². Potentiostatic tests were performed on different voltage levels. The tests were repeated with chloride contents of 1% and 3% in solution. Compared to the test without chlorides, only minor differences could be observed in the curves for small potentials [95]. From a potential of 580 mV vs. NHE oxygen development was observed at the anode, from a potential of 1340 mV vs. NHE a formation of corrosion products was observed at the anode [96].

Rueffer et al [94] have investigated whether graphite is an active or inactive anode with the focus on the interaction with the dissolution in water. They performed a test setup consisting of a graphite microelectrode as the anode, a platinum plate as counter electrode, a saturated mercury-mercurous sulfate reference electrode was tested in various electrolytes. Galvanostatic tests with different polarization durations between one and six hours were carried out and the total organic carbon content (TOC) was determined. The results of this work showed an increase of the total organic carbon content from a potential of 600 mV vs. $Hg/Hg_2SO_4$. The currents varied between 1 and 20 mA. In the experiments a dark discoloration of the electrolyte was observed. A gas evolution was observed above 300 mV vs. $Hg/Hg_2SO_4$. The addition of 1 wt. % sodium chloride to the sodium hydroxide solution produced the same qualitative results, while the addition of 5 wt. % with a mass increase at the anode resulted in the formation of a protective layer. Further experiments refuted an inactive behavior of the graphite electrode and concluded a modified active behavior.

To investigating carbon textiles embedded in mortar specimens. A number of researchers tackle the question which range of current density is needed to make carbon textile act as a satisfactory anode for CP, while minimizing the deterioration of the anode. Current density is either related to the anode surface (carbon textile) or to the reinforcing steel surface, which can lead to confusion and which makes comparison of the results difficult.

Bertolini et al. [98] investigated the behavior of a cementitious conductive overlay anode made of nickel-coated carbon fibers in a cementitious mortar. Applied current densities ranged from 10-100 mA/m$^2$ with respect to the anode surface. The authors concluded that impressed current densities of up to 20 mA/m$^2$ made the cementitious conductive coating a satisfactory anode for CP for over two years. However, an exceedance of 50 mA/m$^2$ led to the destruction of the anode within only 1-2 months. In this range of current densities, acid is produced by anodic reactions, which lead to the degradation of the anode. Furthermore a decomposition of the polymer based binders [113] and of the mineral binders [110] was observed for the presented anode system.

Vennesland et al. [99] introduced a system based on woven carbon textile mesh, which was developed in Norway. This approach was tested on specimens obtained from a concrete

bridge which was demolished due to steel corrosion. A one month polarization with a feeding voltage of 1000 mV and current densities of 3-4 mA/m$^2$ with respect to the reinforcement surface was applied and evaluated. The criterion given in DIN EN ISO standard 12696 [12] to control the efficiency of the cathodic corrosion system was fulfilled by all specimens, verifying that the low current densities were adequate to achieve CP.

A declaration of a definite value concerning the maximum external current to run CP systems was made by Van Nguyen et al. [97]. For carbon fiber fabric anodes applied current should remain below 128 mA/m$^2$ (with respect to the steel surface area). For carbon fiber rod anodes applied current should not exceed 64 mA/m$^2$. The statements are based on laboratory simulations of CP systems, which were operated for 1100 hours.

Lee-Orantes et al. [116] have investigated the performance of a bonded carbon fiber reinforced polymer on reinforced concrete prisms. The carbon anodes were polarized with current densities of 50, 100 and 1000 mA/m² during 175, 50 and 7 days. The results have shown that the carbon fibers used for structural reinforcement can also work simultaneously with a (CP) system. After more than 100 days of CP application, no adverse mechanical influences were found in the system, although the applied currents were 24, 48 and 480 times higher than real constructions.

Anwar et al. [100] delivered surprising results which contrasted the formerly stated ranges of maximum current densities. However, they investigated the effectiveness of lightweight conductive mortar as an anode material, with only 1.1 % addition of carbon fibers. Galvanostatic experiments were performed for a duration of 14 days. Constant current density of 200 mA/m$^2$ related to the anode surface was applied. The attainment of constant potentials proved difficult. However, valuable discoveries were made regarding the durability of carbon fibers. Scanning electron microscope (SEM) images demonstrate that neither high current densities nor high potentials cause significant carbon fiber dissolution.

Zhang et al. [16] carried out experiments on cathodic prevention which is the application of a protective current to a structure prior to chloride exposure. Tests were performed on carbon fiber mesh anodes, embedded in mortar specimens. Test specimens were covered in a 10 % saline solution. Initially defined current densities were applied to all test specimens. Electrochemical accelerated testing was performed for two months. The specimens were sawn open after the two months, annular microstructural changes were detected around the carbon rovings. It was found that, despite the extremely low current densities hydrogen ions were formed around the anode causing locally acidic conditions. Under acidic conditions portlandite ($Ca(OH)_2$) decomposes. With increasing current densities, microstructural and chemical changes at the anode interface are expected to increase considerably.

To forecast the service life, the electrical charge density Φ was used, which is defined according to equation (20) from the current density applied over time [101].

$$\Phi = i_a \cdot t_a = i_e \cdot t_e \quad (20)$$

Here, ϕ is the total amount of electrical charge applied to the system during the entire period of acceleration test in C/m$^2$, where C is the abbreviation for Coulomb, $I_a$, the applied current density into the system in A/m$^2$, $t_a$ is the time that the applied current density is available in seconds, .

The forecast is then made using the equation converted according to time (21).

$$t_e = \frac{i_a}{i_e} \cdot t_a \quad (21)$$

Here, $i_e$ the protective current density which is required in practice in A/m$^2$ and $t_e$ is the estimated equivalent service life of cathodic prevention system in the real case in days.
The predicted service lives were at least 71 years with a protective current density $i_e$ of 2 mA/m². Zhang et al. have made statements about the condition of the carbon meshes [102]. A release of the bond between carbon textile anode and cement was determined [102].
Jing et al [103] developed a conductive mortar by applying carbon fiber as a secondary anode and activated titanium strips as the primary anode. This carbon-filled (0.05-0.8 vol.-%) mortar was studied for its electrical, mechanical and electrochemical properties. Galvanostatic measurement were performed in $Ca(OH)_2$ solution. A current density of 200 mA/m$^2$ related to mortar surface was impressed and the potential was measured. The results of up to 350 hours of polarization have shown that the mortar with increasing carbon content requires less potential to generate similar current densities.
Chini [8] presented results for carbon textile anodes in mortar. Two different carbon textile anodes with two different mortars and different chloride contents were used. Activated titanium reference electrodes (ATME) were concreted into steel pipes which served as counter-electrodes. Potentiostatic tests and EIS measurements were performed. At polarizations between 100 and 1000 mV the anode behavior was found to be active. The results of the EIS measurements on the mortar test specimens on the active areas of the carbon textile anode coincided with the results from the EIS measurements in simulated pore solution [96].
Van Nguyen et al. [97] have tested the suitability of epoxy resin for embedding of carbon textiles to concrete and a carbon fiber reinforced geopolymer for embedding carbon rods in a milled groove. The performance of the carbon anodes were carried out in the alkaline

solution and on mortar specimens. In all solution tests, hydrogen development was observed. In the Potentiostatic experiments, decreasing currents and increasing resistances were observed over time. According to the authors, the drop in current indicates a dissolution of the carbon anode, which, however, seems to reach a stable state after a certain time. After 165 hours, a mass loss of 2.69 % was observed on a carbon fiber anode with an applied supply voltage of 10 volts in solution.

Zhu et al. [104; 105; 106] performed tensile strength tests on the carbon fiber after the anodic polarization. Dumbbell-shaped samples were protected with a seal and only a defined test region was unsealed. Subsequently, the samples were galvanostatically polarized for 25 or 50 days. The current densities were between 770 and 6150 mA/m² related to the unsealed test area. The experiments with lower current densities showed a constant potential over time, whereas at the two highest current densities the potential increased rapidly at first, but decreased with time. The carbon fiber composite was partially heavily destroyed after polarization, especially the epoxy resin matrix. SEM analyses confirmed the decomposition of the epoxy resin matrix, but no decomposition of the carbon fibers was detected. The degree of dissolution increased with increasing current density and longer polarization time. The dissolution of the epoxy resin was attributed to destruction of the C-N compounds, which led to depolymerization of the epoxy resin. The tensile strength decreased with increasing current density and polarization time. The authors presented a proposal for calculating the service life of the material for tensile reinforcement under anodic polarization on the basis of charge density and tensile strength from the tests, which predicts a service life of at least 24 years under dual function at a current density of 20 mA/m² with a fiber strength reduction to 40 %.

Sun et al [107] have continued these investigations, but have focused on the explanation of the electrochemical processes and the determination of a resolution rate. For this purpose, samples were polarized galvanostatically in two alkaline solution for 50 days. Fourier-transform infrared spectroscopy (FTIR) was used to clarify the resolution mechanisms of the epoxy resin, which differed for the two solutions used. On the carbon textile polarized in sodium hydroxide solution, more C-O-C and C=0 compounds were identified, which were formed by the binding of oxygen from oxygen development, which explains the softening of the epoxy resin.

Dissolution of graphite was observed in [94]. An actual decomposition of the carbon fiber itself was only found in [111], the investigations of [95; 96] determined that a decomposition of the carbon fiber is possible, but that a dissolution of the polymer-based coating is more likely.

# 5 Investigations

Figure 10 shows the investigated materials for the four papers. Furthermore Figure 11 shows the different examinations carried out for the tests.

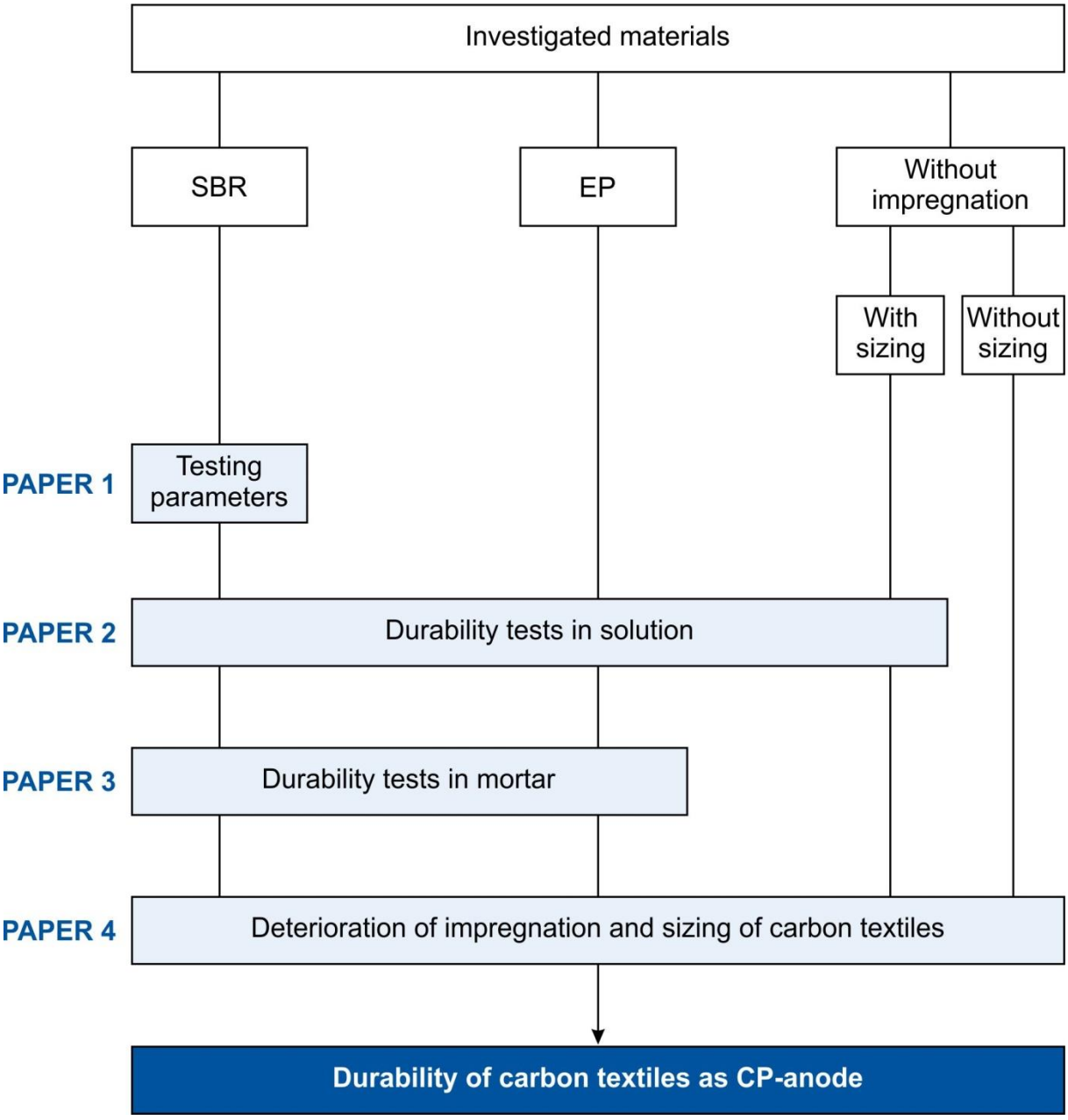


Figure 10: Schematic representation of the investigations of this thesis

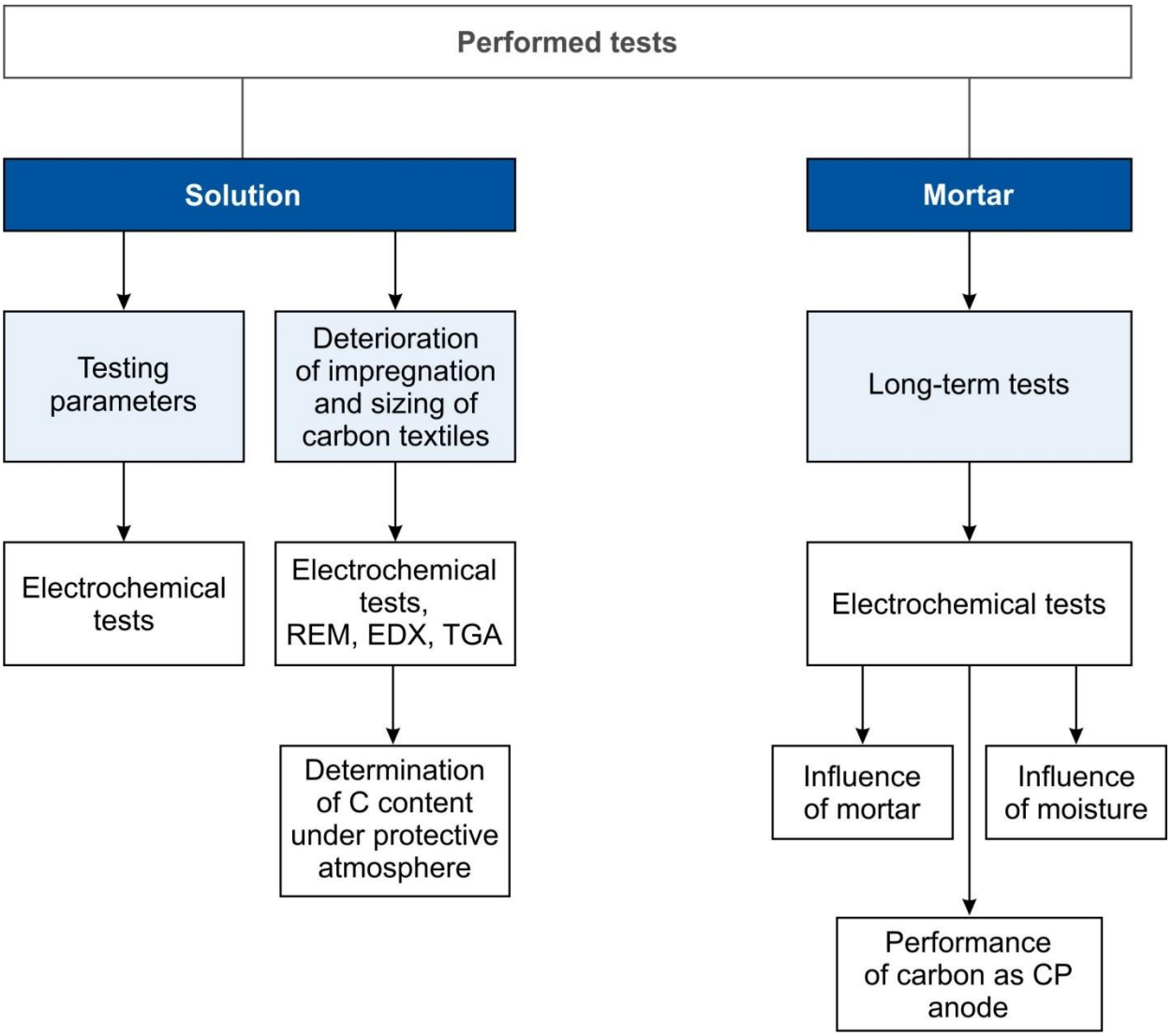


Figure 11: Examinations carried out for the tests

# 6 DISSCUSSION OF MAIN FINDINGS

## 6.1 Influencing parameters on the measurement

In Paper 1, the most important influencing parameters on the planned measurements were examined. The parameters identified that could have an influence on the test results were the orientation of the sample in the solution, the influence of chlorides in the solution, the storing of the sample in the solution for a longer time before polarization, the homogenization of the solution during the experiment and the sealing of the roving ends after cutting of a large mat.

It turned out that the orientation has no influence on the result. The influence of chlorides on the measurement can be clearly seen. Even the two identical test specimens show different results. This influence should be examined more closely. However, due to the large number of tests carried out to investigate the durability of the polymer-impregnated carbon textile, this work was not carried out.

When storing the sample 24 hours before starting the measurement as well as homogenizing the solution during the measurement, there is an influence on polarization. This influence was however found to be insignificant. Therefore, the additional measurements in Paper 2 were carried out with a measurement of the resting potential of 24 hours. The measurement was performed under permanent mixing.

The main influencing factor was found to be the sealing of the roving ends. Because polymer impregnated carbon textile has free unimpregnated carbon textile at the cut surface, these ends are better conductors since no inhibition is exerted by an impregnation. In practice however finished mats are typically used without cutting and the specimens here should represent practical conditions. Therefore, the ends were sealed with epoxy resin.

Carbon textile investigated in paper 1 was a carbon textile impregnated with SBR. The results of the potentiodynamic tests on unimpregnated carbon fibers are presented as a current density potential curve in logarithmic scaling. It should be noted that the current densities are subject to the above assumptions regarding the calculation of the anode surface. All curves have a similar characteristic that can be divided into 5 phases:

1. OCP up to Tafel area 1
2. Tafel area 1
3. Transition area
4. Tafel area 2
5. Area above Tafel area 2

These phases indicate different reactions of the carbon and the change of the active surface by the polarization in solution, whether the reactions to the dissolution of carbon textile or impregnation material indicate. These phenomena were not known at the time of measurements in Paper 1.

At the right end of the curve a turning of the curve can be observed (Figure 12). At first glance, it appears to be overcompensation. However, in Paper 2, a large number of instant-off measurements proved that the IR drop is relatively constant and therefore not responsible for overcompensation in the calculation of the compensated potential. Rather, a destruction of the impregnation materials could cause a change in the active surface area. Another cause could be the electrochemical reactions that occur between impregnated carbon textile and solution at these potentials.

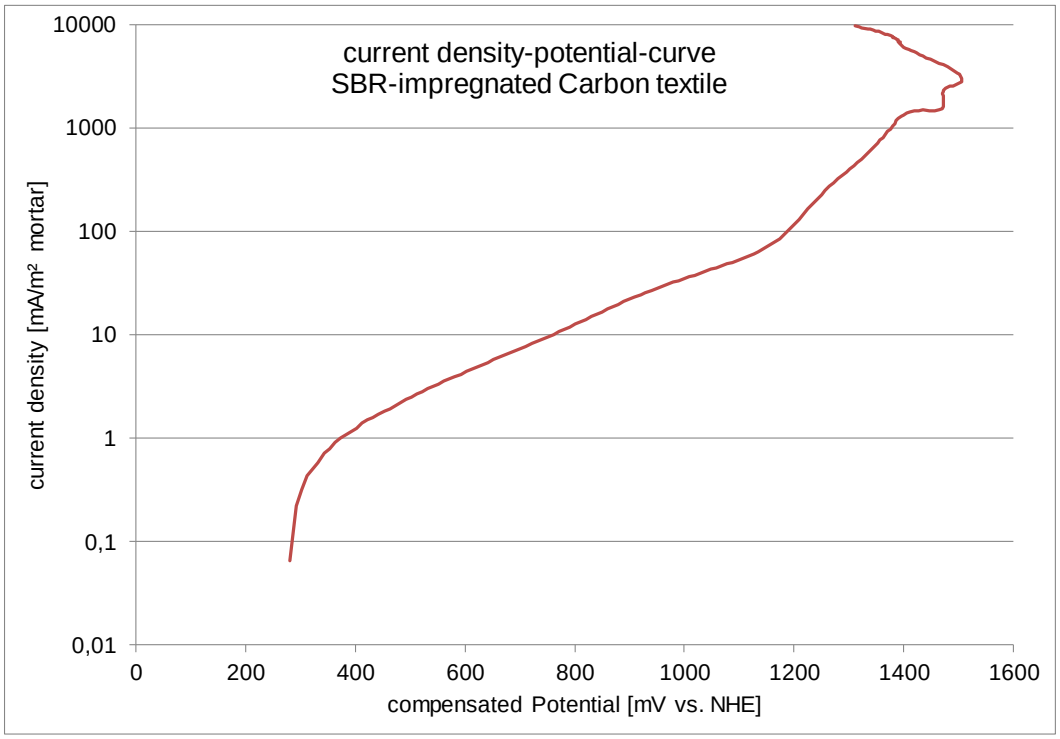


Figure 12: current density-potential-curve of SBR-impregnated Carbon for pretest measurements

## 6.2 Influence of polarization on the impregnation in solution

In paper 2 carbon textiles with two different impregnation materials (SBR and epoxy), graphite and carbon textile without impregnation material but with sizing were investigated. The aim was to determine the influence of impregnation material on polarization and to observe corrosion of carbon textile or destruction of impregnation materials. First potentiodynamic experiments were carried out to get the critical potentials out. Afterwards, potentiostatic tests were carried out on the chosen potentials under argon atmosphere. Subsequently, the solution was examined for carbon content. In the context of an IGF project

[117] authors have measured the carbon content in solution with total organic carbon (TOC), one can measure the carbon content in solution. Since we have a saturated CaOH solution with sediment, carbon compounds with solids can be set which cannot be detected in a TOC measurement. Instead, the solution was dried by evaporating the solvent and then treated with nitrogen prior to performing a DIN EN ISO 15350 [120] carbon analysis. In addition, SEM analysis was performed on polarized and non-polarized carbon textile samples to determine if the breakdown of the material had occurred within the impregnation or carbon textile. Two impregnated carbon textiles were selected for the experiments: a styrene butadiene rubber (SBR) and an epoxy impregnated carbon textile. Unimpregnated carbon textile as a raw material was also provided by the manufacturers. The raw carbon textile was already coated with sizing but the impregnation process had not been carried out.

The results of potentiodynamic experiments have shown that SBR impregnated carbon textile provides more current density at the same potentials, but less than the pure graphite sample. From this, it can be concluded that the impregnation prevents the charge transfer of carbon into the solution. After many carbon textile samples had been examined by SEM, the following observations about the change of the surface after polarization were made:

- The SEM images in paper 2 and 4 show reproducible results for the same materials
- The SEM analysis then showed that the SBR impregnation has many flaws in the starting material which was found to lead to a better polarizability. Epoxy impregnation, on the other hand, is dense and had no flaws, but rather pores that increased in size with polarization. SBR impregnation changed even after polarization so that it is destroyed.

It was also determined that the measured electrical resistivity of SBR is much lower than what is expected from a non-conductive polymer such as SBR, since SBR is normally used as an insulator for the cables. Therefore, an electrical longitudinal conductivity could also be achieved by impregnation.

An oxygen development is not to be expected from the theoretical potential of approximately 480 mV vs. NHE. However oxygen development can be expected after exceeding an overvoltage of 690 mV vs. NHE.

The SBR impregnation is mostly very flat and bright (Paper 2), there are some large pores in the material, which could have been caused by air inclusions during impregnation or due to the shrinkage of the material during drying. The carbon filaments are easily visible at the pore locations in the impregnation. The surface of the polarized SBR-based material looks completely different. One can clearly see a destruction of the SBR. Instead of being flat, the surface is furrowed after polarization of the carbon roving and some carbon filaments have been uncovered. A large part of the surface is covered by a film which, according to EDX analysis in Figure 13, consists mainly of calcium, carbon and oxygen. At higher resolutions,

different types of crystals can be seen: partly tapering, partly with flat, sharp-edged surfaces. The film could therefore consist of calcium carbonate, for example. The calcium carbonate is formed from the calcium of the calcium hydroxide solution and may have been formed from carbon from impregnation or from carbon dioxide in the air.

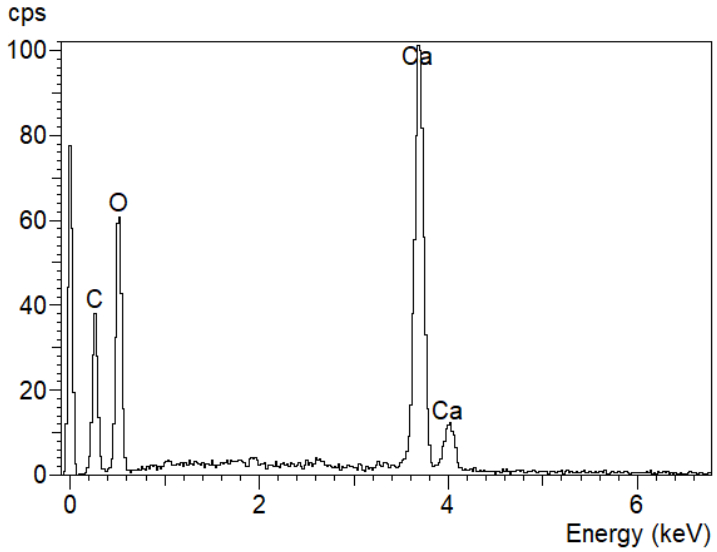


Figure 13: EDX analysis of the film [Paper4]

The position of the carbon filaments can be seen through the impregnation. The surface is less flat than the surface of the S4. Small pores with diameters of up to approximately 10 µm can be seen along the translucent carbon fibers. The number of pores was found to increase significantly as a result of polarization. Furrows are also visible in the direction of the carbon filaments. These will have been created by destruction of the epoxy resin impregnation and reducing the thickness of the impregnation at these points above the carbon filaments.

Since the SBR impregnation was more susceptible to polarization and the preparation for carbon analysis was very time-consuming, the carbon analysis was only performed on S4. According to the course of the graphs, the holding potentials were selected at three points. Distinct changes in the slope could be detected at these points, which, according to previous findings, indicate a change in the electrochemical reaction within the system. These potentials were then potentiostatically polarized on 3 further test specimens for 5 days. All measurements were carried out under an argon protective gas atmosphere in order to minimize carbonation of the alkaline solution. The solution from the holding tests was then collected and prepared by evaporation and subsequent freeze-drying so that a solid sample was available for carbon analysis. The carbon values at the first and second hold points showed similar carbon contents in the solution as the reference sample without polarization. Point three showed a slight increase in carbon content. Subsequently, identical tests were carried out on point 1 with a holding period of 4 weeks. Thus, the change of the carbon

content in the solution was investigated in more detail. The entire test was also carried out in an inert gas environment. No significant difference in carbon content was observed between the polarized samples and the reference sample, which would indicate an accelerated dissolution of the carbon textile within the tested potential range. The detected carbon content was observed to increase with polarization duration of 5 days. This may indicate dissolution of the carbon textile or the penetration of $CO_2$ into the solution despite the protective gas atmosphere. Another possibility could be the detection of carbon from polymeric impregnation materials that are destroyed by polarization and fall into the solution.

The SEM analyses of paper 4 show that the carbon contained in the solution cannot come from the carbon fiber. It should be mentioned that carbon analysis after polarization is only carried out for carbon impregnated with SBR and the SEM results show that the SBR impregnation decomposes with the polarization from the beginning. Thus, it can be said that the decomposed polymers up to holding potential P3 are so low that they cannot be detected in solution by carbon analysis. At holding potential P3 one sees an increase of the carbon content. The decomposition of the polymers often happens through the supply of energy. These processes are also called thermal decomposition. Other sources of energy, such as current, also cause bonds within molecules to split. Therefore, it is assumed that the energy for the decomposition of the SBR impregnation or sizing was reached at P3, which can be found in the carbon analysis.

Further tests were carried out on the unimpregnated carbon. The samples were also potentiostatically polarized at potentiostatic polarization point 1 for 4 weeks. No significant difference in carbon content was observed between the polarized and unpolarized samples. The REM images of paper 4 showed an explanation for this phenomenon. At potentiostatic potential point 1, the sizing is not yet destroyed or decomposed and thus no additional carbon is measured in the solution after polarization. It is presumed that the carbon present in the solution is due to entry of carbon into the solution through contact with air during decanting of the containers.

The results of Paper 2 have shown that impregnation has a greater influence on polarization. SEM analysis after polarization showed that impregnation is destroyed by anodic polarization after specific potentials. Carbon analysis showed that the carbon textile was not attacked. In order to better investigate the destructive mechanism of impregnation, additional experiments were carried out which are summarized in Paper 4.

In Paper 2, tests on carbon textile anodes in alkaline solution were carried out and new findings on the condition of carbon textile under anodic polarization were gained. On the basis of theoretical investigations, the dissolution reactions of carbon fibers under anodic polarization could be clarified. First, different surface oxides are formed on the carbon fiber. The surface oxides are further oxidized under continuous anodic polarization. Carbon dioxide

and carbonates are formed in a strongly alkaline environment. The reaction products and the kinetics of the carbon dissolution are influenced by the electrolyte.

Through Potentiodynamic experiments the behavior of unimpregnated carbon fibers (Paper 4) under anodic polarization in alkaline solution was characterized. The current density potential diagram of unimpregnated carbon fibers shows five phases like the diagrams of impregnated carbon fibers (Paper 1).

SEM images were able to explain why impregnated carbon materials have conductivity at all, even though the impregnation materials epoxy resin and SBR are electrically non-conductive. The electrical conductivity of the materials is based on imperfections, pores, partly low impregnation thicknesses and damage to the impregnation matrix.

The tests and other SEM images in Paper 4 show that the epoxy resin and SBR impregnations and the sizing of the carbon fibers, respectively, are first decomposed. Destruction of the carbon fibers themselves could not be brought about, which is believed to be due to the relatively strong covalent bonds between the carbon atoms of the carbon fibers. There are critical potentials for epoxy resin impregnation and sizing for which dissolution reactions are expected. These potentials likely lie at or above 900 mV vs. NHE for the sizing of the unimpregnated carbon fibers and at 1050 to 1150 mV vs. NHE for the epoxy resin impregnation of E4 and are characterized in the current density potential diagram by the transition range between Tafel slope 1 and Tafel slope 2. The SBR impregnation is expected to be dissolved at a potential of 490 mV vs. NHE. Above the critical potentials, potential and current are jointly responsible for the damage to the impregnation and are related to each other according to Ohm's law.

## 6.3 Polarization of Carbon textile in Mortar

In order to validate findings gained from the solution tests [Paper 1 & 2] and the ongoing research, as well as to obtain further insights into the function in the actual embedding of the carbon textile anodes in mortar, long-term tests were planned on mortar test specimens. The test specimens were prepared, and the performance of the tests started [Paper 3]. Unfortunately, it was not possible to carry out many analyses on the mortar test specimens as in the solution tests, since carbon textile could not be removed from the mortar without imparting mechanical damage to the carbon textile. It was possible to observe the performance of carbon textile as a CP anode over a longer period of time and to apply the knowledge gained from the solution tests to the known potentials in mortar.

Two different mortars, two different storage conditions and three different anode materials were selected for the investigations. Potentiostatic measurements on critical potentials were

planned for a period of approximately 8 months. To determine critical potentials in mortar, potentiodynamic experiments were first carried out and potentials selected. Different storage conditions, different polarization behavior of carbon textile in mortar was to be determined in wet and dry environments.

Higher current densities in wet bodies were expected as compared to dry specimens due to the influence of moisture on polarization. Wet conditions are more favorable for charge transfer since the electrolytic resistance of the mortar decreases due to the moisture in the mortar.

SBR impregnated carbon has also shown better polarizability as epoxy impregnated carbon in mortar. The results showed that the SBR impregnated samples can provide more current density at approximately the same potentiostatic potentials. This can be attributed to the destruction of the SBR impregnation during anodic polarization.

A comparison of the both mortars shows that mortar 1 delivers more current density than mortar 2 at the same potentials. It can be seen that mortar can have a very large influence on the operation of the CP systems.

The samples sawn after potentiostatic measurement show no visual changes in the mortar or carbon. Unfortunately, carbon embedded in mortar cannot simply be separated without destruction of the sample prior to examination under SEM. But the constantly running current density with potentiostatic potentials set indicates that the carbon has remained intact over the time tested. No acidification of the mortar has been observed in the vicinity of the carbon anode.

## 6.4 Damage mechanisms of polymer impregnated carbon textiles

The results of paper 4 have shown that the impregnation and sizing is destroyed with increasing anodic polarization. For this purpose potentiostatic measurements at critical potentials were performed. These critical potentials were determined by the potentiodynamic experiments using current-potential-curves. Epoxy and SBR-impregnated samples as well as samples without impregnation were investigated. In order to show the destroyed sizing, tests were also carried out on carbon rovings without impregnation and without sizing.

First, it was visually observed in all investigated samples that with anodic polarization a white film is deposited on the roving, which grows with increasing anodic polarization.

Afterwards REM pictures and the EDX analysis showed that this film is calcium carbonate and comes from the reaction between calcium from the solution and carbon. Whether this carbon comes from carbon roving or from impregnation or sizing will be discussed in the following section.

It has been seen that the polarization of carbon textiles is possible due to the imperfections in the impregnation. Defects in both epoxy and SBR impregnated samples can be seen with the aid of SEM. Although the imperfections are more significant in SBR impregnated samples. It is assumed that the sizing is so thin that the polarization of carbon through the sizing is possible. With epoxy impregnated samples, the impregnation remains intact up to a certain potential range. Then the sizing starts to be destroyed by the polarization. It is assumed that the sizing is destroyed at a potential where oxygen development and oxygen gas formation are achieved. With increasing anodic polarization, the impregnation is also destroyed.

But with SBR impregnated Carbon the destruction of the impregnation is observed right from the beginning of the polarization. The impregnation is destroyed and thus one has more active surface for the polarization. This also explains the better polarizability of SBR impregnated carbon. The sizing starts to be destroyed by higher potentials; just like with epoxy impregnated carbon.

Comparison of the SEM images of the two unimpregnated carbon textiles with and without sizing showed that the carbon roving remains intact up to an anodic polarization of 2200 mV vs. NHE. The deposited films, which can be seen on the sizing, consist of calcium carbonate. The results of the carbon textile unimpregnated but with sizing have shown that after the destruction of the impregnation by anodic polarization the deposited film sits on the sizing and appears to be a 2 µm thick layer. This film is not visible on unimpregnated Carbon without sizing.

# 7 CONCLUSIONS

Figure 14 and Figure 15 show the main results of this work. Figure 14 shows that in epoxy impregnated carbon at the beginning of the polarization there are pores on the epoxy impregnation but it remains intact until destruction of the sizing. After a potential of 1050-1150 mV vs. NHE the epoxy impregnation is also destroyed. It must be said that the investigations up to 2200 mV vs NHE and current densities between 50 and 80 mA/m$^2$ related to mortar surface showed no destruction of the carbon. This is only valid for the tested materials with tested impregnation materials. If new materials are available, the possible destruction of the impregnation and sizing could be detected by potentiodynamic measurement with a very slow polarization rate in a current density potential curve.

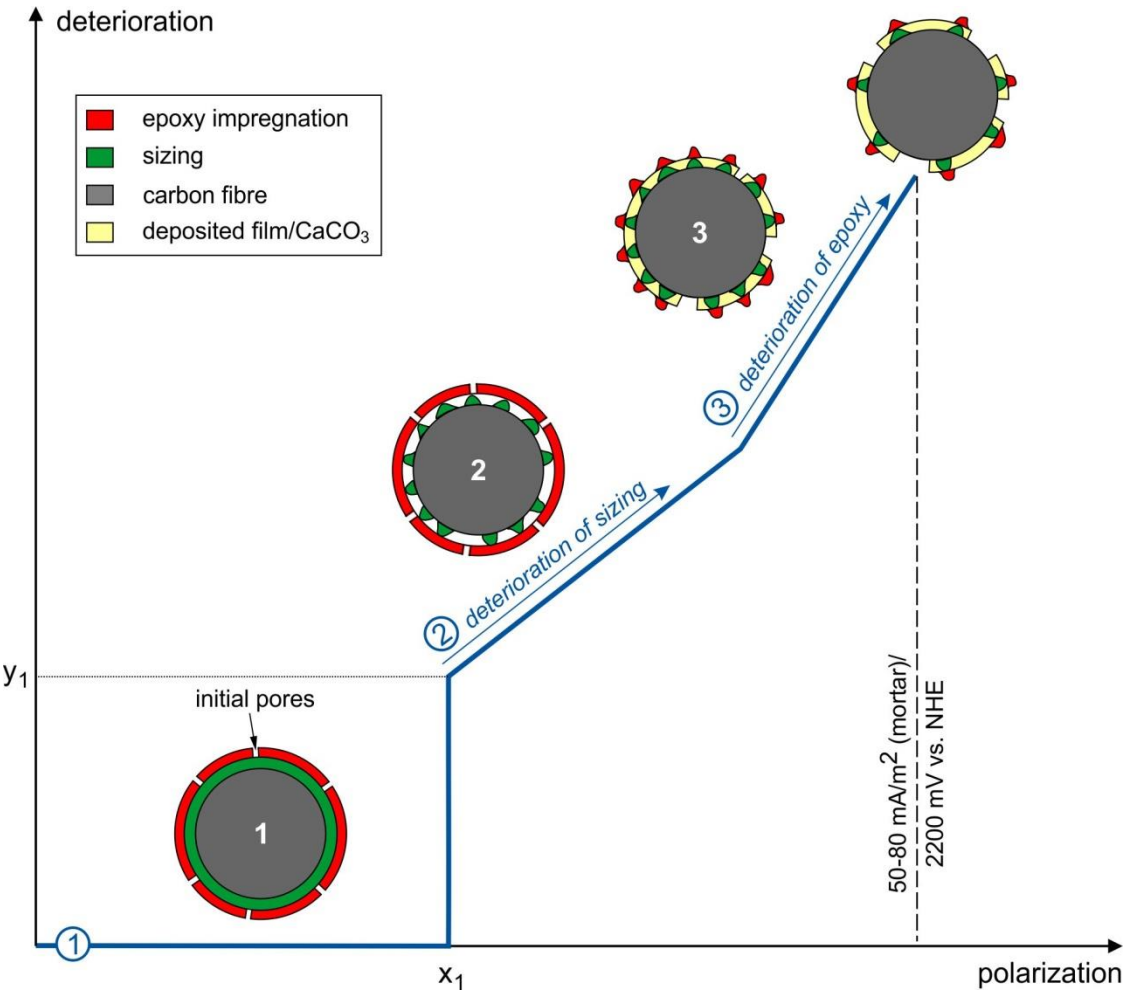


Figure 14: Destruction mechanism of the epoxy impregnated carbon.

Figure 15 shows that with SBR impregnated carbon the impregnation is destroyed from the beginning and thus achieves better polarizability. When the potential of the destruction of the sizing is reached, the deposited films form on the remaining sizing at the same time and increase with increasing polarization.

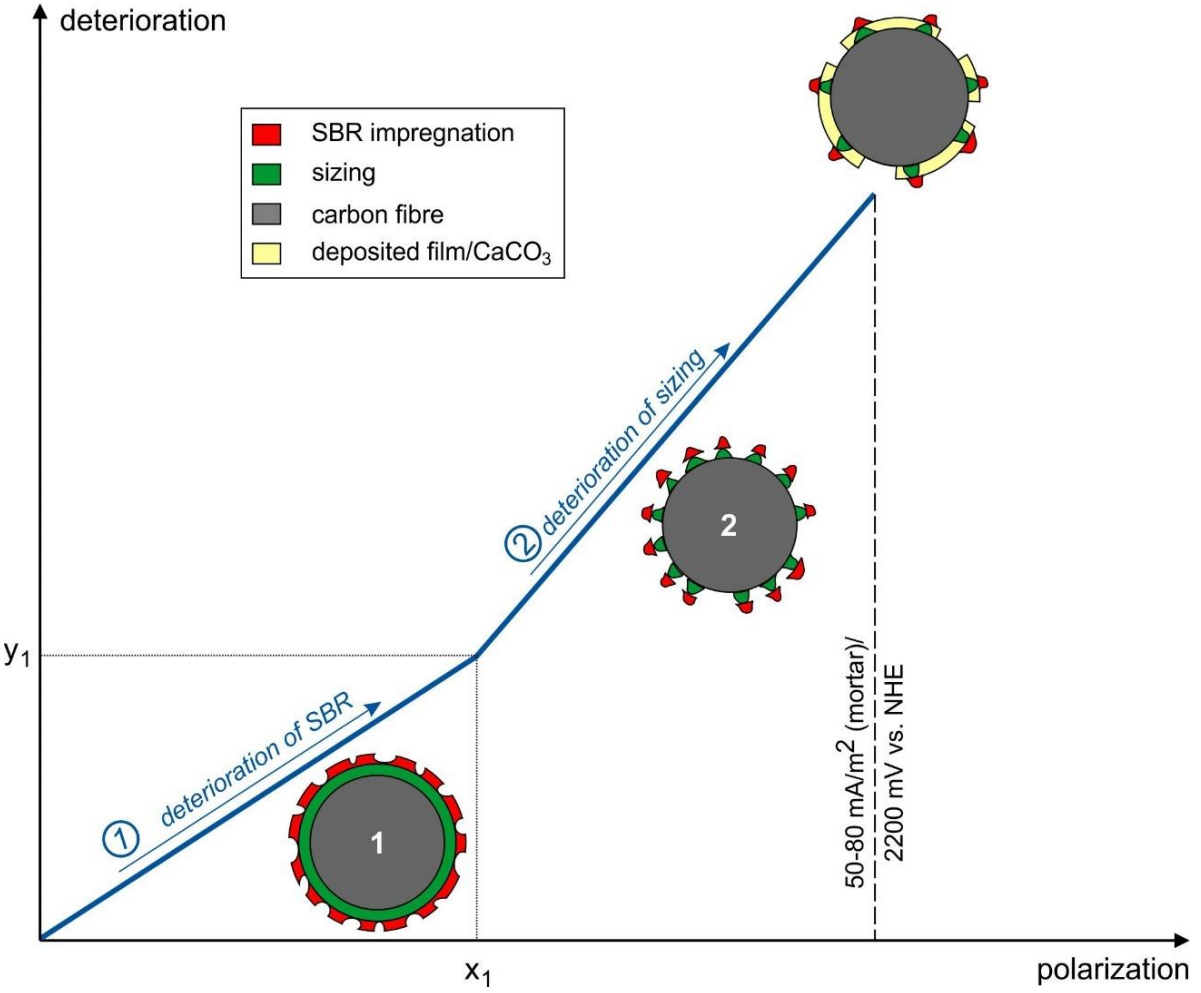


Figure 15: Destruction mechanism of the SBR impregnated carbon.

The conclusion of this work can be summarized as follows:

1. CP with carbon textiles up to 2200 mV vs NHE is possible.
2. The acidification effects that occur to other anode materials also apply to carbon.
3. Potentiostatic tests in mortar have shown that carbon textiles have delivered constant current over the investigation period.

# 8 FURTHER RESEARCH WORK

The critical potentials, which lead to a destruction of parts of the carbon materials, were limited by short-term experiments. However, the slope of the current density potential curves indicates an active anode behavior and a dissolution of the anode. The critical potentials identified through these trials should be validated by experiments with potentials just below the critical potentials in the transition area of the curves over a longer period of time and subsequent review of SEM images of the anode surface.

Carbon textile has excellent mechanical properties. As reinforcement in textile concrete, it has a high potential to be used as reinforcement in thin components and to reduce crack widths in concrete elements. The possibility of utilizing carbon textiles as both a CP anode and reinforcing material shows promise. The modification and destruction of the impregnation material under polarization can however lead to loss of bond between mortar and carbon textile. Therefore, the effects of anodic polarization on the tensile strength of carbon textiles and on the adhesive strength between carbon textile and mortar must be investigated. These investigations could be used to estimate the changes in strength over the service life of structurally strengthened members or structures built with carbon textile reinforcing with an impressed current applied. First, pull-out and three-point bending tests after polarization in mortar should be performed to determine the influence of polarization. If a negative influence is detected, new impregnation materials should be developed that maintain the carbon roving / concrete bond over time and are not destroyed by anodic polarization.

Furthermore, the influence of chlorides on the measurements and destruction of impregnation and sizing should be investigated.

Investigations should be carried out on higher potentials in order to determine possible destruction of the carbon and present its limiting potentials.

A very important aspect would be whether the combination of CP and strengthening can be used together. For this purpose, various experiments must be carried out. On the one hand, carbon textiles embedded in mortar must be polarized at the limit potentials determined from solution tests where the impregnation and sizing is destroyed. Then pull-out and three point bending tests must be carried out. The results should be compared with the identical reference specimens, which are not to be polarized. Additionally, carbon roving must be placed under tensile stress and polarized at the same time. This should show whether stress crack corrosion occurs in carbon rovings.

# 9 REFERENCES


[1] Pourbaix, M. (1974): Atlas of electrochemical equilibria in aqueous solutions. NACE International, Houston, Texas, USA.

[2] Helm, C.; Raupach, M. (2016): Development of a numerical simulation model considering the voltage drops within CP anode systems in RC structures. Materials and Corrosion 67(6), pp. 621–630.

[3] Nürnberger, U. (1995): Korrosion und Korrosionsschutz im Bauwesen, Band 1: Grundlagen Betonbau, Bauverlag GmbH, Wiesbaden und Berlin.

[4] Ashworth, V. (2010): Principles of cathodic protection. In: Cottis, B. et. Al. (eds.): Shreir's Corrosion, Elsevier, Oxford, pp. 2747-2762.

[5] Raupach, M. (1992): Kathodischer Korrosionsschutz im Stahlbetonbau. Beton 42(12), pp. 674–676.

[6] Eichler, T.(2012): Zu den sekundären Schutzmechanismen beim kathodischen Korrosionsschutz von Stahl in alkalischen Medien, Dissertation, Fakultät für Bauingenieurwesen der Rheinisch-Westfälischen Technischen Hochschule Aachen

[7] Chini, M.; Antonsen, R.; Vennesland, Ø.; Arntsen, B.; Mork, J.H. (2007): A review of utilization of carbon fibers as an anodic material in cathodic protection. In: Ferreira, R.M. et al. (eds.): Proceedings of the International RILEM Workshop on Integral Service Life Modeling of Concrete Structures, pp. 397-402.

[8] Chini, M. (2010): Pan-based carbon fiber as anode material in cathodic protection systems for concrete structures, PhD Thesis, Norwegian University

of Science and Technology, Faculty of Engineering Science and Technology (Department of Structural Engineering), Trondheim, Norway.

[9] Pedeferri, P. (1996): Cathodic protection and cathodic prevention. Construction and Building Materials 10(5), pp. 391-402.

[10] Page, C.L. (1997): Cathodic protection of reinforced concrete-principles and applications. In: Proceedings of the International Conference on Repair of Concrete Structures. From Theory to Practice in a Marine Environment, Svolvear, Norway, 28-30 May 1997 (pp. 123-131).

[11] Isecke, B. (1988): Korrosion und zerstörungsfreie Prüfung im Bauwesen, Technisches Messen 55, 4, pp. 152-156

[12] Deutsches Institut für Normung (2017): DIN EN ISO 12696: 2017-05. Kathodischer Korrosionsschutz von Stahl in Beton.

[13] Sekar, A.S.S.; Saraswathy, V.; Parthiban, G. T. (2007): Cathodic Protection of Steel in Concrete Using Conductive Polymer Overlays. International Journal of Electrochemical Science 2(11), pp. 872-882.

[14] Raupach, M.; Büttner, T. (2014): Concrete Repair to EN 1504. Diagnosis, Design, Principles and Practice, CRC Press Francis & Taylor Group, Boca Raton.

[15] Isecke, B. (1987): Kathodischer Schutz kann Bauwerke aus Stahlbeton retten, Neues aus der Forschung, Beratende Ingenieure, 12, pp. 14-17

[16] Zhang, E.Q.; Tang, L.; Zack, T. (2016): Carbon Fiber as Anode Material for Cathodic Prevention in Cementitious Materials. In: Proceedings of the 5th International Conference on the Durability of Concrete Structures, Shenzhen, China, 30 June – 1 July 2016.

[17] Nerland, C.; Polder, R. (2002): Cathodic protection of RC Structures far more than Bridge Decks. In: 15th International Corrosion Congress (ICC), Granada, Spain, 2-27 September 2002.

[18] Montemor, M.F.; Simoes, A.M.P.; Ferreira, M.G.S (2003): Chlorid-induced corrosion on reinforcing steel: from the fundamentals to the monitoring techniques. Cement and Concrete Composites 25(4-5), pp. 491-502.

[19] Berke, N. (2012): Environmental Degradation of Reinforced Concrete. In: Kutz, M. (Ed.): Handbook of Environmental Degradation of Materials, Elsevier, Great Britain.

[20] Graef, H.; Thielen, G. (1995): Influences of concrete technology affecting the initiation and progress of steel corrosion in concrete. Beton 45(9), pp. 640-646.

[21] Page, C.L.; Treadaway, K.W. (1982): Aspects of the electrochemistry of steel in concrete. Nature 297(5862), pp. 109-115.

[22] Andrade, C.; Merino, P.; Novoa, X.R.; Perez, M.C.; Solar, L. (1995): Passivation of reinforcing steel in concrete. Materials Science Forum 192-194, pp. 891-898.

[23] Bentur, A.; Diamond, S.; Berke, N.S. (1998): Steel corrosion in concrete—fundamental and civil engineering practice, E&FNSpon, London.

[24] Berke, N.S. (1986): The use of anodic polarization to determine the effectiveness of calcium nitrite as an anodic corrosion inhibitor. In: Chaker, V. (Ed.): Corrosion effects of stray currents and the techniques for evaluating corrosion of rebars in concrete, ASTM, Philadelphia, pp. 78-91.

[25] Bommer, H. (1998): Kathodischer Korrosionsschutz von Magnesium-

Werkstoffen durch neue Magnesium-Legierungen, Herbert Utz Verlag, München.

[26] Brett, C.M.A; Brett, A.M.O (1993): Electrochemistry – Principles, Methods and Applications, Oxford University Press, Oxford.

[27] Bard, A.J.; Faulkner, L.R. (2001): Electrochemical Methods: Fundamentals and Applications, Wiley, New York.

[28] Pourbaix, M. (1973): Lectures on electrochemical corrosion, Plenum Press, New York/London.

[29] Hoar, T.P. (1961): Electrochemical principles of the corrosion and protection of metals. Journal of applied chemistry banner 11(4), pp. 121-130

[30] Roos, E.; Maile, K. (2008): Werkstoffkunde für Ingenieure, Springer Vieweg, Berlin/Heidelberg.

[31] Wendler-Kalsch, E.; Gräfen, H. (1998): Grundlagen der Korrosion. In: Wendler-Kalsch, E.; Gräfen, H. (Eds.): Korrosionsschadenkunde. Springer Verlag, Berlin, Heidelberg, pp. 10–46.

[32] Reinhardt, H.W (2001): Korrosion und Korrosionsschutz, WILEY-VCH Verlag GmbH, Weinheim.

[33] Fernández-Solis, C.D.; Vimalanandan, A.; Altin, A.; Mondragon Ochoa, J.S.; Kreth, K.; Keil, P. (2016): Fundamentals of Electrochemistry, Corrosion and Corrosion Protection, Springer International Publishing, Switzerland.

[34] Thull R., Schaldach M:. Fretting corrosion of metallic implants. Pp. 1-6. 2nd Annual Meeting of the European Society for Artificial Organs (ESAO), Berlin

1975

[35] Creegan, P.J.; Graham, J.R.; Tatro, S.R.; Herreryherrera, A.E.; Kaden, R.A.; McDonald, J.E.; Schrader, E.K. (1994): Compendium of case-histories on repair of erosion-damaged concrete structures. ACI Materials Journal 91(4), pp. 408-409.

[36] Thuresson, T.I. (1996): Electrochemical Monitoring of the Influence of Concrete Quality on the Reinforcing Steel Corrosion in Industrial Effluent, Thesis (M.Sc.), Queen's University, Kingston.

[37] Glass, G.K.; Buenfeld, N.R. (2000): Chloride-induced corrosion of steel in concrete. Progress in Structural Engineering and Materials Banner 2(4), pp. 448-458.

[38] Hafenbautechnische Gesellschaft e.V. Hamburg, Fachausschuss für Korrosionsfragen (1994): Kathodischer Korrosionsschutz für Stahlbeton. Sanierung und Erhaltung von Hafenbauwerken aus Stahlbeton durch Kathodischen Korrosionsschutz, Hafenbautechnische Gesellschaft e.V., Hamburg.

[39] Poursaee, A. (2016): Corrosion of Steel in Concrete Structures, Woodhead Publishing, UK.

[40] Dauberschmidt, C. (2010): Chloridbelasteter Beton – immer ein Entsorgungsfall? In: Regionaltagung des Deutschen Beton- und Bautechnikvereins, München, 23 February 2010.

[41] Glass, G.K.; Reddy, B.; Buenfeld, N.R. (1998): The inhibitive properties of concrete in a chloride containing environment. In: 39th Corrosion Science Symposium, University of Northumbria, Newcastle, UK, 8-10 September 1998.

[42] Arup, H. (1983): The Mechanisms of the Protection of Steel by Concrete. In: Crane, A.P. (ed.): Corrosion of Reinforcement in Concrete Construction, Ellis Horwood Limited, Chichester, pp. 151-157.

[43] Tuutti, K. (1982): Corrosion of steel in concrete, PhD Thesis, Swedish Cement and Concrete Research Institute, Stockholm.

[44] Raupach, M.; Schnell, J. (2015): DAfStb-Positionspapier zum kritischen korrosionsauslösenden Chloridgehalt, Deutscher Ausschuss für Stahlbeton e.V., Berlin.

[45] Hansson, C.M.; Sørensen, B. (1990): The threshold concentration of Chloride in Concrete for the Initiation of Reinforcement Corrosion. In: Berke, N. et al. (Ed.): Corrosion Rates of Steel in Concrete, ASTM International, West Conshohocken, PA.

[46] Zhang, J.Y. (2008): Corrosion of Reinforcing Steel in Concrete Structures: Understanding the Mechanisms, National Research Council (NRC)-Institute for Research in Construction, Ottawa.

[47] Angst, U.; Elsener, B.; Larsen, C.K.; Vennesland, Ø. (2009): Critical chloride content in reinforced concrete. A review. Cement and Concrete Research 139 (12), pp. 1122-1138.

[48] Breit, W.; Kritischer Chloridgehalt – Untersuchungen an Stahl in chloridhaltigen alkalischen Lösungen. Materials and Corrosion, 1998

[49] Wetjen, D. (2016): Wechselwirkung von Carbonfasern, Schlichte und epoxidbasierter polymerer Matrix in carbonfaserverstärkten Kunststoffen, Dissertation, Universität Augsburg, Mathematisch-Naturwissenschaftlich-Technische Fakultät, Augsburg, Germany.

[50] Sato, N.; Tatsuda, N.; Kurauchi, T. (1992): Application of laser Raman spectroscopy to the analysis of stress distribution of fibres in composites. Journal of Materials Science Letters 11(6), pp. 365-366.

[51] Larson, B.K.; Drzal, L.T. (1994): Glass fibre sizing/matrix interphase formation in liquid composite moulding: effects on fibre/matrix adhesion and mechanical properties. Composites. 25(7), pp. 711-721.

[52] Thomason, J.L. (1995): The interface region in glass fibre-reinforced epoxy resin composites: 3. Characterization of fibre surface coatings and the interphase. Composites 26(7), pp.487-498.

[53] Berg, J.; Jones, F.R. (1998): The role of sizing resins, coupling agents and their blends on the formation of the interphase in glass fibre composites. Composites Part A: Applied Science and Manufacturing 29(9-10), pp. 1261–1272.

[54] Désarmot, G.; Favre, J.P. (1991): Advances in pull-out testing and data analysis. Composites Science and Technology 42(1-3), pp. 151-187.

[55] Drzal, L.T.; Rich, M.J.; Koenig, M.F.; Lloyd, P.F. (1983): Adhesion of graphite fibers to epoxy matrices: II. The effect of fiber finish. Journal of Adhesion 16(2), pp.133-152.

[56] Bischof, C.; Possart, W. (1983): Adhäsion – Theoretische und experimentelle Grundlagen, Akademie Verlag, Berlin.

[57] Morley, J.G. (2009): Fabrication and Properties of Carbon Fibers. Materials 2(4), pp. 2369-2403.

[58] Morgan, P. (2005): Carbon Fibers and Their Composites, CRC Press,

BocaRaton.

[59] Fitzer, E. (1989): Pan-based carbon fibers – present state and trends of the technology from the viewpoint of possibilities and limits to influence and to control the fiber properties by the process parameters. Carbon 27(5), pp. 621-645.

[60] Ehrenstein, G.W. (2006): Faserverbund-Kunststoffe, Hanser Verlag, München/Wien.

[61] Flemming, M.; Ziegmann, G.; Roth, S. (1995): Faserverbundbauweisen – Fasern und Matrices, Springer Verlag, Berlin/Heidelberg.

[62] Chawla, K.K (2012): Composite Materials. Science and Engineering, Springer Verlag, New York.

[63] Park, S.J. (2015): Carbon Fibers, Springer Dordrecht, Heidelberg.

[64] Dai, Z.; Shi, F.; Zhang, B.; Li, M.; Zhang, Z. (2011): Effect of sizing on carbon fiber surface properties and fibers/epoxy interfacial adhesion. Applied Surface Science 257(15), pp. 6980–6985.

[65] Tong, Y.; Wang, X.; Su, H.; Xu, L. (2011): Oxidation kinetics of polyacrylonitrile-based carbon fibers in air and the effect on their tensile properties. Corrosion Science 53(8), pp. 2484-2488.

[66] Qian, X.; Wang, X.; Ouyang, Q.; Chen, Y.; Yan, Q. (2012): Effect of ammonium-salt solutions on the surface properties of carbon fibers in electrochemical anodic oxidation. Applied Surface Science 259(15), pp. 238–244.

[67] Kozlowski, C. (1984): X-Ray Photoelectron Spectroscopic Studies of Carbon Fibre Surfaces, phD Thesis, Newcastle University, Newcastle, UK.

[68] Sherwood, P.M.A. (1996): Surface Analysis of Carbon and Carbon Fibers for Composites. Journal of Electron Spectroscopy and Related Phenomena 81(3), pp. 319-342.

[69] Viswanathan, H.; Wang, Y.Q., Audi, A.A.; Allen, P.J.; Sherwood, P.M.A. (2001): X-ray Photoelectron Spectroscopic Studies of Carbon Fiber Surfaces. 24. Interfacial Interactions between Polyimide Resin and Electrochemically Oxidized PAN-Based Carbon Fibers. Chemistry of Materials. 13(5), pp. 1647-1655.

[70] Hamann, C.H.; Vielstich, W. (1985): Elektrochemie I. Elektrolytische Leitfähigkeit, Potentiale, Phasengrenzen. VCH Verlagsgesellschaft GmbH, Oldenburg und Bonn.

[71] Yang, Y.; Lin, Z.G. (1995): In situ FTIR characterization of the electrooxidation of glassy carbon electrodes. Journal of applied Electrochemistry 25(3), pp. 259-266.

[72] Weitzsacker, C.L.; Xie, M.; Drzal, L.T. (1997): Using XPS to Investigate Fiber/Matrix Chemical Interactions in Carbon-fiber-reinforced Composites. Surface and Interface Analysis. 25(2), pp. 53-63.

[73] Yumitori, S.; Nakanishi, Y. (1996): Effect of anodic oxidation of coal tar pitch-based carbon fibre on adhesion in epoxy matrix. Part 1. Comparison between H2SO4 and NaOH solutions. Composites Part A: Applied Science and Manufacturing 27(11), pp. 1051–1058.

[74] Yumitori, S.; Nakanishi, Y. (1996): Effect of anodic oxidation of coal tar pitch-based carbon fibre on adhesion in epoxy matrix. Part 2. Comparative study of

three alkaline solutions. Composites Part A: Applied Science and Manufacturing 27(11), pp. 1059–1066.

[75] Gao, S. L.; Mäder, E.; Plonka, R. (2007): Nanostructured coatings of glass fibers: improvement of alkali resistance and mechanical properties. Acta Materialia 55(3), pp. 1043-1052.

[76] Zhang, R. L.; Huang, Y. D.; Liu, L.; Tang, Y. R.; Su, D.; Xu, L. W. (2011): Effect of emulsifier content of sizing agent on the surface of carbon fibres and interface of its composites. Applied surface science 257(8), pp. 3519-3523.

[77] Lesko, J.J.; Swain, R.E.; Cartwright, J.W.; Chin, J.W.; Reifsnider, K.L.; Dillard, D.A.; Wightman, J.P. (1994): Interphases developed from fiber sizings and their chemical-structural relationship to composite performance. The Journal of Adhesion 45(1-4), pp. 43-57.

[78] Xu, L. (2003): Interfacial engineering of the interphase between carbon fibers and vinyl ester resin, PhD Dissertation, Michigan State University, Department of Chemical Engineering and Materials Science, East Lansing, MI, USA.

[79] Broyles, N.S.; Verghese, K.N.E.; Davis, S.V.; Li, H.; Davis, R.M.; Lesko, J.J.; Riffle, J.S. (1998): Fatigue performance of carbon fibre/vinyl ester composites: the effect of two dissimilar polymeric sizing agents. Polymer 39(15), pp. 3417-3424.

[80] Zhang, R.L.; Liu, Y.; Huang, Y.D.; Liu, L. (2013): Effect of particle size and distribution of the sizing agent on the carbon fibers surface and interfacial shear strength (IFSS) of its composites. Applied Surface Science 287, pp. 423-427.

[81] Kim, J.K.; Mai, Y.W.; Mai, Y.W. (1998): Engineered interfaces in fiber reinforced composites, Elsevier Science, Amsterdam.

[82] Kulas, C. (2013): Zum Tragverhalten getränkter textiler Bewehrungselemente für Betonbauteile, Dissertation, RWTH Aachen University, Lehrstuhl und Institut für Massivbau, Aachen.

[83] Raupach, M.; Orlowsky, J.; Büttner, T.; Dilthey, U.; Schleser, M. (2006): Epoxy-impregnated textiles in concrete – load bearing capacity and durability. In: Hegger, J. et. al. (Ed.): Textile Reinforced Concrete. RILEM Publications S.A.R.L., Bagneux, France, pp. 77-88.

[84] Benedix, R. (2008): Bauchemie – Einführung in die Chemie für Bauingenieure und Architekten, Vieweg+Teubner, Wiesbaden.

[85] Schwarz, O.; Ebeling, F.W. (2007): Kunststoffkunde, Vogel Industrie Medien GmbH & Co. KG, Würzburg.

[86] Li, G.; Wang, L.; Leung, C.; Hu, R.; Zhao X.; Yan, B; Zhou, J. (2015): Effect of styrene-butadiene rubber on the electrical properties of carbon black/cement mortar. Royal Society of Chemistry

[87] Elsner, P.; Eyerer, P.; Hirt, T. (2012): Kunststoffe – Eigenschaften und Anwendungen, Springer-Verlag, Berlin/Heidelberg.

[88] Dick, J.S.; Rader, C.P. (2014): Raw Materials Supply Chain for Rubber Products. Overview of the Global Use of Raw Materials, Polymers, Compounding Ingredients, and Chemical Intermediates, Carl Hanser Verlag GmbH & Co. KG, München.

[89] Mortimer, C.E.; Müller, U. (2003): Chemie. Das Basiswissen der Chemie, Thieme, Stuttgart.

[90] Polder, R.B.; Peelen, W.H.A. (2011): Service life aspects of cathodic protection of concrete structures. In: Grantham, M.G. (Ed.): Concrete Repair. A Practical

Guide. Taylor & Francis, Hoboken.

[91] Poltavtseva, M.; Ebell, G.; Mietz, J. (2015): Electrochemical investigations of carbon-based conductive coatings for application as anodes in ICCP systems of reinforced concrete structures. Materials and Corrosion 66(7), pp. 627–634.

[92] Mork, J.H.; Mayer, S.; Rosenbom, K.; Tuveson-Carlström, L.; Sandberg, B. (2006): Cathodic protection of concrete structures with a carbon fibre mesh anode. In: EUROCORR conference, Maastricht, The Netherlands, 25-28 September 2006.

[93] Mork, J.H.; Mayer, S.; Rosenbom, K. (2007): Cathodic protection of reinforcement in concrete. In: EUROCORR conference, Freiburg, Germany, 9-13 September.

[94] Rueffer, M.; Bejan, D.; Bunce, N.J. (2011): Graphite. An active or an inactive anode. Electrochimica Acta 56, pp. 2246–2253.

[95] Chini, M.; Antonsen, R.; Vennesland, Ø.; Mork, J.H.; Arntsen, B. (2008): Polarization Behavior of Carbon Fiber as an Anodic Material in Cathodic Protection. In: 11DBMC International Conference on Durability of Building Materials and Components, Istanbul, 11-14 may 2008.

[96] Chini, M.; Arntsen, B.; Vennesland, Ø.; Mork, J.H.: Electrochemical impedance monitoring of carbon fiber as an anode material in cathodic protection. In: Alexander, M. et al. (Ed.): Concrete Repair, Rehabilitation and Retrofitting II, CRC Press, Boca Raton, pp. 299–300.

[97] van Nguyen, C.; Lambert, P.; Mangat, P.; O'Flaherty, F.; Jones, G. (2012): The Performance of Carbon Fibre Composites as ICCP Anodes for Reinforced Concrete Structures. ISRN Corrosion 2012, pp. 814923(1)- 814923(9).

[98] Bertolini, L.; Bolzoni, F.; Pastore, T.; Pedeferri, P. (2004): Effectiveness of a conductive anode for cathodic protection of steel in concrete. Cement and Concrete Research 43(4), pp. 681-694.

[99] Vennesland, O.; Haug, R.; Mork, J.H. (2006): Cathodic protection of reinforced concrete – a system with woven carbon mesh. In: Alexander, M. et al. (Eds.): Concrete Repair, Rehabilitation and Retrofitting, Taylor and Francis Group, London, UK, pp. 811-815.

[100] Anwar, M.S.; Sujitha, B.; Vedalakshmi, R. (2014): Light-weight cementitious conductive anode for impressed current cathodic protection of steel reinforced concrete application. Construction and Building Materials 71, pp. 167–180.

[101] Chang, J. (2002): A study of the bond degradation of rebar due to cathodic protection current. Cement and Concrete Research 32, pp. 657–663.

[102] Zhang, E; Tang, L. (2014): A Novel Anode Material for Cathodic Prevention of Steel Reinforced Concrete Structures with Hybrid Functions. In: Proceedings of XXII Concrete Research Symposium, Rykjavik, Iceland, 13-15 August 2014 (pp.435–438).

[103] Jing, X.; Wu, Y. (2010): Conductive Mortar as Anode Material for Cathodic Protection of Steel in Concrete. Journal of Wuhan University of Technology-Mater Sci Ed 25(5), pp. 883-888.

[104] Zhu, J.H.; Zhu, M.; Han, N.; Liu, W.; Xing, F. (2014): Electrical and Mechanical Performance of Carbon Fiber-Reinforced Polymer Used as the Impressed Current Anode Material. Materials (Basel, Switzerland) 7(8), pp. 5438–5453.

[105] Zhu, J.H.; Guo, G.; Wei, L.; Zhu, M.; Chen, X. (2016): Dual Function Behavior of Carbon Fiber-Reinforced Polymer in Simulated Pore Solution. Materials

(Basel, Switzerland) 9(2), pp. 103(1)-103(12).

[106] Zhu, J.H.; Wei, L.; Guo, G.; Zhu, A. (2016): Mechanical and Electrochemical Performance of Carbon Fiber Reinforced Polymer in Oxygen Evolution Environment. Polymers 8(11), pp. 393(1)-393(12).

[107] Sun, H.; Memon, S.A.; Gu, Y.; Zhu, M.; Zhu, J.H.; Xing, F. (2016): Degradation of carbon fiber reinforced polymer from cathodic protection process on exposure to NaOH and simulated pore water solutions. Materials and Structures 49(12), pp. 5273–5283.

[108] Chung, D. D. L. (2002): Review Graphite. Journal of Materials Science 37(8), pp.1475–1489.

[109] Eastwood, B.J.; Christensen, P.A.; Armstrong, R.D.; Bates, N.R. (1999): Electrochemical oxidation of a carbon black loaded polymer electrode in aqueous electrolytes. Journal of Solid State Electrochemistry 3(4), pp. 179–186.

[110] Peelen, W.H.A.; Polder, R.B.; Redaelli, E.; Bertolini, L. (2008): Qualitative model of concrete acidification due to cathodic protection. Materials and Corrosion 59(2), pp. 81–89.

[111] Bismarck, A.; Kumru, M.E.; Springer, J.; Simitzis, J. (1999): Surface properties of PAN-based carbon fibers tuned by anodic oxidation in different alkaline electrolyte systems. Applied Surface Science 1999(143), pp. 45–55.

[112] Tang, L.; Zhang, E.Q.; Fu, Y.; Schouenborg, B.; Lindqvist, J.E. (2012): Covercrete with hybrid functions – A novel approach to durable reinforced concrete structures. Materials and Corrosion 63(12), pp. 1119–1126.

[113] Kobayashi, T.; Wu, C. (2005): New cathodic protection system for concrete

structures using nickel-coated carbon fibers sheet anodes. In: 21st US-Japan Bridge Engineering Workshop, Tsukuba, Japan, 3-5 October 2005.

[114] Atkins, P.W.; de Paula, J. (2013): Physikalische Chemie, Wiley-VCH, Weinheim.

[115] Liu, X.; Yang, C.; Lu, Y. (2012): Contrastive study of anodic oxidation on carbon fibers and graphite fibers. Applied Surface Science 258(10), pp. 4268–4275.

[116] Lee-Orantes, F.; Torres-Acosta, A.A.; Martínez-Madrid, M.; López-Cajún, C. (2007): Cathodic Protection in Reinforced Concrete Elements, using Carbon Fibers Base Composites: ECS Transactions. ECS Transactions 3(13), pp. 93–98.

[117] Mietz, J.; Raupach, M. (2015): Untersuchungen zur Anwendbarkeit leitfähiger Beschichtungen auf Karbonbasis für den Einsatz als Fremdstromanode im Kathodischen Korrosionsschutz von Stahlbetonbauteilen, Schlussbericht IGF-Vorhaben 17076 N/1

[118] Martin-Perez, B.; Zibara, H.; Hooton, R.D.; Thomas, M.D.A. (2000): A study of the effect of chloride binding on service life predictions. Cement and Concrete Research 30(8), pp. 1215-1223.

[119] Corrosion of metals and alloys (2015), Basic terms and definitions (ISO 8044)

[120] Deutsches Institut für Normung 82010: DIN ES ISO 15350: 2010-08. Stahl und Eisen, Bestimmung der Gesamtgehalte an Kohlenstoff und Schwefel, Infrarotabsorptionsverfahren nach Verbrennung in einem Induktionsofen

# Development of a Test Method for the Durability of Carbon Textiles Under Anodic Polarisation


**Amir Asgharzadeh and Michael Raupach**

**Abstract** Cathodic protection (CP) is a widely used method to protect steel reinforcements against corrosion. In the course of the last half century, it has been established as a proven method for repairing corrosion-affected reinforced concrete structures, exposed mainly to chlorides. The impressed current anode system for the protection of steel in concrete is already known and applied in practice for more than 30 year. The CP anodes can be embedded in mortar, applied as coating or distinct anode on the repair structure surface. Using CP, the potential of the steel reinforcement is shifted in cathodic direction towards more negative values and consequently the anodic dissolution of iron is suppressed. The current densities on the surface of the reinforcement play a key role in shifting of the potential in cathodic direction. For the anode material nowadays Mixed Metal Oxide coated Titanium (MMO) is often used due to its high durability under anodic polarization. As an alternative anode material, Carbon Textiles embedded in mortar, which provide extraordinary mechanical properties and are also conductive, have already been studied. The results demonstrate that Carbon Textiles are generally suitable as an anode material for CP on reinforced concrete. Deterioration of Carbon is likely to occur in CP systems using carbon as anode material, when critical current densities are exceeded. Therefore the durability of Carbon Textiles at typical CP current densities of less than 20 mA/m$^2$ with respect to concrete surface is considered of special interest.

## 1 Introduction

In the past decade in certain cases Carbon fibres have been used as anode material for CP on steel reinforced concrete. In comparison to conventional anode materials, such as MMO coated titanium, carbon offers several benefits e.g. reduced costs depending on the type of Carbon Textile, flexible installation, structural strengthening or

A. Asgharzadeh (✉) · M. Raupach
Institute of Building Material Research, RWTH Aachen University, Schinkelstrasse 3, 52062 Aachen, Germany
e-mail: Zadeh@ibac.rwth-aachen.de



C. Andrade et al. (eds.), *Service Life and Durability of Reinforced Concrete Structures*, RILEM Bookseries 17, https://doi.org/10.1007/978-3-319-90236-4_11

limitation of crack widths. Beside these benefits, first investigations of various carbon textiles embedded in mortar specimen under laboratory conditions show promising results concerning the performance of carbon textiles as anode material for CP [10].

The use of Carbon reinforced concrete provides many new opportunities for building and construction industries. In comparison to the traditionally used steel rebars, which need a minimum thickness of concrete cover to provide sufficient corrosion protection, carbon reinforced concrete is not susceptible to corrosion. As a result, it can be used to build very thin and light element structures, while still offering high strength, see e.g. Fig. 1.

However, there are still few investigations about the long term durability of carbon when in direct contact with alkaline environments.

In order to investigate the suitability of carbon textiles as anode material for CP, different experiments focussing on the anodic polarisation behaviour of carbon were performed. So far, the exposure conditions of the experiments were limited to aqueous solutions, simulating the alkaline environment of uncarbonated concrete. In a next step, carbon textiles are embedded in mortar specimens to simulate realistic conditions. In addition, the influence of chlorides on the durability of the textiles, as well as on the polarisation behaviour of carbon textiles, will be further investigated.

## 2 Literature Review

According to the Pourbaix diagram (Fig. 2), carbon is a not stable material in the pH range of normal concrete at its own free corrosion potential. Instead, carbon will rather dissolve into substances like carbon acid, carbonate and bicarbonate, or it dissolves into gaseous molecules such as $CO_2$, CO or $CH_4$ [1]. The same products of reaction can occur due to high anodic polarization (cf. Eqs. (1)–(3)).

In the following, results of different authors are reflected, which agree in principle. In 1999, Eastwood et al. [2] presented results about the anodic reaction of carbon


**Fig. 1** Example for a textile concrete structure at the RWTH Aachen

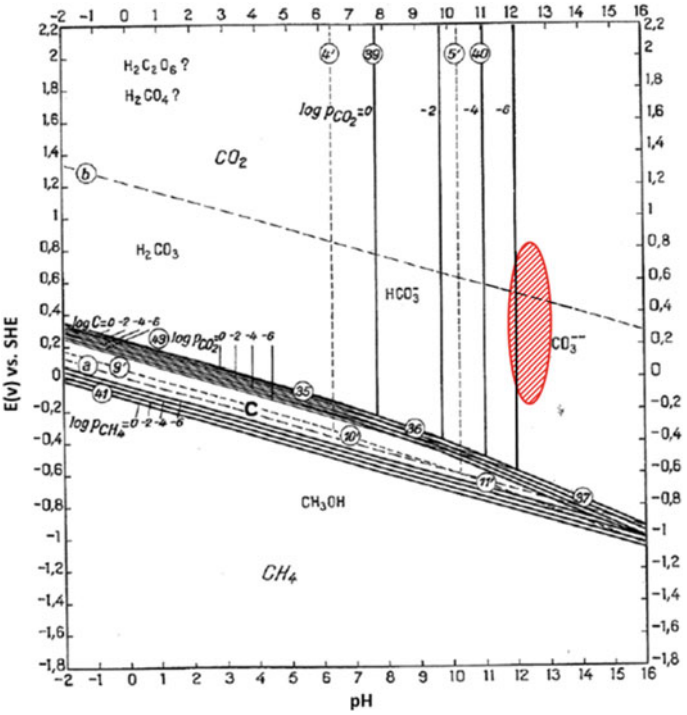


**Fig. 2** Pourbaix diagram of graphite

under the presence of carbonate and bicarbonate. They discovered that the anodic reaction(s) occur at much lower anodic potentials compared to solution with the same pH, but without carbonate or bicarbonate. Their investigations also show, that an increased graphite content of the carbon increases the oxidation resistance. Chini carried out some tests regarding the polarization behaviour of carbon in synthetic alkaline solution with pH 13.2 [1]. The results indicate that carbon shows a passive behaviour up to a polarization of 300 mV versus OCP (Open Circuit Potential).

In the case of more positive potentials, carbon acts as a corrosion active material in concrete structures, even though there is a second passive section above 2500 mV versus SCE (Fig. 3). For low pH values, Maaß, as well as Eastwood et al. defined the critical potential where carbon gets electrochemically oxidised with 207 mV versus NHE in acids [2, 3]. According to [4, 5] the anodic reactions of carbon when exposed to acids can be described as follows:

$$C + 2H_2O \rightarrow CO_2 + 4H^+ + 4e^-, \varphi_{00} = 0,207VNHE \quad (1)$$

$$C + H_2O \rightarrow CO + 2H^+ + 2e^-, \varphi_{00} = 0,518VNHE \quad (2)$$

$$CO + H_2O \rightarrow CO_2 + 2H^+ + 2e^-, \varphi_{00} = -0,103VNHE \quad (3)$$

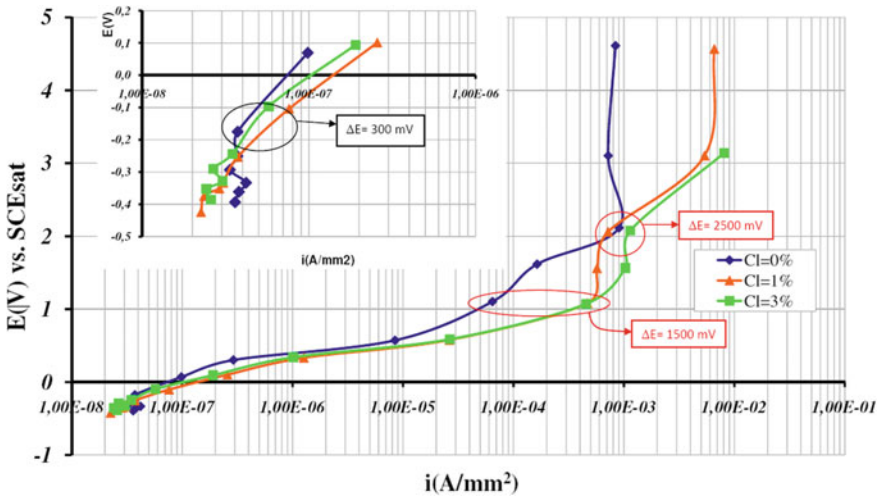


**Fig. 3** Current density-potential-curve for carbon in simulated concrete pore solution with different chloride contents [9]

with:

$\varphi_{00}$ Standard reduction potential of the half-cell reaction at 25 °C, 1013 mbar, pH = 0 (vs NHE)

Since the reaction rate is limited in the range below 207 mV versus NHE due to the kinetics, Maaß stated that the corrosion rates here are very low. Furthermore he described the corrosion rate depending on the applied imposed anodic potential. Corresponding to the Butler–Volmer–Equation, the corrosion rates rise exponentially above the thermodynamic steady-state potential of 203 mV versus NHE [3]:

$$i = i_0\left[\exp\left(\alpha\frac{zF}{RT}\eta_D\right) - \exp\left(-(1-\alpha)\frac{zF}{RT}\eta_D\right)\right] \tag{4}$$

with:

i Current density [A/m$^2$]
$i_0$ Exchange-current-density [A/m$^2$]
α Transfer coefficient [-]
z Number of electrons transferred [-]
F Faraday constant [C/mol]
R Gas constant [J/mol K]
T Absolute temperature [K]
$\eta_D$ Overpotential [V]

Vennesland et al. [6] presented results, which are in conformity with Maaß. By carrying out laboratory experiments they showed, that the electrochemical reactions are changing according to the applied potential. Thus, the potential is one of

the key factors affecting the corrosion rate. They proofed their results by measuring the mass loss of carbon after different levels of sustained anodic polarizations. While the carbon specimen polarized with 2 V versus OCP lost 3% of its mass in 168 h testing, the specimen polarized with 3 V versus OCP lost 44%. However, such deterioration rates would be unacceptable for CP-systems, if used on real concrete structures.

A very important factor concerning the boundary conditions seems to be the chloride content of the concrete structure, as it could affect the pH-value of the pore solution as well as the whole binding behaviour of the concrete. This may, as a consequence, lead to a different electrochemical behaviour of the carbon. Here, Chini discovered ambivalent results. While 1 M.-% of mixed-in chloride results in a higher polarisation resistance, 3 M.-% reduced the polarisation resistance of the specimen [1]. Therefore further investigations should be carried out, to investigate the influence of chlorides on the polarisation behaviour of carbon embedded in concrete.

In addition to the factors above, also the temperature, as well as the quality and humidity of the concrete and it´s chemical composition have to be taken into account, when using carbon as anode material for CP for real concrete structures [1].

Furthermore, Raupach et al. performed some test on a CarboCath® area of a parking construction in 2007. Here, the results showed a significantly higher influence of the temperature on the protective current output than of the reduction of the humidity of the test area, as water is consumed during anodic reactions [7].

Pruckner describes in his work the installation process of a carbon anode system for CP. In view of the previous results, a waterproof sealing has been applied to the carbon anodes, as well as a coating on the concrete surface, to reduce the ingress of chlorides [8].

Despite all the existing concerns, Chini rates carbon as generally suitable for use as an anode material for CP, provided that the polarisation (potential shift) of the carbon will remain less than 300 mV versus OCP. For higher potential shifts, the lifetime can be calculated by estimating the mass loss of the carbon, according to Eqs. (5) and (6) [1].

$$\frac{dW}{dt} = \frac{I_{OX} \cdot W_0}{n \cdot F} \tag{5}$$

$$W = \frac{W_0 \cdot Q}{n \cdot F} \tag{6}$$

W Mass loss per unit of time [kg/s]
$W_0$ Mole mass of carbon [12.01 g/mol]
n Number of the electrons involved in the electrochemical reaction [equiv. $mol^{-1}$]
F Faraday constant [964853 A sol]
$I_{OX}$ Current because of oxidation [A]

Here, the relation between the mass loss of the carbon and the measured electrical current, as well as the Evan's diagram, have been used to calculate the life time of the CP system. Chini has shown that a system will theoretically remain operative for

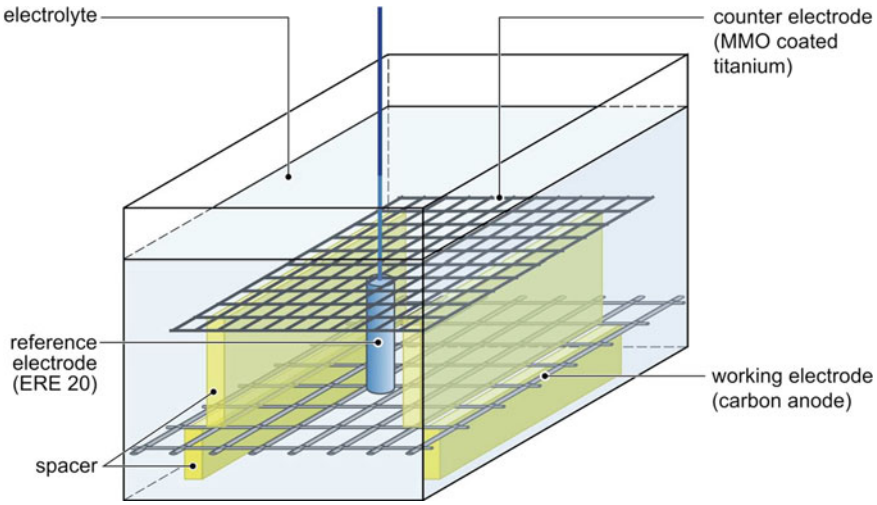


**Fig. 4** Schematical test set-up

more than 50 years, if a potential shift between 500 and 750 mV versus SCE is used, which are common values in practice. However, it is important to notice that Chini has only tested the longitudinal properties of the carbon fibers whereas the durability of carbon as textile mesh has not yet been clarified [9].

## 3 Experimental Program

### *3.1 General Set-up*

Before the durability of carbon textiles embedded in mortar specimen will be tested, basic investigations on Carbon Textiles in synthetic concrete pore solutions were performed. Preliminary pre-tests were executed in order to determine the relevant influencing factors to the measurement results. Figure 4 shows the test set-up for both pre- and main tests in synthetic pore solution schematically.

In order to perform electrochemical investigations an electrochemical cell has been designed. While carbon mesh acts as the working electrode, titanium mesh is used for the counter electrode. Both electrodes are completely immersed in electrolyte solution. In addition a reference electrode is installed to measure the electrode potential of the working electrode. Non-conductive polymer spacers were used to maintain a constant distance between the working and the counter electrode.

### 3.2 Materials

Table 1 shows the investigated carbon textile as well as other materials that were needed for the Potentiodynamic experiment.

### 3.3 Specimen Preparation

For the preparation of the working electrodes, carbon textile mesh was cut into pieces with dimensions of 10.5 cm × 5 cm. The electrical connection with the carbon textile was enabled through the use of wire ferrules. A special resin on epoxy basis has been used for the sealing and to eliminate the corrosion of the wire. Figure 5 shows the stepwise preparation of the cable connection and the working electrode.

For the counter electrode MMO coated titanium mesh was cut into elements with similar dimensions as the carbon working electrode. The electrical connection with the mesh cathode was ensured using luster terminals. Spacers were used to maintain the distance between the working and counter electrode as well as to position the reference electrode. Finally the three-electrode cell arrangement was placed in a container having a horizontal cross section of about 15 cm × 8 cm. 630 mg saturated calcium hydroxide solution was required to ensure total covering of the cell arrangement. Figure 6 shows the completed three-electrode-cell. A total number of 24 cell arrangements were prepared in order to investigate the relevant influencing factors (see Table 2).

**Table 1** Materials used for electrochemical tests

| Element | Material |
|---|---|
| Working electrode | styrene-butadiene-rubber impregnated Carbon Textile roving distance 20 mm in both directions |
| Counter electrode | MMO coated titanium |
| Reference electrode | ERE 20, $MnO_2$ |
| Electrolyte solution | Saturated $Ca(OH)_2$<br>Saturated $Ca(OH)_2$ + 3% NaCl |
| Spacer | Non-conducting synthetic material from PVC |

### 3.4 Testing Program

The Pre-tests were carried out to determine which factors for this test set-up will have a significant influence on the measurement results. Table 2 provides an overview of the factors which were investigated in particular.

The sealing of the roving-tips was achieved by an epoxy-based resin. Figure 7 shows the roving with unsealed as well as with sealed tips.

### 3.5 Test Procedure

The same measuring cycle was applied for all 24 cell arrangements. The test procedure was implemented as follows:

A Gamry G300 potentiostat in combination with $MnO_2$-based reference electrodes (type ERE-20) were used for the measurements. First of all, the Open circuit

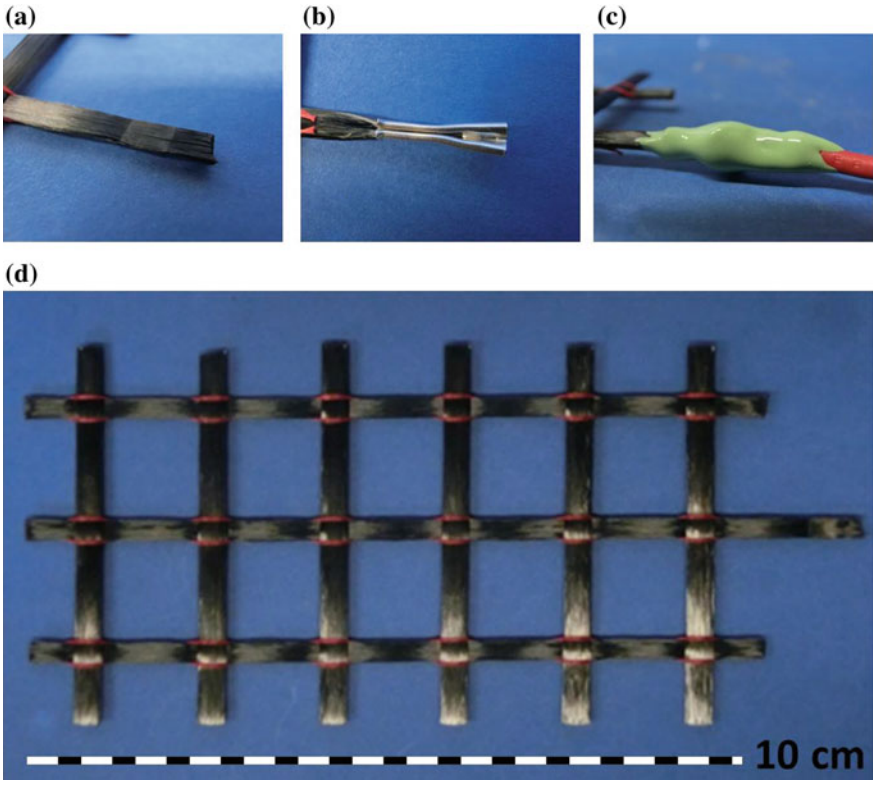


**Fig. 5** Preparation of cable connection and working electrode

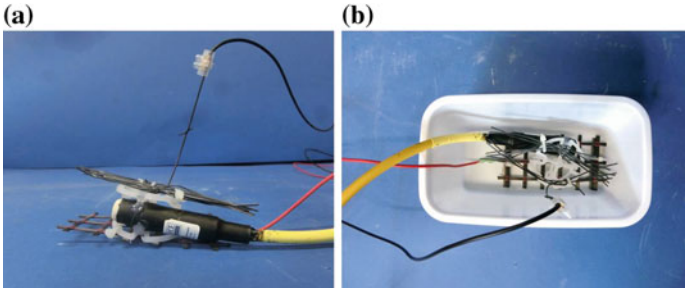


**Fig. 6** Completed three-electrode-cell

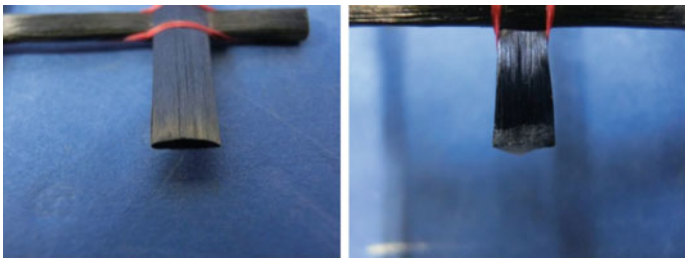

**Fig. 7** Unsealed and sealed roving-tip

**Table 2** Shows the factor which were investigated in particular

| Influencing Factor | Variations | Sample description |
|---|---|---|
| Specimen orientation (Figs. 8 and 9) | • Vertical position<br>• Horizontal position | • NV_S_Ca_1/2<br>• NV_L_Ca_1/2 |
| Sealing of roving-tips (Fig. 7) | • Sealed<br>• Unsealed | • V_L_Ca_1/2<br>• NV_L_Ca_1/2 |
| Electrolyte solution | • Saturated $Ca(OH)_2$<br>• Saturated $Ca(OH)_2$ + 3% NaCl | • NV_S_Ca_1/2<br>• NV_S_Ca + 3Cl_1/2 |
| Storing of specimens | • Exposure to solution 24 h before test procedure<br>• No pre-exposure to solution | • NV_L_Ca_24_1/2<br>• NV_L_Ca_1/2 |
| Homogenization-level of solution | • Permanent stirring of solution<br>• Solution without motion | • NV_S_Ca_G_1/2<br>• NV_S_Ca_NG_1/2 |

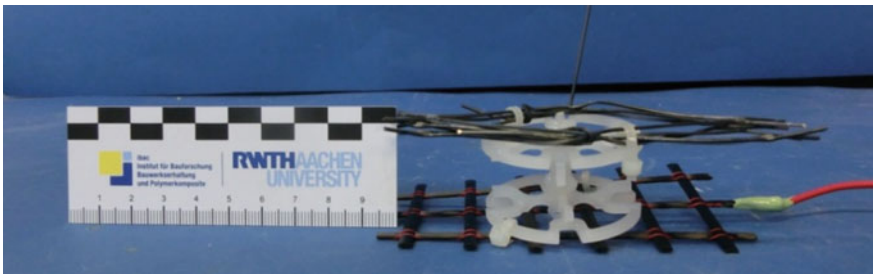


**Fig. 8** Side view of a prefabricated cell arrangement

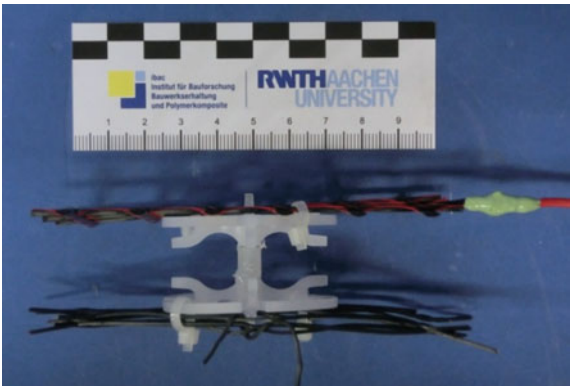


**Fig. 9** Top view of a prefabricated cell arrangement

potential (OCP) was measured as an indication for the free corrosion state. For this purpose data points were recorded every five seconds over a total duration of 200 s. Subsequently potentiodynamic polarization with constantly increasing electrical potential was carried out. Starting with the open circuit potential, the applied potential was increased at a constant rate of 0,033 mV per second until an overall potential shift of 2000 mV was achieved. Hence, this resulted in a test duration of approximately 18 h. Automatic data collection took place every 300 s. Finally Instant-off potential measurements were performed to ensure that IR-drop compensated potentials were measured. Overrating of the actual polarization of the anode material can thus be avoided.

Following this anodic polarization, the obtained results were plotted with current-density versus (compensated) potential in order to evaluate the performed tests. The compensated potential can be calculated according to Ohm's law (Eqs. 7 and 8) as follows:

$$U_{compensated} = U_{measured} - \Delta U_{IR} \tag{7}$$

$$\Delta U_{IR} = R \cdot I \tag{8}$$

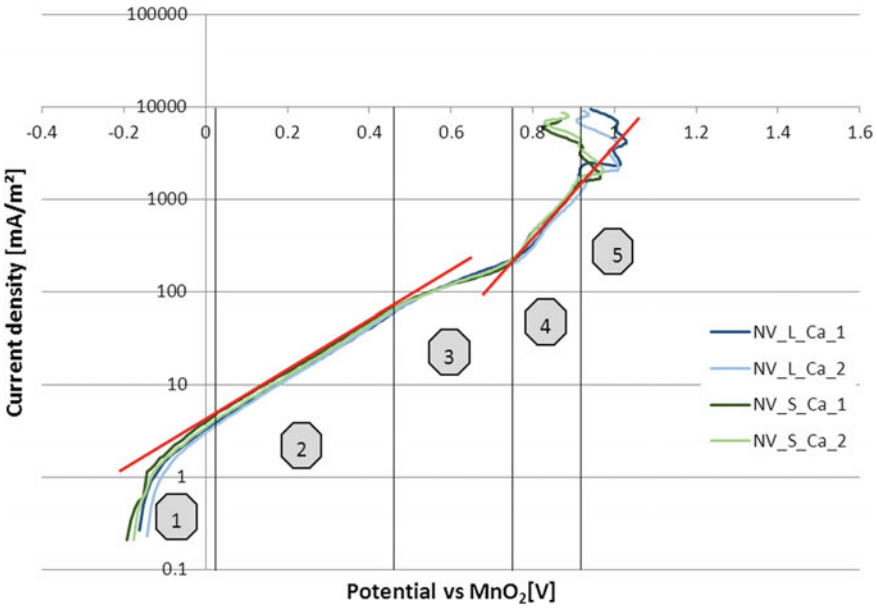


**Fig. 10** Influence of specimen orientation

Substracting the voltage ($\Delta U_{IR}$) resulting from the IR-drop ensures that the actual net polarization of the anode material is taken into account.

## 4 Test Results

For each influencing factor two identical cell arrangements were investigated and the results were compared to their counterparts. Figures 10, 11, 12, 13 and 14 show the test results obtained for both cell arrangements. Note that the current density in the graphs is plotted on a logarithmic scale.

All measured curves show similar typical characteristics, which can be divided into five phases:

1. OCP to Tafel area 1
2. Tafel area 1
3. Transition area
4. Tafel area 2
5. Above Tafel area 2

It should be noted, that for CP-systems in reinforced concrete structures the current density is typically not higher than around 20 mA/m$^2$ with respect to the concrete surface area. This means, that only phases 1 and 2 are of practical interest.

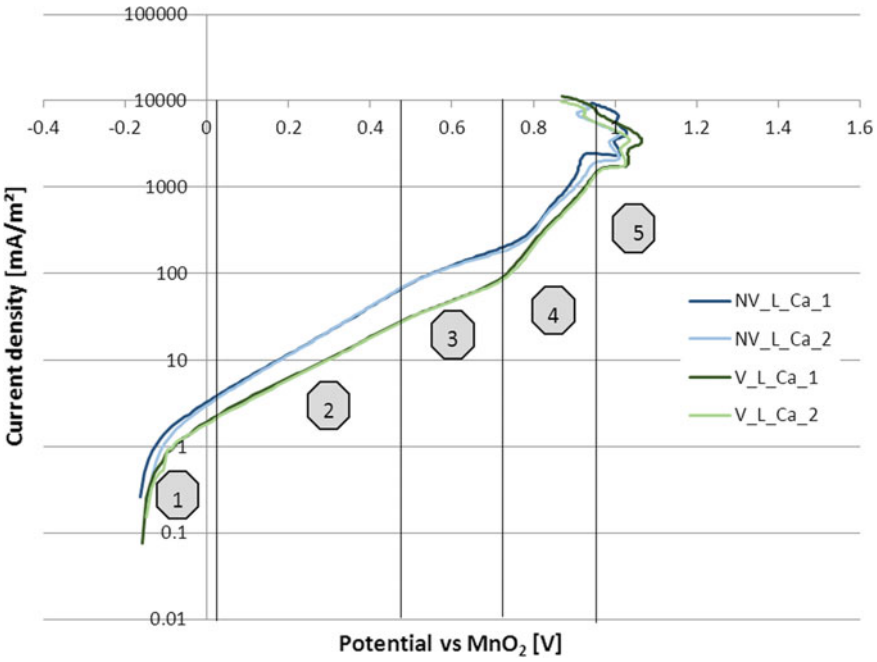


**Fig. 11** Influence of sealing of specimen-tips

Figure 10 visualizes the influence of the orientation of the cell arrangement. Since all curves show a very good agreement, the position of the cell arrangements obviously has no significant influence on the measurement results. Conversely, the sealing of roving tips, the storing of the cell arrangements and the homogenization level of electrolyte solution show significant influences on the test results as will be described in the following.

Figure 11 shows the current-density potential curves for the influencing factor *sealing of roving-tips.* A significant gap between the development of the curve for cell arrangements with sealed tips on the one hand (V_L_Ca_1 and V_L_Ca_2) and for cell arrangements without sealed tips (NV_L_Ca_1 and NV_L_Ca_2) on the other hand can be observed. If the same potential is imposed, cell arrangements with no sealing of roving-tips allow a significantly higher current density than cell arrangements with sealed roving-tips. Thus sealing of roving-tips strongly influences the test results, because the sealing of roving tips prevents the passage of electrical current into solution.

Similarly the difference in storing of cell arrangements shows significant effects on the measurement results, as can be seen in Fig. 12. Pre-exposure to electrolyte solution 24 h before the polarization test-procedure leads to an increased current flow during the electrochemical investigations.

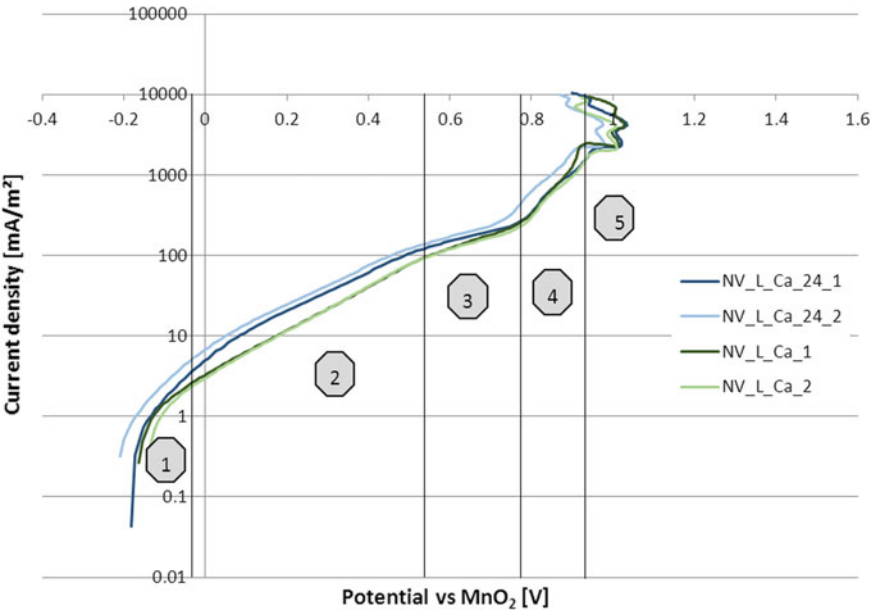


**Fig. 12** Influence of specimen storing

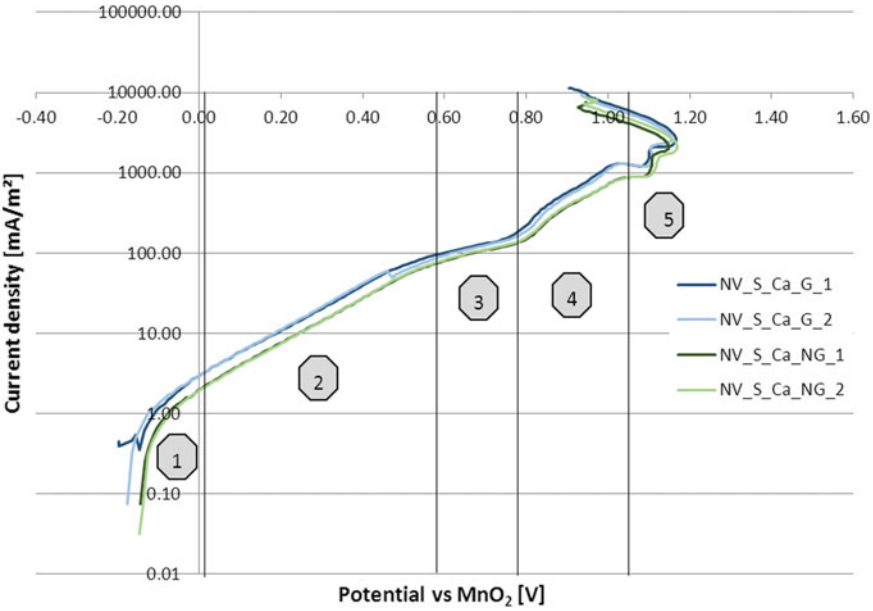


**Fig. 13** Influence of homogenization-level of electrolyte solution

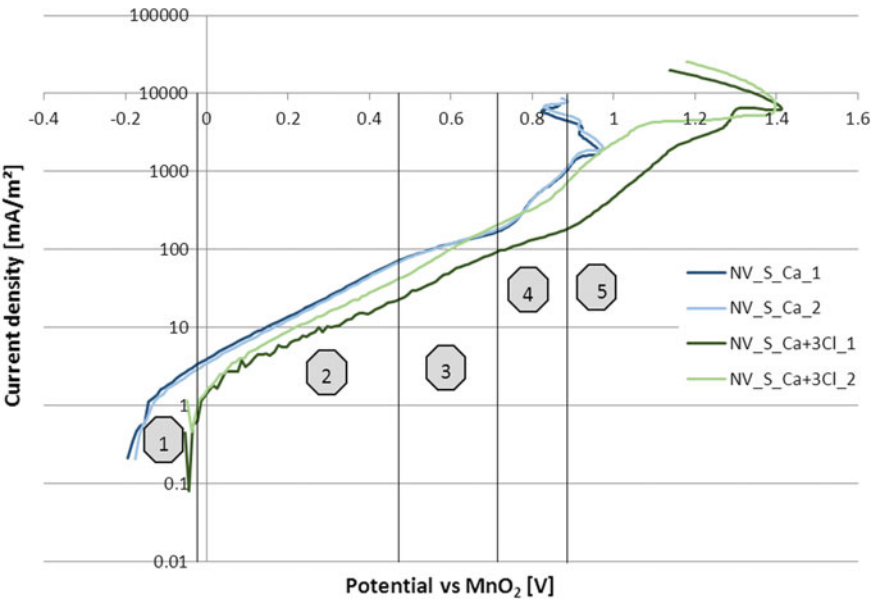


**Fig. 14** Influence of electrolyte solution

Figure 13 shows the current-density potential curve with variations concerning the homogenization level of the electrolyte solution. The stirring of the solution shows an impact on the development of the polarization curve as well. The approximation of the curve representing specimen NV_S_Ca_G_2 to the curves representing the specimens in unstirred solution (NV_S_Ca_NG_1 and NV_S_Ca_NG_2) can be explained by the technical impact of the stirring process.

The influence of the electrolyte solution, which is presented in Fig. 14 has to be investigated in further tests since the data obtained from these tests does not have sufficient validity.

Table 3 summarizes the results of the pre-tests. In order to qualify the influence as being significant, a potential criterion was established: A potential shift of more than 50 mV at a current density of 20 mA/m$^2$ was graded as a significant change.

## 5 Conclusions and Outlook

A test method has been developed to investigate the durability of Carbon Textiles under anodic polarization. In a first test series the influence of relevant factors regarding the testing procedure in a simulated concrete pore solution has been examined. For the main experiments the following factors are taken into account:

- Horizontal position of the carbon mesh

**Table 3** Summary of the pre-test results

| Influencing factor | Variations | Significant influence |
|---|---|---|
| Specimen orientation | • Vertical position<br>• Horizontal position | No |
| Tips of carbon rovings | • Sealed<br>• Unsealed | Yes |
| Electrolyte solution | • $Ca(OH)_2$<br>• $Ca(OH)_2$ + 3% NaCl | To be investigated |
| Storing of specimens | • Exposure to solution 24 h before test procedure<br>• No pre-exposure to solution | Yes |
| Homogenization-level of solution | • Permanent stirring of solution<br>• Solution without motion | Yes |

- Sealed tips of the carbon roving
- Storing of the cell arrangement 24 h before test procedure starting
- Permanent stirring of exposure solution.

Looking at the anodic polarization curves obtained for the carbon mesh, two different sections can be detected at each curve. The two different slopes indicate a different electrochemical reaction of carbon in each of these two potential regions. These different slopes have to be considered in more detail in a future work.

After evaluation of the main test series in simulated concrete pore solution Carbon Textiles will be applied to concrete specimens by casting them into cement-based mortar. Then, long-time experiments will be carried out in order to finally gain information on the long-term durability as anode material for CP. The objective for such long-term experiments is to find out how the durability of carbon under real operating conditions will develop over time.

## References

1. Chini M, Antonsen R, Vennesland, Ø, Arntsen B, Mork JH (2013) A review of utilization of carbon fibres as an anodic material in cathodic protection. In: International RILEM workshop on integral service life modelling of concrete structures, p 395–402
2. Eastwood BJ, Christensen PA, Armstrong RD, Bates NR (1999) Electrochemical oxidation of a carbon. Black loaded polymer electrode in aqueous electrolytes. Journal of Solid State Electrochemistry 3(4):179–186

3. Maaß S (2007) Langzeitstabilität der Kathoden-Katalysatorenschicht in Polymerelektrolyt-Brennstoffzellen. Dissertation, Institut für Chemische Verfahrenstechnik der Universität Stuttgart, Göttingen (in German)
4. Pourbaix M (1974) Atlas of electrochemical equilibria in aqueous solutions. Nat. Assoc. of Corrosion Engineers, Houston, Texas, Chapter IV, 17.1
5. Kinoshita K (1988) Carbon, electrochemical and physicochemical properties. Wiley & Sons, New York
6. Vennesland Ø, Haug R, Mork JH (2005) Cathodic protection of reinforced concrete—a system with woven carbon mesh. In: International conference on concrete repair, rehabilitation and retrofitting (ICCRRR), Cape Town, South Africa
7. Raupach M, Bruns M, Wolff L (2007) Installation and investigation of a field test area with the carbo cath CP-System and different surface coatings at the parking Garage Scheibenstrasse in Düsseldorf. Aachen, Germany
8. Pruckner F (2006) New anode for cathodic protection of car parks. Concr Eng Int 10(1):54–57
9. Mork JH, Mayer S, Rosebom K, Tuveson-Carlstrom L, Sederholm B, Sandberg B (2006) Cathodic protection of concrete structure with a carbon fibre mesh anode. In: EUROCORR 2006, Maastricht
10. Chini Mahdi (2010) Pan-based carbon fibre as anode material in cathodic protection systems for concrete structures. Doctoral Thesis, Faculty of Engineering Science and Technology, Department of Structural Engineering of the Norwegian University of Science and Technology
11. Asgharzadeh A, Raupach M, Koch D (2015) Investigations on the suitability of technical textiles for cathodic corrosion protection: Untersuchung zur Eignung von technischen Textilien für den kathodischen Korrosionsschutz. In: Proceedings of the 4th International Conference on Concrete Repair, Rehabilitation and Retrofitting (ICCRRR), Leipzig, Germany

Received: 9 February 2018 | Accepted: 14 August 2018
DOI: 10.1002/maco.201810098

ARTICLE

Materials and Corrosion

# Durability behavior of polymer impregnated carbon textiles in alkaline solution as CP anode

**Amir Asgharzadeh** | **Michael Raupach**

Institute of Building Materials Research, RWTH-Aachen University, Schinkelstrasse 3, Aachen 52062, Germany

**Correspondence**
Amir Asgharzadeha, Institute of Building Materials Research, RWTH-Aachen University, Schinkelstrasse 3, Aachen 52062, Germany.
Email: zadeh@ibac.rwth-aachen.de

Cathodic corrosion protection (CP) is a cost-effective option for maintenance of concrete structures. CP is an electrochemical method that can be used to reduce the corrosion rate to an acceptable level. Thus, service life of reinforced concrete can be increased considerably. In this work, carbon textiles with varying polymer impregnations, cross sections, and mesh widths have been used as CP anodes and have been tested for their durability. The main goal of this research is to determine the behavior of carbon textile under permanent anodic polarization while stored in saturated calcium hydroxide solution. The outcome will serve as a basis for further investigations in which textiles will be permanently polarized and tested after embedding in mortar.

**KEYWORDS**
anodic dissolution, cathodic protection, potentiostatic, steel reinforced concrete, weight loss

## 1 | INTRODUCTION

Corrosion of steel in concrete raises major concerns. Decreasing stability of affected buildings endangers public safety. To provide the required safety, maintenance work is essential but poses considerable economic problems for the owners of such buildings as well as the construction industry. In many cases the method of cathodic corrosion protection (CP) of reinforced concrete components is a cost-effective option and has become more and more important in the last decades. The main purpose of CP is the reduction of corrosion to an acceptable level. For the implementation, the potential of the reinforcement is shifted in cathodic direction by introducing an external current via embedded or surface-mounted anodes. CP is an effective approach for the treatment of reinforced concrete structures, which are attached or already damaged by chlorides. Figure 1 shows the principle of CP using an impressed current anode. The reinforcement is exposed to an external current via direct current source using an embedded insoluble anode.[1]

Textile reinforced concrete, consisting of technical textiles (in particular carbon fibers, but also basalt- and AR-glas fibers) and a concrete matrix is already used in practice in the course of repair measures as well as for strengthening of building surfaces.[2]

Usually, the reinforcement of textile reinforced concrete consists of thousands of single filaments which are bundled into rovings. In particular carbon fibers are used as reinforcement material, due to their outstanding mechanical properties (tensile strength and elastic modulus). Before carbon fibers are combined to rovings, each fiber is coated by a mixture of various chemicals (sizing). To improve adhesion and handling for further application, carbon rovings are again impregnated. In practice, mainly epoxy resin or styrene-butadiene rubber (SBR) based coatings are used for impregnation. Generally, epoxy resins result from the mixture of a base resin and a hardener component, while the SBR-based coating is an aqueous dispersion consisting of rubbery butadiene particles and polystyrene. General statements about exact compositions can not be given due to security issues of the producers.[3]

  

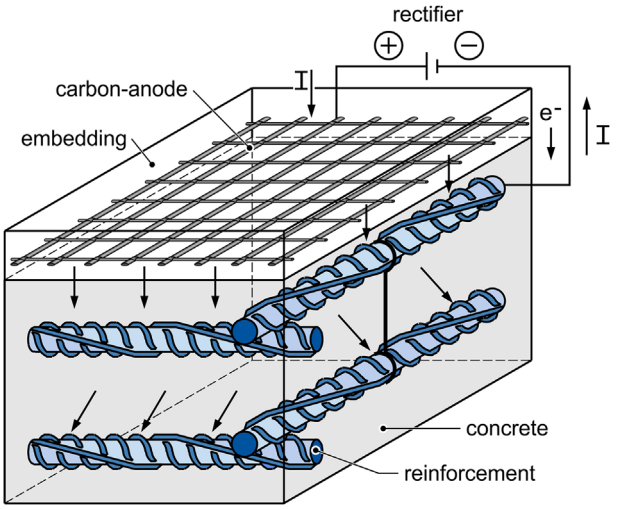


**FIGURE 1** Priciple of cathodic corrosion protection with carbon textile anode. [Color figure can be viewed at wileyonlinelibrary.com]

In recent times, carbon fibers are also used as anode materials in cathodic corrosion protection systems, since they additionally exhibit good electrical characteristics. However, experience concerning their durability is rare and extensive research is required.

In Ref. [4] the reasons for the use of carbon textile as a CP-anode and its advantages are explained in detail. Here, relevant factors, regarding the testing procedure in a simulated concrete pore solution have been examined.

It was noted, that carbon can oxidize in high-pH solutions under polarization with high anodic potentials to carbon dioxide and carbonate or bicarbonate.[5] Temperature, humidity, concrete quality, and especially the chemical composition of the concrete pore solution can influence the electrochemical properties of the carbon embedded in concrete. In a synthetic pore solution (pH 13.2) carbon does not show any corrosion phenomena up to an anodic potential of 300 mV corresponding to −108 mV versus SCE.[6] Beyond this level it is active (in concrete as well as in concrete pore solution). Chini has shown that the presence of chlorides increases the corrosion rate of carbon. He concluded that carbon is generally suitable as CP-anode if the potential does not exceed 300 mV. The life expectancy has been calculated on the basis of the mass loss of the carbon network.[6]

Chini et al.[7] have attempted to investigate the long-term stability of carbon under anodic polarization. Applied potential between 1000 and 6000 mV were used to assess the carbon behavior. The tests were carried out on an area of 11 $m^2$ on the Oland Bridge in Sweden. The driving voltage has been identified as the decisive parameter for the control of the dismantling processes. For example, there was a mass loss of 3% after 168 h at an anodic polarization of 2000 mV (not IR-compensated) and a loss of 44% at 3000 mV. No defects were found below anodic polarization of 1800 mV polarizations. After a polarization of 3 years with a protection current density of 1–2 mA/$m^2$ they have found that the 100 mV criterion was fulfilled.

Van Nguyen et al.[8] have applied carbon fiber anodes as rods and textile on already corroding steel reinforced concrete beams and used them as CP-anodes. The DC voltages between 5000 and 20 000 mV were applied and observed for 7 days. They have found that the current flow between the anode and the reinforcement decreases significantly over time. The reason for this has been identified as the dissolution of the carbon fiber anode. A weight loss of 0.33–0.56% was found in the rod and between 0.66 and 2.69% in the fabric, which was judged to be relatively low. They have rated the durability of carbon as a CP-anode as possibly problematic. The investigation in calcium hydroxide solution with applied current of 10 mA has shown that no damage to the carbon is observed at the rod at anodic current densities up to 64 mA/$m^2$ of steel area and with the fabric up to 128 mA/$m^2$ of steel area.

Zhang et al.[9] carried out an accelerated procedure by significantly increasing the current density. Thereby, life expectancy of carbon has been estimated depending on the current density. The procedure is based on the following linear model:

$$\Phi = i_{\text{applied}} \cdot t_{\text{applied}} = i_e \cdot t_e$$

$$t_e = \frac{i_{\text{applied}}}{i_e} \cdot t_{\text{applied}} \quad (1)$$

where Φ is polarization parameter according to Chang[10] (Coulomb/$m^2$). $i_{\text{applied}}$ is applied current density. $t_{\text{applied}}$ is test duration. $i_e$ is current density for CP (between 0,2 and 20 mA/$m^2$; here 2 mA/$m^2$), and $t_e$ is estimated life expectancy.

For the investigations concerning life expectancy specimens were produced consisting of two single rovings, which were stored in calcium hydroxide solution as well as carbon fabrics, which were embedded in mortar. During the tests, very high current densities were applied in order to induce damages. The applied current densities varied between 800 and 4615 mA/$m^2$ of steel area for the specimens which were stored in solution and 4777 mA/$m^2$ of steel area for the specimens which were embedded in the first mortar. After test duration of 60 days for solution and 30/60 days for first mortar specimens, the carbon was separated from its environment and optically analyzed. With this method damages could be reliably determined. However, the study concluded that carbon fibers are suitable for CP. The life expectancy of carbon as anode material in CP-systems was estimated to last over 100 years.

Eastwood et al.[11] describe, that the reactions in the alkaline environment are more complex than in the acidic

medium. Here, the high concentration of hydroxyl ions causes the formation of oxygen and less of carbon dioxide, especially at low anodic potentials. Above a pH of 9, the formation of oxygen is even catalyzed by the presence of carbonate ions in the electrolyte.[12] At the same time, the accumulation of oxygen always causes the formation of humic acid in the solution.[13] Studies show that increasing the graphite content of the carbon causes its resistance to oxidation to carbon dioxide.[14] In alkaline solutions (pH between 11 and 13) at high current densities, carbon dioxide accumulation prevails and at low current densities oxygen enrichment prevails.[11]

Pruckner[15] applied conductive coating as strips over and between the primary anode wires, which were fixed in concrete before. Conductive coating is from binder and carbon pigmentation and is both electrically conductive. Only low protection current is needed to achieve average current densities at low polarizations. The measurements showed that the corrosion rate of reinforcement after repair over a period of 4 years was only 1% compared to the pre-repair corrosion rate.

According to the Pourbaix diagram of carbon in water (Figure 7), carbon is not chemically stable under anodic polarization, especially in alkaline media. Even at low anodic potentials corrosion of carbon is indicated, actually disabling carbon as suitable anode for CP systems.[5] However, a direct transfer of the Purbaix diagram to the question of suitability of carbon fibers for CP is not possible. Several restrictions must be considered. Firstly, the Pourbaix diagram is only valid for pure carbon in aqueous solution. In the case of cathodic protection pure carbon is not applied as anode material, but a carbon fiber composite. Carbon fibers are always coated with sizing and often additionally impregnated with SBR-based material or epoxy resin. In addition, the Pourbaix diagram by its thermodynamic nature provides no information on corrosion rates. It is possible that limited corrosion rates might be tolerated in the case of CP. In the Pourbaix diagrams, the pH value at the contact surface between solution and carbon is considered as influencing factor of the carbon's stability. However, it does not take the process of acidification at the anode's surface into account, which is a general and commonly reported issue[8,9,16–20] leading to locally strongly acidic conditions.

Taking these aspects into account, further considerations are required to the discussion of the Pourbaix diagram to evaluate the suitability of carbon as sufficiently durable CP-anode in practice.

Dissolution of graphite was observed in Rueffer et al.[21] Actual decomposition of the carbon fiber has been demonstrated in Yumitori and Nakanishi[22] and Bismarck and Kumru.[23] According to the investigations published in Ref. [6] a decomposition of the carbon fiber is possible, but a degradation of the polymer-based sizing more likely.

The Pourbaix diagram, the underlying equations and a number of previous works show that critical potentials exist.[5] The service life of carbon anodes previously predicted on the basis of simple models is promising.[6,9,24] However, further investigations must be carried out in order to determine the potentials and current densities which lead to the lowest possible degradation rates of the carbon anodes, but nevertheless ensure sufficient protection of the structure.

In previous works[4] different sections regarding the current density-potential curves of carbon meshes under anodic polarization have been detected. Different slopes, which indicate different electrochemical reactions of carbon, depending on the potential regions aroused interest. These findings are further investigated in the present work. Studies have been performed with both styrene-butadiene-rubber and epoxy impregnated textiles.

## 2 | EXPERIMENTAL

### 2.1 | Materials and methods

The experiments on the durability of carbon textiles as a CP anode are divided into three steps. The first series of experiments was carried out for the determination of the influencing parameters on the anodic polarization of carbon textile and results were published in Asgharzadeh and Raupach.[4] The main parameters have been used to investigate the durability of carbon textiles as a CP anode. Carbon textiles were permanently polarized while stored in calcium hydroxide solution. As a last step, permanent anodic polarization of carbon textile will be investigated in mortar.

This paper contains the potentiodynamic experiments to determine the current density-potential curve. On the basis of the results, interesting areas were identified and potentiostatic test experiments were carried out in saturated calcium hydroxide solution. After different anodic polarizations the solution was analyzed to identify the carbon content. Furthermore SEM investigations have been carried out. With this investigation it was possible to identify critical potentials regarding the destruction of polymer impregnated carbon textiles and the damage mechanisms in saturated calcium hydroxide solution.

### 2.2 | Current density-potential curves in calcium hydroxide solution

#### 2.2.1 | Specimen preparation

In consequence of the preparatory pre-test results,[4] several modifications were implemented to reduce external effects. As the specimen orientation had no influence on the measurement results, a horizontal position was chosen, due to handling advantages.

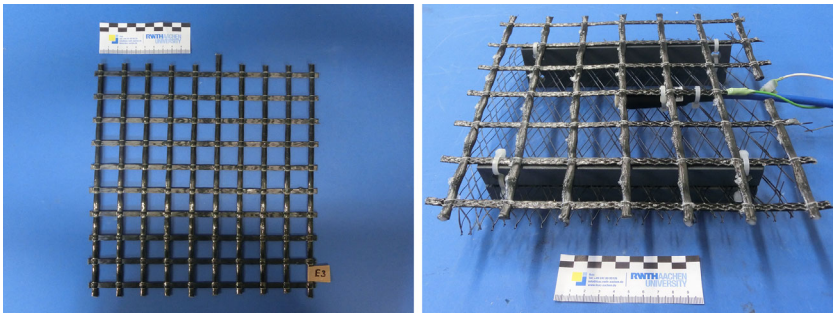

**FIGURE 2** Carbon textile and test setup. [Color figure can be viewed at wileyonlinelibrary.com]

The dimensions of the textiles were increased to 25 × 25 cm. With a total height of the specimen structure including spacer, carbon textile, another spacer, and mixed metal oxides (MMO) coated titanium mesh (bottom to top) of around 6 cm, 8 L of saturated calcium hydroxide solution were necessary to ensure an adequate covering. All textiles were stored in saturated calcium hydroxide solution for 24 h before test procedure.

To keep the saturated calcium hydroxide solution as homogenous as possible paddle stirrers were added to continuously blend the solution and reduce deposition of calcium hydroxide. As paddle stirrer material, polytetrafluorethylene (PTFE) was used.

The dimensions of the textiles as well as the test set-up can be seen in Figure 2.

### 2.2.2 | Test variations

In comparison to the pre-tests, the main tests now focused on the variation of textile dimensions as well as on textile impregnation/coating material. In addition to SBR-based coating, epoxy impregnated textiles were investigated. The mesh-sizes and the roving cross-sections were varied, as shown in Table 1. In addition, the current density-potential relationship of pure graphite was also determined in the solution and compared with other two materials.

### 2.2.3 | Test Procedure

First of all, the open circuit potential (OCP) was measured as an indication for the free corrosion state. Subsequently anodic potentiodynamic polarization was carried out. Starting with the open circuit potential, the applied potential was increased at a constant rate of 2 mV/min until an overall potential shift of 2200 mV in the anodic direction was achieved. Finally Instant-off potential measurements were performed to ensure that IR-drop compensated potentials were calculated. Overrating of the actual anodic polarization of the anode material can thus be avoided.

Following this anodic polarization, the obtained results were plotted as current–density versus (compensated) potential curves. Selected examples of the results are shown in Figure 3.

For comparability, measured potentials were converted to the normal hydrogen electrode (NHE). The real potentials of the $MnO_2$-electrodes itself according to manufacturer information have been considered and potentials shifted accordingly in order to obtain comparable results.

**TABLE 1** Specimen specifications

| Specimen specification | Impregnation/coating material | Mesh size (mm/mm) 0°/90° | Cross-sectional area ($mm^2$/m) 0°/90° |
|---|---|---|---|
| E1 | Epoxy | 21/21 | 85/85 |
| E2 | Epoxy | 38/38 | 95/95 |
| E3 | Epoxy | 25/25 | 142/142 |
| E4 | Epoxy | 38/38 | 142/142 |
| S1 | SBR-based | 21/21 | 85/85 |
| S2 | SBR-based | 38/38 | 95/95 |
| S3 | SBR-based | 25/25 | 142/142 |
| S4 | SBR-based | 38/38 | 142/142 |
| UG | Unimpregnated | – | – |

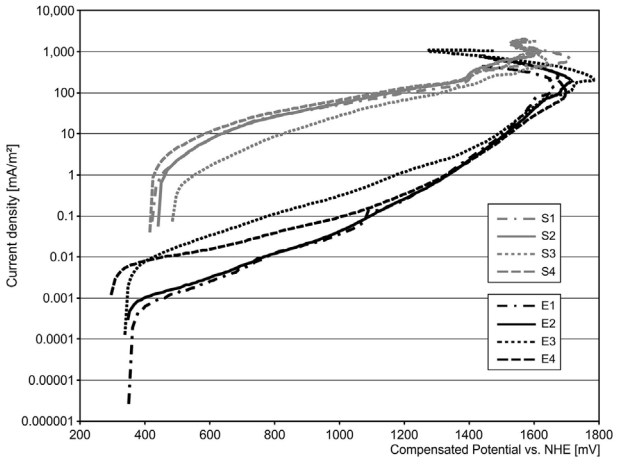


**FIGURE 3** Current density-potential graph of carbon textiles with SBR-based coating (S1–S4) and epoxy impregnation (E1–E4)

It can also be clearly seen from the curves of all materials that the potential value strikes back at very high current densities. This is contradictory to what is expected in the potentiodynamic experiment. This effect is discussed in section 4.1.

With respect to these curves, three potentials were selected at S4, which were chosen on the interesting points that can give information about the possible dissolution of the carbon or destruction of the impregnation material. Potentiostatic tests were performed at these potentials. Thereafter, the solution was examined for the carbon content and also the surface of the carbon examined by means of SEM.

## 2.3 | Loss of carbon after polarization tests

In order to eliminate possible influences of carbonation of the solution and analyze the carbon content in the solution, tests were carried out within protective atmosphere. Therefore the containers were additionally filled with argon and sealed with tape. Textiles coated with SBR-based material were used as anode material. S4 was chosen because of its prior results of the polarization tests. Detailed specimen specification can be seen in Table 1.

### 2.3.1 | Specimen preparation

In order to increase the surface of the working electrode a second layer was added to the carbon specimen (Figure 4). The dimensions of the textiles were about $10.5 \times 10.5$ cm. Spacers were installed to keep the electrodes in position. "ERE20" were used as reference electrodes, while MMO coated titanium mesh was still used as counter electrode.

### 2.3.2 | Test Procedure and results

Potentiodynamic tests starting with the open circuit potential to 2200 mV were carried out. Results were plotted in a current-density against (compensated) potential curve.

For further examination of the phenomenon, characteristic potentials P1, P2, and P3 were chosen (Figure 5). Based on these data, further potentiostatic tests were performed with new specimens. Thereby, nine specimens were polarized up to the characteristic potential P1, P2, and P3. These potentials were kept constant for 5 days.

Subsequently, a potentiostatic test was performed at 856 mV versus NHE (P1) for a duration of 4 weeks. Thus, changes concerning the carbon content of the solution could be further investigated. The entire experiment was carried out under inert gas atmosphere, in order to minimize carbon uptake through the air. In addition, a reference test specimen was integrated into the test series. This "blank sample" was stored under the same conditions but without polarization.

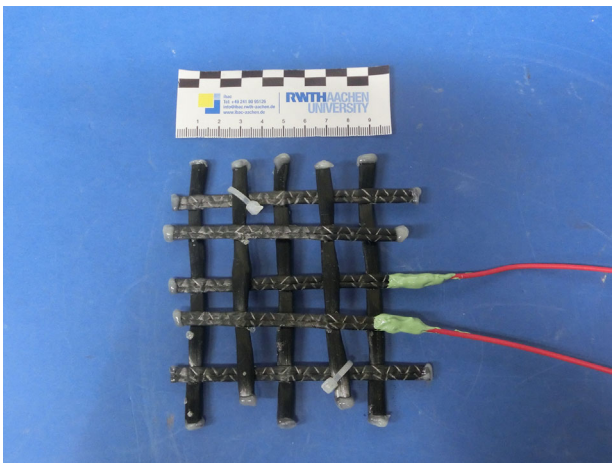


**FIGURE 4** Working electrode with two layers of carbon textile. [Color figure can be viewed at wileyonlinelibrary.com]

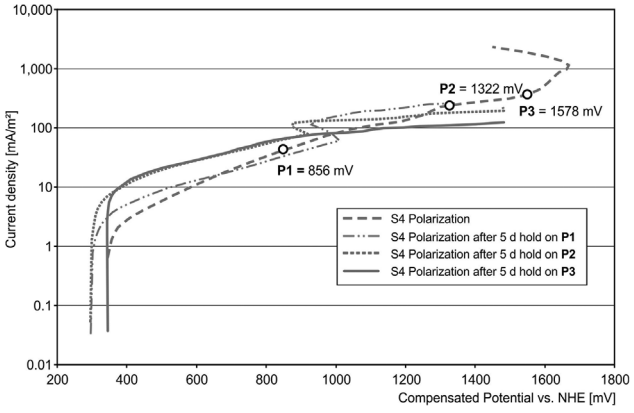


**FIGURE 5** Current density-potential curves with and without interposed potentiostatic experiments

## 2.4 | SEM examinations of the carbon textile surface after polarization

To understand the different behaviors of textiles coated with SBR-based material and EP-impregnated textiles, carbon textile surfaces of both unpolarized and polarized specimens were analyzed via scanning electron microscopy (SEM).

For conventional imaging in the SEM, specimens must be electrically conductive at the surface. Therefore materials are coated with ultra thin coating of electrically conducting material. To prepare EP-impregnated textile, graphite was used for coating.

The SEM images of the samples were taken before and after the polarization to detect the influence of polarization. In addition, reference samples were put in solution for the same polarization time but not polarized. Subsequently, SEM images were taken. In order to determine the homogeneity and the distribution of the filaments as well as the impregnation, SEM images of cross section of the two materials were carried out.

# 3 | RESULTS

## 3.1 | Current density-potential curves in calcium hydroxide solution

Figure 3 shows the mean values of three identical specimens of the tested textiles in saturated calcium hydroxide solution. It is clearly visible, that the textiles coated with SBR-based material reveal significant higher current densities at the same compensated potentials in comparison to the epoxy impregnated material.

Furthermore, Figure 3 shows the order of the textiles concerning their polarization behavior. In specific, textiles S1, S2, and S4 show the highest current densities of the textiles coated with SBR-based material in the performed tests. Focussing on the epoxy impregnated ones, E3 shows the highest current densities, followed by E4. The textiles E1 and E2 show almost the same polarization behavior.

The current density-potential curves of a textile coated with SBR-based material and pure graphite show a similar trend whereas the current density-potential curve of EP-impregnated textile indicates a quite different behavior (Figure 6). Here, the change in the slope of the curve is initiated by a considerably smaller (compensated) potential (Figure 3).

## 3.2 | Loss of carbon after polarization tests

In the Figure of Pourbaix (Figure 7), the holding potentials are plotted in the given pH value of 12.6.

After 5 days, the calcium hydroxide solution was removed to carbon analysis and replaced with fresh saturated calcium hydroxide solution. After the solution exchange, carbon fabric was depolarized until the open circuit potential was reached. Subsequently, applied voltage was increased again up to the achievement of 2200 mV. In this way a comparison of the curve progression with and without interposed hold experiments was possible (Figure 5).

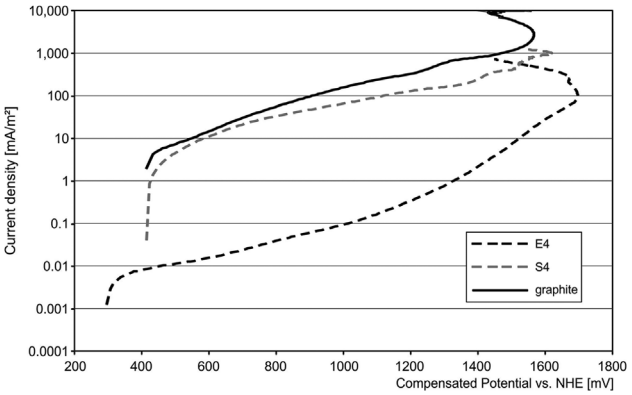


**FIGURE 6** Current density-potential graph: SBR-based coating and EP impregnated carbon textile versus graphite

Figure 5 shows that after holding at P1 and P2 an unknown effect occur in the curve progression when potential is between 900 and 1100 mV versus NHE. This effect is not observed for the original curve (S4 polarization). After the permanent polarization at P3 the slope change of the curve, which was between 1300 and 1400 mV versus NHE in the original polarization curve, is no longer present. Instead, current density increases steadily with rising potential.

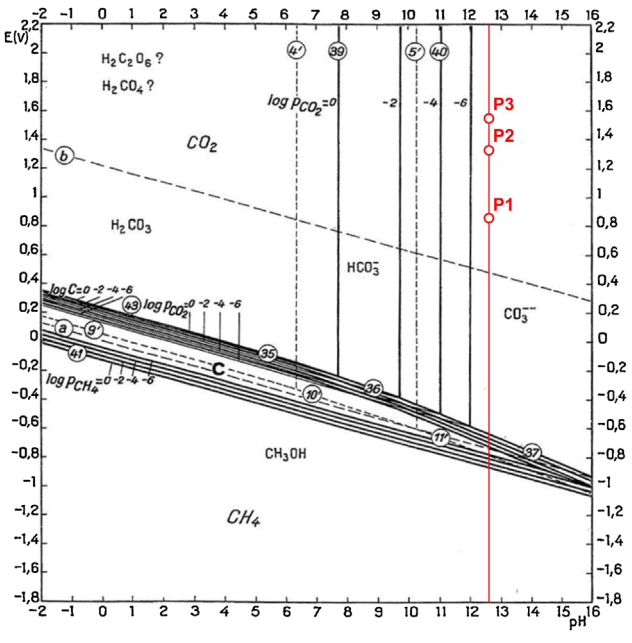


**FIGURE 7** Pourbaix diagram of carbon in water with chosen potentials.[5,25] [Color figure can be viewed at wileyonlinelibrary.com]

**TABLE 2** Carbon content of the solutions after different polarizations (S4)

| Specimen (−) | Potential (mV) | Duration of experiment | Current densities ($mA/m^2$) | Carbon content | |
|---|---|---|---|---|---|
| | | | | Single values (wt%) | Mean values (wt%) |
| Potentiodynamic test | 2200 vs. OCP | 18 h | – | 2.28 | 2.28 |
| P1-1 | 856 vs. NHE | 5 d | 8.8 | 2.38 | $2.03 \pm 0.43$ |
| P1-2 | 856 vs. NHE | 5 d | 5.5 | 1.42 | $2.03 \pm 0.43$ |
| P1-3 | 856 vs. NHE | 5 d | 8.4 | 2.29 | $2.03 \pm 0.43$ |
| P2-1 | 1322 vs. NHE | 5 d | 91.3 | 2.25 | $2.26 \pm 0.21$ |
| P2-2 | 1322 vs. NHE | 5 d | 57.7 | 2.01 | $2.26 \pm 0.21$ |
| P2-3 | 1322 vs. NHE | 5 d | 130.0 | 2.53 | $2.26 \pm 0.21$ |
| P3-1 | 1578 vs. NHE | 5 d | 551.2 | 3.35 | $3.81 \pm 0.32$ |
| P3-2 | 1578 vs. NHE | 5 d | 487.8 | 4.01 | $3.81 \pm 0.32$ |
| P3-3 | 1578 vs. NHE | 5 d | 496.6 | 4.06 | $3.81 \pm 0.32$ |

It is clearly visible, that the initial current density-potential curve of carbon textile after polarization up to 2200 mV versus OCP cannot be reproduced after permanent polarization at the above-mentioned potentials. However, the current densities which were achieved are sufficient for cathodic protection of concrete structures.

### 3.2.1 | Carbon content after potentiostatic tests

After 5 days of constant polarization at the characteristic potentials P1, P2, and P3, the solution was removed in order to analyze carbon contents. The results of the carbon analysis as well as the occurring current densities for each of the specimens can be seen in Table 2.

The chemical analysis is carried out according to ISO 15350, which determines the total carbon content in the solid state. For this, the tested solutions are freeze-dried. This method allows analysis of the total carbon content in solution, including sediment of the pore solution.

Regarding the carbon contents which were measured for the storing solutions of the specimens P1_1–P3_3, the following must be kept in mind: The values listed in Table 2 include carbon which entered the solution during the 5 days of permanent polarization as well as carbon which entered the solution during the preceding polarization up to 2200 mV versus OCP. For the assessment in view of future application of CP, the amount of carbon entering the solution during potentiodynamic tests needs to be subtracted. The values in Table 2 show, that up to 1322 mV versus NHE no additional carbon has gone into the solution. It can be seen small increase in carbon content in solution at a holding potential of 1578 mV versus NHE.

Results of the carbon analysis for the samples after 4 weeks of potentiostatic loading are shown in Table 3. With respect to the carbon content, no significant difference was observed between the polarized samples and the reference test specimen. Thus, accelerated dissolution of the carbon fiber due to the applied voltage range was not indicated.

In order to further investigate the influence of the impregnation to the polarization behavior in solution, experiments were carried out with unimpregnated rovings (UG). The test specimens were also polarized to 856 mV versus NHE and held for 4 weeks under inert gas. Again, a reference test specimen was integrated into the test series. Results of the subsequent carbon analysis are also shown in Table 3. There is no significant difference in carbon content between the polarized and unpolarized specimens.

**TABLE 3** Carbon content of the solutions after 4 weeks potentiostatic test of S4 and unimpregnated carbon

| Specimen (−) | Potential (mV) | Duration of experiment | Current densities ($mA/m^2$) | Carbon content |
|---|---|---|---|---|
| | | | | Mean values (wt%) |
| P1-4W-UG | 856 vs. NHE | 4 wk | 43 | $7.85 \pm 0.22$ |
| P0-4W-UG | 0 | 4 wk | 0 | $7.13 \pm 0.57$ |
| P1-4W-S4 | 856 vs. NHE | 4 wk | 8 | $7.40 \pm 0.68$ |
| P0-4W-S4 | 0 | 4 wk | 0 | $7.42 \pm 0.23$ |

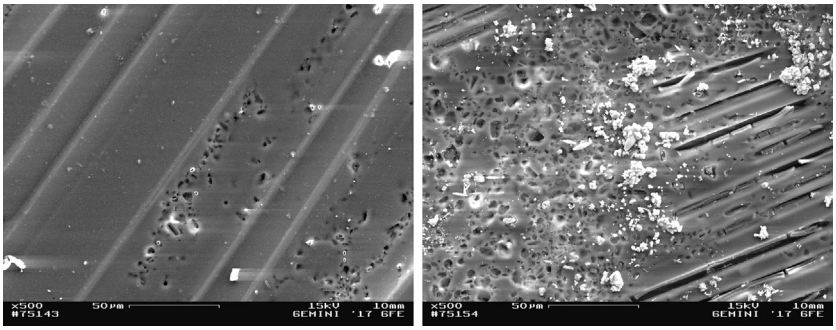


**FIGURE 8** SEM image of unpolarized (left) and polarized (right) EP-impregnated textile

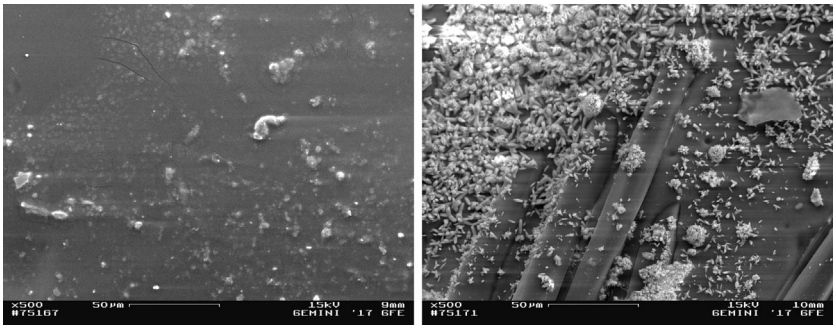


**FIGURE 9** SEM image of an unpolarized (left) and polarized (right) textile coated with SBR-based material

## 3.3 | SEM examinations of the carbon textile surface after polarization

Figure 8 shows the produced SEM images of EP-impregnated textile. The left picture shows the initial material. The impregnation is already characterized by a slight porosity. After polarization (right picture) the porosity increases significantly which results in the increased conductivity. Therefore, the active surface increases for the transport of the current, and thus, the current increases to a certain potential.

Rapid growing current strength after exceeding a certain potential, which was observed before, may be due to the destruction of impregnation material as visible in Figure 8. No change in surface was seen on the epoxy impregnated carbon after storing in the solution without polarization.

To prepare textiles coated with SBR-based material, graphite was unsuitable as coating material for SEM, which indicates that SBR-based coating is thicker and less conductive. Instead, platinum–palladium was used for specimen preparation. Nevertheless, the SEM picture of unpolarized textile coated with SBR-based material (Figure 9) shows a non-conductive surface of the specimen without any visible filaments. However, after the polarization of the textile, SBR-based coating disperses and filaments become clearly detectable. This extensive destruction of impregnation explains why textiles coated with SBR-based material reach higher current densities compared to EP-impregnated textile, when potential is identical. The white particles at the surface of the polarized textile are calcium carbide, which is a reaction product that forms by the contact of calcium hydroxide solution and carbon fibers.

Figure 10 clearly shows the damaged impregnation material. After holding the potential on P3, SBR-based coating has exfoliated and the subjacent carbon filaments are

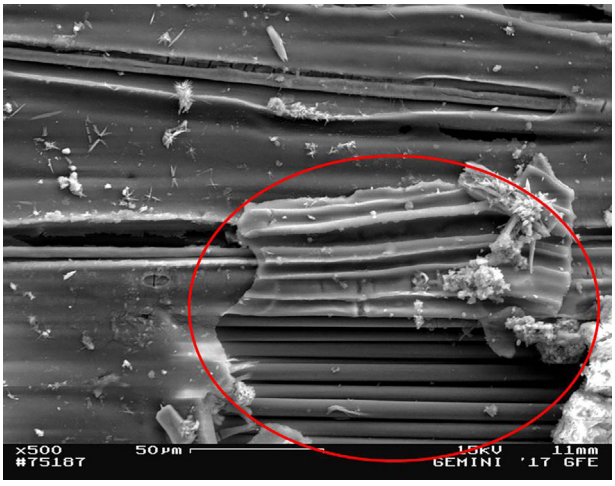


**FIGURE 10** SEM picture of polarized (P3-1) textile coated with SBR-based material. [Color figure can be viewed at wileyonlinelibrary.com]

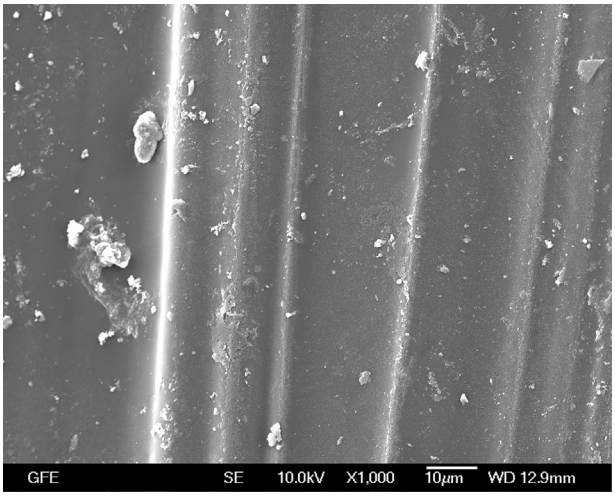


**FIGURE 11** SEM image of an unpolarized textile coated with SBR-based material stored in $Ca(OH)_2$

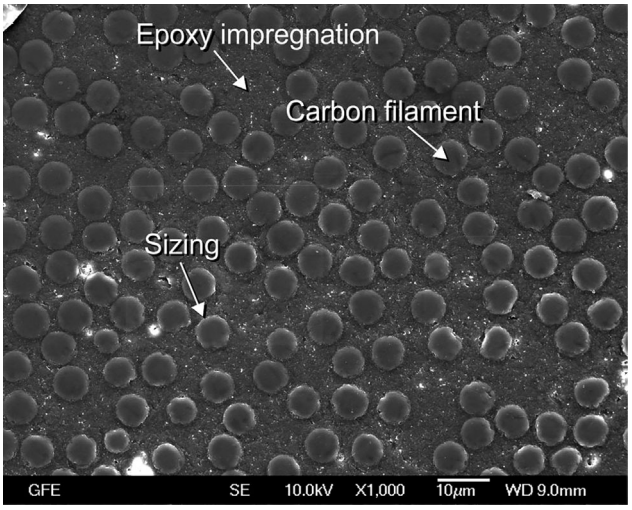


**FIGURE 13** SEM image of cross section of an unpolarized epoxy-impregnated carbon textile

directly exposed to the surrounding material. The underside of the exfoliated SBR-based coating clearly shows the filament imprints.

Figure 11 shows the SEM picture of an unpolarized textile coated with SBR-based material which was stored in solution for the same duration as the polarized textiles. The SEM picture shows no change in surface amorphology. Thus, the exfoliation is clearly a result of polarization.

Regarding the SEM images of the cross section, the single filaments in SBR-impregnated (Figure 12) rovings are close together and the SBR-based material content between filaments is low. The contact of the filaments leads to an enlargement of the active surface of the material. In epoxy impregnated rovings (Figure 13), the filaments are almost isolated from each other. Only on the surface they slightly touch each other. This leads to enhanced mechanical properties, but less polarizability. However, these observations are only valid for the investigated materials and do not allow conclusions for epoxy impregnation and SBR-based coating in general.

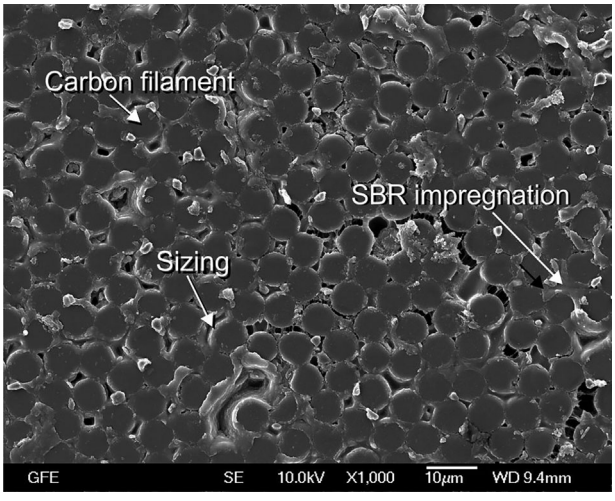


**FIGURE 12** SEM image of cross section of an unpolarized textile coated with SBR-based material

## 4 | DISCUSSION

### 4.1 | Current density-potential curves in calcium hydroxide solution

Here, the different polarization curves of carbon textiles with SBR-based coating and EP impregnation will be discussed.

E3 and E4 show similar courses in the current density-potential curve (Figure 3). This is due to the almost equal surfaces area. These two curves run below the E1 and E2 curves, as the same current is distributed over a larger surface area, resulting in smaller current densities.

For the textiles coated with SBR-based material, curve progressions differ considerably without any discernible trend. Textiles coated with SBR-based material delivers significantly more current at the same potential than EP-impregnated carbon. This is because the SBR used for impregnation has about 35 wt% solids, loses a lot of weight on drying out and also shrinks a lot. Therefore it acts as a coating. The shrinkage can cause defects. Through these defects, carbon is directly connected to the surrounding electrolyte. Potentials in the range of oxygen evolution lead to a damage of the coating by the gas formation on the carbon surface. This assumption is confirmed by SEM investigation. In addition, the resistivity of the SBR-based coating was measured and found to be between 10 and 100 Ωm at a frequency of 10 Hz. This shows a quite low resistance.

For EP-impregnated textiles, water ingress is limited. For the investigated EP it can be assumed, that charge transport primarily takes place via the detected pores in the impregnation, which increase after polarization.

Because this system is assumed to be a charge transfer controlled system, one starts from Butler–Volmer kinetics. The multiple slope changes in the current density-potential relationship can be explained by the reactions. In solution experiments, it is assumed that the limiting current density is not reached. That is why the broad gradient explains the different possible reactions in these curves. In the polarization experiment of carbon in $Ca(OH)_2$ solution, carbon from a potential of 1.2 V is an oxygen electrode with $z = 1$ (the number of electrons involved in the electrode reaction). If $z$ increases to 2 or 3, the slope of the curve changes, which indicates different reactions to be discussed below.

Electrochemical oxidation of carbon in water can lead to the formation of hydroxy, carbonyl, and carboxyl groups. That could be the explanation for the first hump in the curve. These products can be oxidized to $CO_2$ by further polarization. This may be an alternative explanation for the behavior of the curve at the end of the diagram. It is also possible that vicinal diols are formed, which contain two OH groups on neighboring C atoms. These molecules cannot be detected in the solution or on the carbon surface because the surface of the anode is so large that you cannot see the small defects. For such experiments suitable samples and test equipment should be set up.

Regarding potential-decrease at the right curve end, this effect can have at least three reasons. First, overcompensation can be assumed. Because the determination of the instant-off potential at the end of the measurement and compensation for all other potentials can lead to overcompensation. Secondly, polarization can increase the active surface, resulting in a rapid increase in current density when the initial surface area is not taken into account due to the destruction of the impregnation. Finally, it is suggested that new reactions may occur at certain potentials. However, these potentials are for CP by far too high and therefore technically not relevant.

In order to take a closer look at this effect, new potentiostatic tests were carried out on S4 in the saturated calcium hydroxide solution. During each stage, the on potential was turned off to look at the instant-off potentials. Figure 14 shows the ratio of current density to compensated potential. At the end of the curve, it is considered that the current density increases rapidly while the potential remains constant. This proves that at a certain potential, the surface of carbon is changed and thereby leads to higher currents.

The results of the performed hold experiments, which are shown in Figure 15, confirm the validity of the assumptions. Lower potential of 856 mV as well as 1322 mV versus NHE initiates a more or less stable current for the experimental duration. At potential of 1578 mV versus NHE however, causes a rapidly growing current.

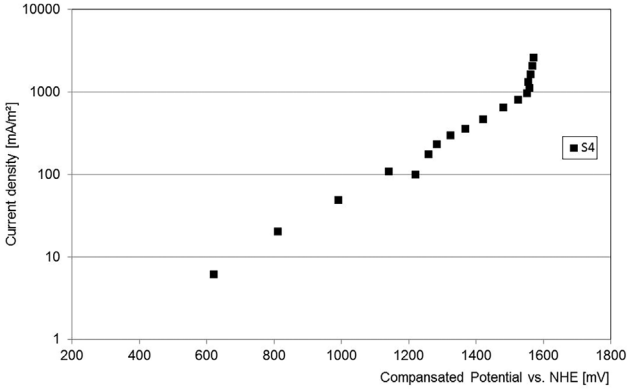


**FIGURE 14** Potentiostatic step tests of S4 with increasing potential

## 4.2 | Loss of carbon after potentiostatic tests

Current density potential curves provide an interesting effect of the polarization of carbon textile. There is a small hill to see at the textiles coated with SBR-based material at 1322 mV versus NHE. Therefore, three holding potentials were selected before, at, and after this potential. These points are P1 = 856 mV versus NHE, P2 = 1322 mV versus NHE, and P3 = 1578 mV versus NHE designates.

The results of the carbon analysis show that up to a potential of 1322 mV versus NHE no additional carbon goes into the solution. The potentiostatic experiments at 1578 mV versus NHE show an insignificant increase in the carbon content in solution. Analyzed carbon after a potential of 1322 mV versus NHE has to be investigated, whether it

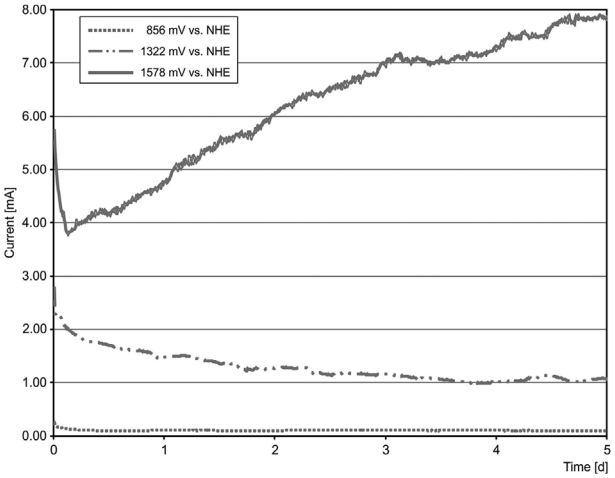


**FIGURE 15** Potentiostatic tests of S4 under different polarizations

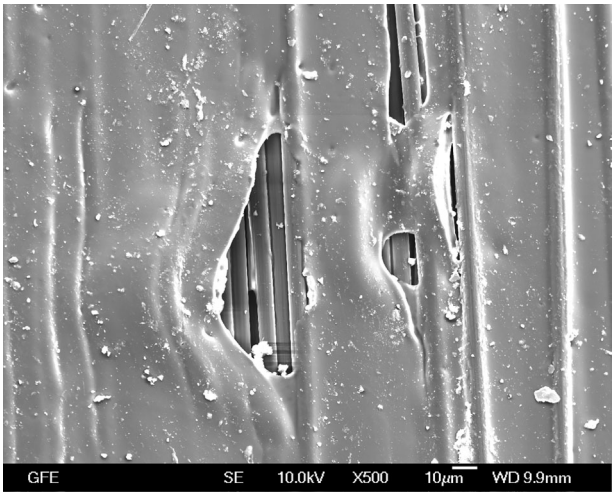


**FIGURE 16** Textile coated with SBR-based material before polarization

comes from carbon or impregnation material. Therefore, investigations were carried out with unimpregnated material. The results in Table 3 show that the carbon, which was found in solution neither comes from the carbon fiber fabric itself nor from the impregnation material. Due to the very similar carbon contents in all test specimens, a significant carbon input due to polarization or the existing impregnation can be excluded. It is assumed that the carbon originates from the air and entered the solution during filling the containers.

After potentiostatic tests at different potentials, the initial current density-potential curve of carbon textile after one-time polarization from OCP up to 2200 mV cannot be reproduced. That is because of the change in the surface due to the destruction of the impregnation.

### 4.3 | SEM examinations of the carbon textile surface after polarization

SEM images indicate that EP-impregnation is significantly porous. After polarization, porosity further increases. Thus, electrical-conductivity is present.

In order to prove the polarizability of the textiles coated with SBR-based material, investigations were carried out. First, the surface of the sample was examined more closely and extensively before polarization. Figure 16 shows that carbon, coated with the SBR-based material gives defects which in turn allow contact between carbon and the solution. In the anodic polarization after the oxygen evolution potential was achieved (theoretically at 1.2 V vs. NHE at pH 14), by gas formation, the SBR-based coating is disbanded and separated from the carbon surface.

Incidentally, Figures 12 and 13 show that the filaments are close to each other for SBR-based material. There are also pores between the filaments, which can be filled with solution during the measurements and thereby may increase the charge transfer. Here, the charge transfer can be possible both over the outer surface as well as through the adjacent filaments. In the case of epoxy, charge transfer may only be possible through the pores and only on the outer surface.

## 5 | CONCLUSIONS AND OUTLOOK

The following conclusion can be drawn from the experimental study:

1 The results of the polarization experiments show that textiles coated with SBR-based material delivers by a factor of 100–1000 more current than EP impregnated carbon at equal potentials, but still less than graphite.
2 No dissolution of carbon in saturated solution of calcium hydroxide up to 1322 mV versus NHE (P2) has been observed.
3 Carbon has been detected at 1578 mV versus NHE (P3) in solution, which was not from carbon filaments. At this potential the disbanding of the SBR-based coating can be seen.
4 SEM pictures do not indicate any damages of the carbon filaments at potentials up to 1578 mV versus NHE (P3).

The conductivity of the SBR-based coating, which is used for the coating, will be examined more closely.

Currently investigations are running on the durability of carbon textile anodes in concrete structures by carrying out long-time potentiostatic experiments. Carbon textiles will be applied also to concrete and mortar specimen. Then, long-time experiments will be carried out in order to finally gain information concerning the durability as anode material for CP in concrete structures.

## ORCID

*Amir Asgharzadeh* http://orcid.org/0000-0001-6318-2532

## REFERENCES

[1] M. Raupach, T. Büttner, *Diagnosis, Design, Principles and Practice*. CRC Press Francis & Taylor Group, Boca Raton **2014**.
[2] T. Büttner, C. Morales Cruz, M. Raupach, *Bautechnik*. **2013**, *90*, 485.
[3] D. Wetjen, *Doctoral Thesis*. University of Augsburg, Germany **2016**.
[4] A. Asgharzadeh, M. Raupach, *Service Life and Durability of Reinforced Concrete Structures (RILEM Bookseries)*. Springer International Publishing, Basel **2018**.
[5] M. Pourbaix, *Atlas of electrochemical equilibria in aqueous solutions*. National Association of Corrosion Engineers, Houston **1974**.

[6] M. Chini, *Doctoral Thesis*. Norwegian University of Science and Technology Trondheim, Norway **2010**.
[7] M. Chini, R. Antonsen, Ø. Vennesland, B. Arntsen, J.H. Mork, **2007** presented at *International RILEM Workshop on Integral Service Life Modelling of Concrete Structures*, Guimaraes, Portugal, 5–6 November 2007, pp. 395–402.
[8] C. Van Nguyen, P. Lambert, P. Mangat, F. O'Flaherty, G. Jones, *ISRN Corros. 2012*, **2012**, 814923.
[9] E. Zhang, L. Tang, T. Zack, presented at *The 5th International Conference on the Durability of Concrete Structures*, Shenzhen, China, 30 June – 1 July 2016, pp. 300–308.
[10] J. Chang, *Cem. Concr. Res*. **2002**, *32*, 657.
[11] B. Eastwood, P. Christensen, R. Armstrong, N. Bates, *J. Solid State Electrochem*. **1999**, *3*, 179.
[12] L. I. Krishtalik, Z. A. Rotenburg, *Sov. Electrochem*. **1966**, *2*, 322.
[13] H. Thiele, *Trans. Faraday Soc*. **1938**, *34*, 1033.
[14] N. Staud, H. Sokol, P. N. Ross, *J. Electrochem. Soc*. **1989**, *136*, 3570.
[15] F. Pruckner, *Concr. Eng. Int*. **2006**, *10*, 54.
[16] L. Bertolini, F. Bolzoni, T. Pastore, P. Pedeferri, *Cem. Concr. Res*. **2004**, *34*, 681.
[17] W. H. A. Peelen, R. B. Polder, E. Redaelli, L. Bertolini, *Mater. Corros*. **2008**, *59*, 81.
[18] R. B. Polder, W. H. A. Peelen, *Concrete Repair – A Practical Guide. Service life aspects of cathodic protection of concrete structures*. Taylor & Francis, Hoboken **2011**.
[19] M. Poltavtseva, G. Ebell, J. Mietz, *Mater. Corros*. **2015**, *66*, 627.
[20] L. Tang, E. Q. Zhang, Y. Fu, B. Schouenborg, J. E. Lindqvist, *Mater. Corros*. **2012**, *63*, 1119.
[21] M. Rueffer, D. Bejan, N. J. Bunce, *Electrochim. Acta*. **2011**, *56*, 2246.
[22] S. Yumitori, Y. Nakanishi, *Composites, Part A*. **1996**, *27*, 1051.
[23] A. Bismarck, M. E. Kumru, J. Springer, J. Simitzis, *Appl. Surf. Sci*. **1999**, *143*, 45.
[24] J. H. Zhu, G. Guo, L. Wei, M. Zhu, X. Chen, *Materials*. **2016**, *9*, 103.
[25] N. Takeno, *Geol. Surv. Jpn*. **2015**, 419.

**How to cite this article:** Asgharzadeh A, Raupach M. Durability behavior of polymer impregnated carbon textiles in alkaline solution as CP anode. *Materials and Corrosion*. 2018;1–12. https://doi.org/10.1002/maco.201810098

**Cite this article**
Asgharzadeh A and Raupach M
Durability of impregnated carbon textiles in mortar as cathodic protection anodes.
*Magazine of Concrete Research*,
https://doi.org/10.1680/jmacr.18.00402

**Research Article**
**Paper 1800402**
Received 27/08/2018; Revised 07/01/2019;
Accepted 24/01/2019



**Keywords:** durability-related properties/electrical properties/fibre-reinforced concrete

Magazine of Concrete Research

ice Publishing

# Durability of impregnated carbon textiles in mortar as cathodic protection anodes

**Amir Asgharzadeh** Dipl.-Ing
Graduate Research Assistant, Institute of Building Materials Research, Aachen, Germany (corresponding author: zadeh@ibac.rwth-aachen.de)
(Orcid:0000-0001-6318-2532)

**Michael Raupach** Dr.-Ing
Professor, Institute of Building Materials Research, Aachen, Germany

**Current research focuses on the use of carbon (C) textiles as cathodic protection (CP) anodes. Carbon fibres are of particular interest due to their excellent mechanical properties. However, the influence of anodic polarisation on the durability of carbon anodes is still not sufficiently understood. In previous works, the durability of carbon anodes was examined by experimental investigations in saturated calcium hydroxide ($Ca(OH)_2$) solution. In this work, various anodes (carbon textiles with different impregnations, as well as mixed-metal-oxide-coated titanium (Ti)) were investigated after embedding in mortar. The type of mortar as well as the environmental conditions were varied in order to represent diverse conditions. Potentiostatic polarisation was implemented for 8 months. Results of this work show that CP with impregnated carbon textiles is, at least under the investigated conditions, possible.**

## Introduction

To protect corroding components of reinforced structures against corrosion and to limit the reduction in cross-section of the reinforcing steel, repairs are required. To achieve this goal, it is necessary to inhibit one of the two partial corrosion reactions in such a way that the corrosion processes are reduced to an accepted level. Cathodic protection (CP) refers to methods that prevent anodic partial reaction. The advantage of CP is that the chloride-contaminated concrete does not need to be removed. Conventional CP systems currently on the market use mixed-metal oxide (MMO)-coated titanium (Ti) as the anode material. Research work on carbon (C) textiles as CP anodes is currently under way because of their additional excellent mechanical properties. However, the durability of carbon textiles as CP anodes is not sufficiently understood.

Carbon textiles consist of woven or laid carbon fibre (CF) rovings and are impregnated or soaked, for example, with styrene-butadiene rubber (SBR) or epoxy resins, in order to obtain a more rigid and stronger material. In construction, carbon textiles are increasingly used as reinforcement in textile concrete because of their low weight, crack-bridging ability and excellent mechanical properties.

Bertolini *et al*. (2004) investigated the behaviour of a cementitious conductive overlay anode made of nickel (Ni)-coated CF in a cementitious mortar. Measurements on concrete specimens with two layers of rebars were performed. Current densities in the range of 10–100 mA/m$^2$ with respect to the anode surface were applied, and the distributions of current and potential as well as 4 h decay were regularly measured. The authors found that the application of current densities up to 20 mA/m$^2$ for over 2 years makes the cementitious conductive coating a satisfactory anode for CP. However, the application of current densities of 50 or 100 mA/m$^2$ leads to the destruction of the anode within only 1–2 months. The reason for this has been found to be the production of acidity by anodic reactions.

Anwar *et al*. (2014) investigated the effectiveness of lightweight conductive cementitious mortar as an anode material for CP. The anode is made of pumice aggregate, CFs and cement with MMO-coated titanium as a primary anode. Galvanostatic experiments were performed with a constant current density of 200 mA/m$^2$ related to the anode surface for a duration of 14 d. Achievement of constant potentials was rare, but interesting discoveries were made regarding the durability of CFs. Scanning electron microscope (SEM) images demonstrate that neither high current densities nor high potentials cause significant CF dissolution.

In order to provide CP, the protective current densities for common reinforced components are less than 20 mA/m$^2$. For example, Vennesland *et al*. (2006) demonstrated a system based on a woven carbon mesh installed on specimens obtained from a concrete bridge, which had been demolished due to steel corrosion. A month-long polarisation with a feeding voltage of 1 V and with a 3–4 mA/m$^2$ current density resulted in satisfactory protection.

A maximum external current to run CP systems is given by Van Nguyen *et al*. (2012). For CF fabric anodes, applied current should not exceed 10 mA (128·4 mA/m$^2$ with respect to the steel surface area), and for CF rod anodes, applied current should not exceed 5 mA (64·2 mA/m$^2$ with respect to the steel surface area). The statements are based on laboratory simulations of impressed current cathodic protection systems, which were operated for 1100 h.

Zhang *et al*. (2016) carried out experiments on cathodic prevention. While CP is typically applied to structures which are already affected by corrosion, it is also applied to structures that are exposed to the risk of chloride contamination. Applied current densities for cathodic prevention are much lower (0·2–2 mA/m$^2$), but the fundamental procedure is generally identical (Zhang and Tang, 2014). After 2 months of electrochemical accelerated testing, specimens were sawn into slices to investigate compositional changes in the anode zone. Chemical and microstructural analyses were performed by laser ablation inductively coupled plasma mass spectroscopy as well as SEM. It was found that, under electrochemical treatment, hydrogen ions are formed around the anode, causing locally acidic conditions. Under acidic conditions, portlandite ($Ca(OH)_2$) is neutralised. The positive calcium ions ($Ca^{2+}$) mobilise, moving away from the zone around the anode. Thus, a ring pattern develops around the anode with decreasing ratios of calcium (Ca)/silicon (Si). After completion of the electrochemical treatment, sodium (Na) ions diffuse from the surrounding cement paste matrix to the anodic region to neutralise the negatively charged zone. Thus, peaks of sodium/silicon are formed around the anode. With increasing current density, stronger changes in microstructural and chemical changes at the anode interface can be expected.

The objective of the present work is to experimentally investigate the durability of impregnated carbon textiles as an anodic material in mortar at usual current densities for CP. In previous work it has been shown that significant carbon surface reaction occurred in solution with potentiodynamic polarisation after deterioration of the impregnation (Asgharzadeh and Raupach, 2018b). The present work aims at assessing whether potentiostatic polarisation of impregnated carbon textiles in mortar also leads to the detrimental effects previously observed or whether the mortar provides an additional protective means. Without deterioration, impregnated carbon textiles embedded in mortar could be considered as an interesting anode material to be used in CP, because of its additional structural performance.

## Research significance

Conventional CP systems currently on the market mostly use MMO-coated titanium as the anode material. Carbon as an anode material does not only provide sufficient current densities for CP at moderate polarisations. In the form of impregnated textiles, it can simultaneously provide load-bearing capacities for structural strengthening. Hence, durability is a major issue from both the structural and the CP point of view. This work focuses on the durability of carbon textiles employed as the anodic material in mortars with respect to CP application.

## Experimental programme

### Materials

Two commercially available mortars used for CP were selected. Both are polymer-modified and exhibit high freeze–thaw resistance. Mortar M2 has a higher stiffness than M1 and is therefore mainly used for the repair of vertical components such as walls in car parks or tunnel walls. It can also be used for horizontal surfaces. Some properties are listed in Table 1.

Two carbon textiles with the same rovings in longitudinal and lateral directions and a mesh size of 38 mm with different impregnation materials were used as the anode material in the investigations.

Figure 1 show the epoxy- and SBR-impregnated textiles, respectively.

As an anode material, the styrene–butadiene rubber (SBR-based) coated S4 was selected because this material achieved highest current densities (and thus the best polarisation behaviour) in previous experiments (Asgharzadeh and Raupach, 2018b). For reasons of comparability, the epoxy-impregnated E4 was selected, as it has the same mesh size as S4. In addition, some specimens were equipped with MMO-coated titanium anodes. Thus, a comparison between carbon and titanium anodes was possible as well. Test specimens with titanium anodes were produced only with mortar M1.

### Specimen preparation

The carbon textile used as the anode material and the MMO-coated titanium mesh – employed as the counter electrode – have outer dimensions of 25 × 25 cm$^2$. A gap of 2·5 cm between them is ensured by PVC spacers (Figure 2; left). The reference electrodes (magnesium oxide, $MnO_2$) are attached to the carbon anode. Due to its MMO coating, the titanium mesh serves as an active electrode, ensuring a uniform

**Table 1.** Properties of Mortars 1 and 2

| | Mortar 1 | Mortar 2 | Unit |
|---|---|---|---|
| Density | 2·14 | 2·06 | kg/dm$^3$ |
| Flexural strength (28 d) | 10 | 8·5 | N/mm$^2$ |
| Compressive strength (28 d) | 45–55 | 55 | N/mm$^2$ |
| Elastic modulus (28 d) | 22 300 | 32 500 | N/mm$^2$ |
| Maximum grain size | 4 | 2 | mm |
| Mixing ratio | 100:9–10 | 100:15 | mass of dry material:water |

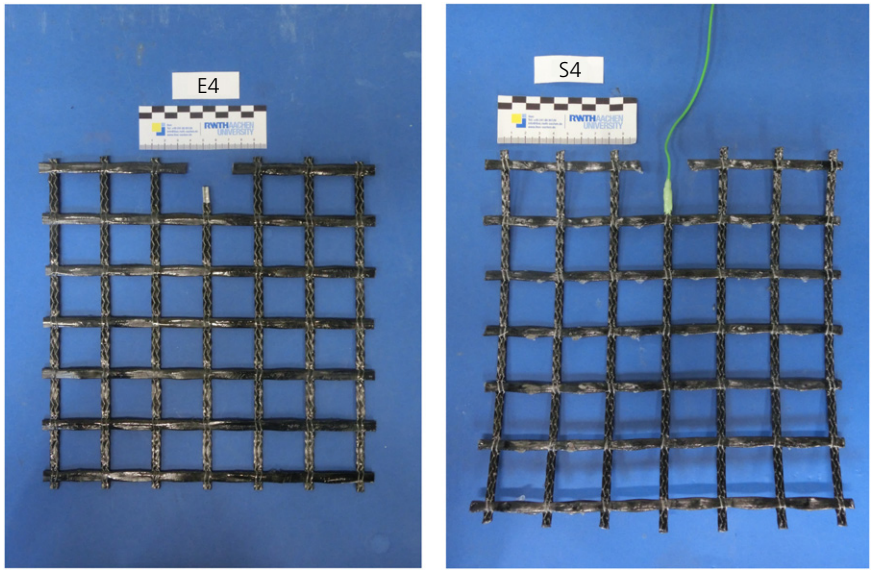


**Figure 1.** Carbon textile impregnated with epoxy (left), with SBR-based material (right)

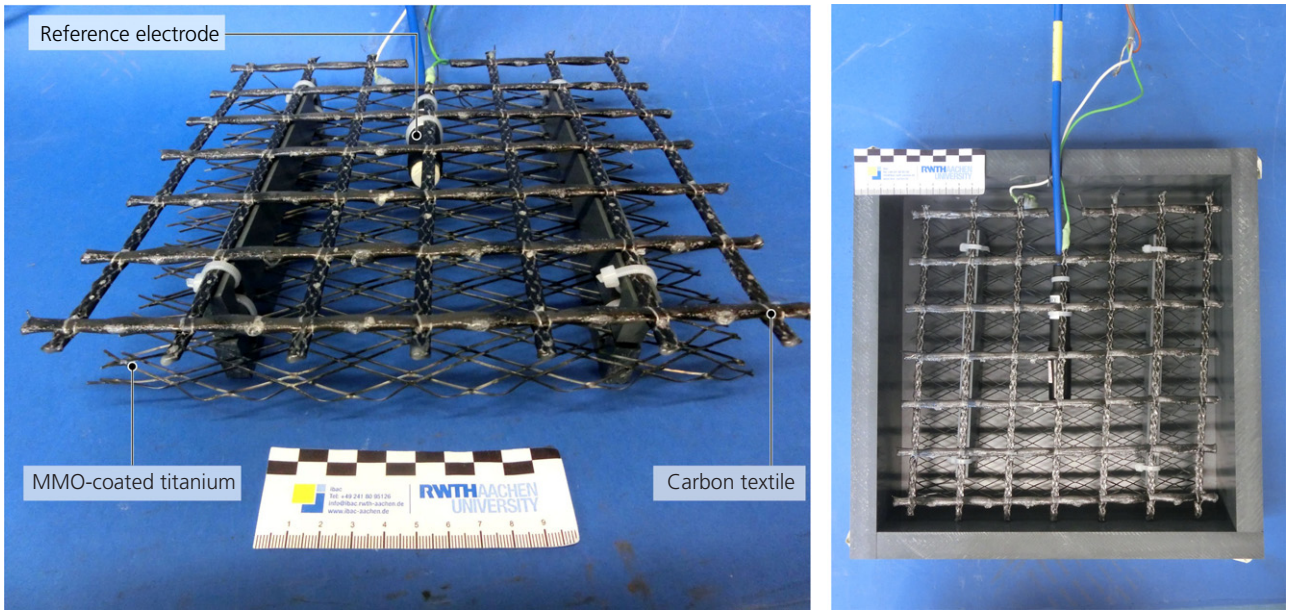


**Figure 2.** Three-electrode design with S4 anode (left), placed in mould (right)

distribution of current. A homogeneous current distribution is required in order to allow comparability of the individual test specimens.

The electrode arrangement (E4, S4 and MMO-coated titanium) is placed at mid-height in mortar moulds of dimensions $27 \times 27 \times 7{\cdot}5$ cm$^3$ (Figure 2; right). The mortars were mixed according to the manufacturers' guidelines and filled into the moulds with vibrational compaction to ensure proper embedding of the electrodes. To prevent uneven drying of the mortar specimens, the vertical surfaces were coated with an epoxy resin. In the completed specimens, as shown in Figure 3, the anode surface is located 2·5 mm below the mortar surface.

## Polarisation

The specimens were connected to single-cell potentiostats under potentiostatic conditions. Carbon textiles were used as a working electrode, MMO-coated titanium as a counter electrode and a magnesium oxide electrode as a reference electrode.

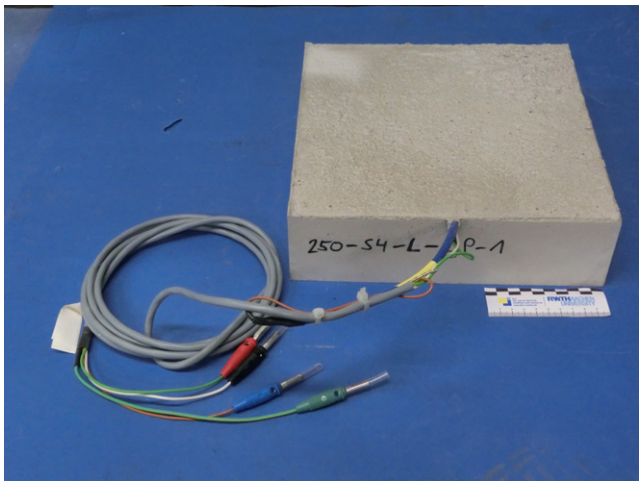

Figure 3. Completed test specimen

Specimens were polarised with constant potential against a reference electrode for 8 months. The first 60 d were used for conditioning. After 57 d, an instant-off measurement was made to adjust the instant-off potentials. After 60 d, the samples were polarised potentiostatically with their potential over the time.

### Simulation of environmental conditions

Two storage conditions were chosen to represent different environmental conditions. To simulate an idealised climate of a tween deck of a parking garage, a temperature of 20°C and a constant relative humidity of about 80% were adjusted in a climate cell (indication: 20/80). In order to mimic puddles on a parking deck, a water layer was established on the mortar surface of some specimens by means of a PVC casing. The wetted specimens were stored at 20°C as well. The different storing conditions and the specimens' design are sketched in Figures 4 and 5, showing

(*a*) mortar
(*b*) working electrode (carbon textile)
(*c*) counter electrode (MMO-coated titanium)
(*d*) reference electrode (magnesium oxide)
(*e*) PVC upstand
(*f*) water
(*g*) protective cover.

The labelling of the test specimens consists of mortar type, anode material, storage and the type of polarisation. Table 2 summarises the labels used. Specimen M1-E4-UW-P-2, for example, is made of M1, has an anode of epoxy-impregnated carbon fabric, is stored at 20°C and 50% relative humidity with water on top, and is permanently polarised at polarisation level 2 (see below). For each environmental condition, six specimens were prepared (see Figure 6). Five of them were polarised according to the section titled 'Polarisation'. The

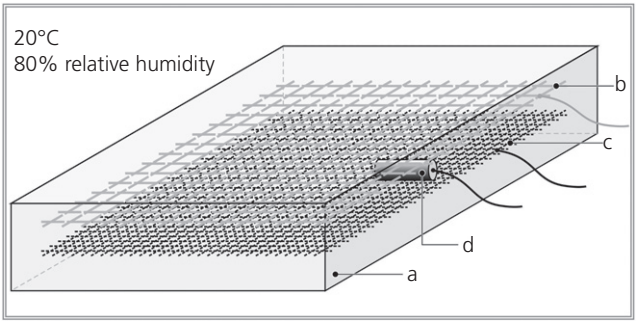


Figure 4. Storage conditions, case: 20/80

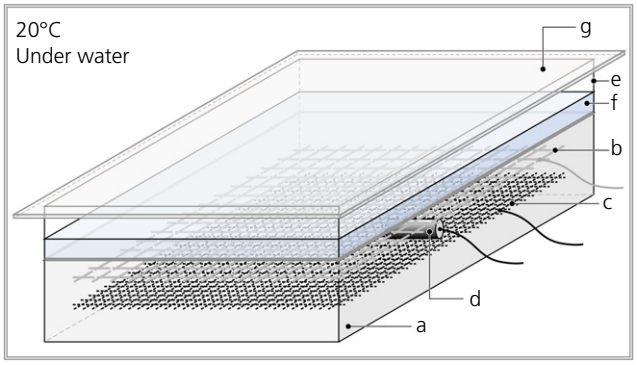


Figure 5. Storage conditions, case: UW

Table 2. Labelling of specimens

| | Material | Label |
|---|---|---|
| Mortar | Mortar 1 | M1 |
| | Mortar 2 | M2 |
| Anode | Epoxy-impregnated carbon | E4 |
| | Carbon with SBR-based coating | S4 |
| | MMO-coated titanium | Ti |
| Storage | 20°C, covered by water | UW |
| | 20°C, 80% relative humidity | 20/80 |
| Polarisation | Long-term polarisation | P |

sixth specimen served for referential potentiostatic measurements. In addition, three identically constructed test specimens for each carbon textile and mortar combination were produced and potentiodynamically polarised (see section 'Preliminary potentiodynamic measurements'), so that the interesting hold potentials could be determined. These specimens are termed pre-test specimens and are not shown in Figure 6.

## Results

### Preliminary potentiodynamic measurements

In order to choose suitable potential levels for the long-term polarisation, potentiodynamic tests on identical pre-test

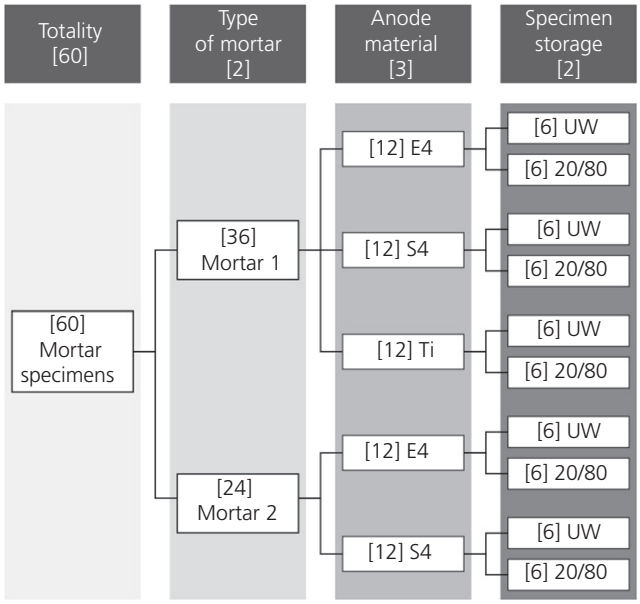


**Figure 6.** Overview of specimen variations

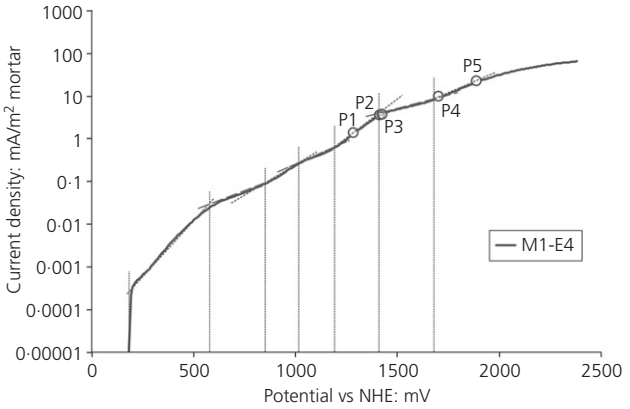


**Figure 7.** Method for selecting the hold points for potentiostatic polarisation

samples were performed. The pre-test specimens were potentiodynamically polarised from resting potential to 2200 mV at a rate of 2 mV/min. From sudden changes in the slope of the otherwise smoothly increasing curves of current density over potential (see Figure 7), it was inferred that detrimental processes in the impregnation of the carbon anode occurred. The corresponding potentials, P1 to P5 in Figure 7, were considered of major interest and hence chosen for the long-term potentiostatic measurements. As a further condition, the chosen potentials should produce current densities between 1 and 20 mA/m$^2$ with respect to the mortar surface. This range is interesting for typical CP applications. Curves similar to those shown in Figure 7 for M1-E4 were obtained for the other mortar and electrode combinations. All selected hold

**Table 3.** Potential levels for potentiostatic polarisation

| | Potential against NHE: mV | | | | |
|---|---|---|---|---|---|
| | P-1 | P-2 | P-3 | P-4 | P-5 |
| M1-E4-(20/80)/UW | 1281 | 1408 | 1411 | 1701 | 1891 |
| M1-S4-(20/80)/UW | 1075 | 1205 | 1345 | 1515 | 1875 |
| M1-Ti-(20/80)/UW | 475 | 545 | 645 | 793 | 1440 |
| M2-E4-(20/80)/UW | 1292 | 1402 | 1472 | 1772 | 2181 |
| M2-S4-(20/80)/UW | 1002 | 1122 | 1212 | 1342 | 1672 |

**Table 4.** Polarisation on individual specimens at different polarisation points

| | Polarisation: mV | | | | |
|---|---|---|---|---|---|
| | P-1 | P-2 | P-3 | P-4 | P-5 |
| M1-E4-20/80 | 1122 | 1246 | 1251 | 1570 | 1773 |
| M1-E4-UW | 1090 | 1235 | 1258 | 1545 | 1708 |
| M1-S4-20/80 | 827 | 954 | 1103 | 1289 | 1680 |
| M1-S4-UW | 964 | 1096 | 1121 | 1410 | 1750 |
| M1-Ti-20/80 | 250 | 316 | 418 | 564 | 1222 |
| M1-Ti-UW | 254 | 323 | 421 | 570 | 1201 |
| M2-E4-20/80 | 1133 | 1252 | 1325 | 1653 | 2079 |
| M2-E4-UW | 1152 | 1224 | 1292 | 1575 | 2038 |
| M2-S4-20/80 | 706 | 864 | 927 | 1062 | 1414 |
| M2-S4-UW | 781 | 895 | 916 | 1112 | 1371 |

potentials are listed in Table 3. The same potentials were then used for both storage conditions, 20/80 and under water (UW).

### Potentiostatic measurements

The rest potential was determined for each of the specimens before polarising and the standard potentials of Table 3 were converted to polarisation, which are more easily applied in practice. The overpotentials applied in the potentiostatic measurements are given in Table 4.

In what follows, current densities are always related to the mortar surface. The potential values do not compensate for internal resistance (IR).

At the beginning of the polarisation, the current density drops sharply but then reaches a nearly constant level after 57 d (see Figure 8 for M1-E4-20/80). This also applies to the wetted specimens M1-E4-UW before wetting. On day 6, however, all current density curves show a sudden drop in current density (Figure 9). The jumps are mainly due to a change in temperature due to the filling of the casings with cold water. After the application of water, the current density of almost all specimens in storage UW increases, except for the sample P4. The increase is probably due to a reduction in the concrete resistance due to the higher humidity. On day 32, a cover was placed on the filled casings in order to reduce evaporation, which led to a renewed jump in the current density curves. At the time of the instant-off measurements (day 57), the change

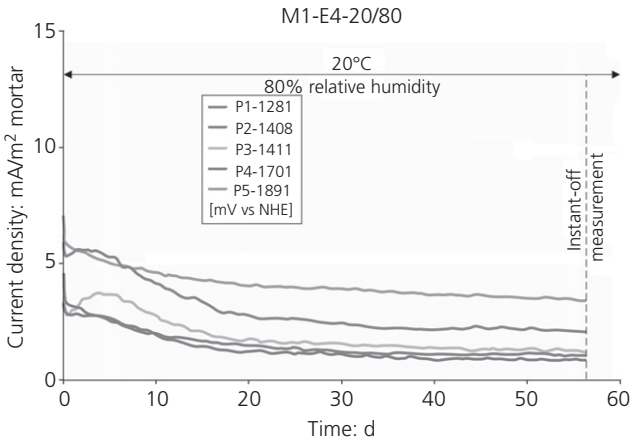


**Figure 8.** Current density plotted against time for M1-E4-20/80 in the first 60 d for all hold potential points

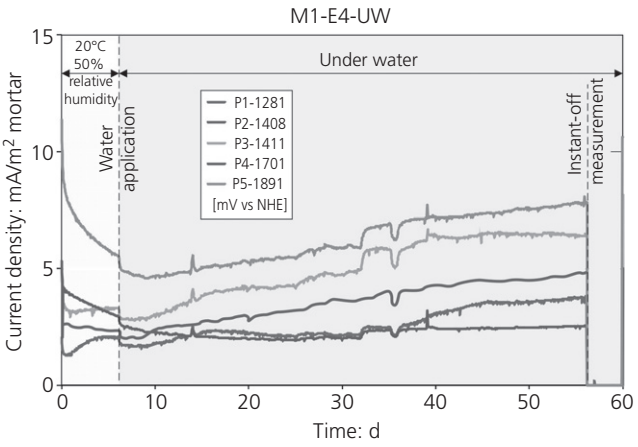


**Figure 9.** Current density plotted against time for M1-E4-UW in the first 60 d for all hold potential points

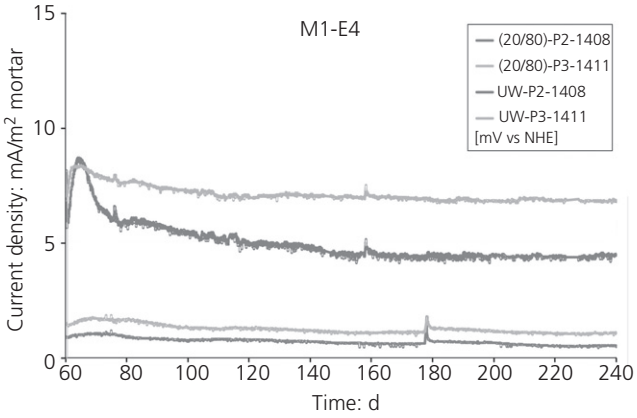


**Figure 10.** Current density plotted against time for M1-E4 at P2 and P3 for both storages

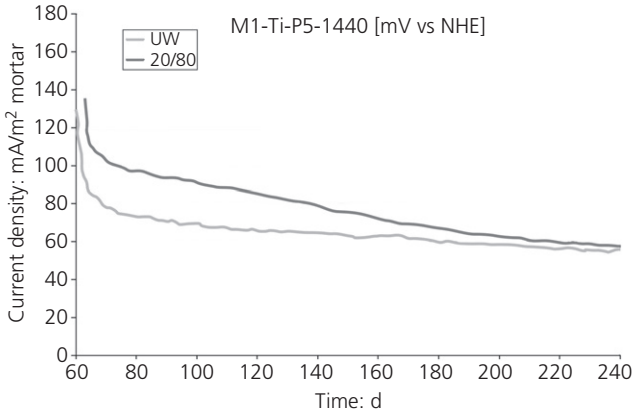


**Figure 11.** Current density plotted against time for M1-Ti at P5 for both storages

in the concrete resistance in three specimens seems to be largely completed and a nearly constant level of current densities is achieved.

Similar effects were observed with the other mortar electrode combinations. In the following, these initial effects are ignored and only the development of currents from day 60 on will be discussed.

Figure 10 shows current densities plotted against time from day 60 to 240 for M1-E4 with potentials P2 and P3 in 20/80 and UW storage.

All four curves show that the current density first increases after starting polarisation and then decreases. The decrease continues for about 60 d until the curves reach nearly constant current densities. This effect is more pronounced in UW storage than in 20/80 storage. The reason could be that at UW the pores are full of water, and oxygen takes more time to transfer. At 20/80, which simulates a relatively dry storage, oxygen is able to reach the cathode without obstruction by the air in pores.

Final current densities are lower with 20/80 storage due to drying and ensuing higher mortar resistance. The causes for the decreasing current densities and thus for the loss of performance have already been observed by Bertolini *et al.* (2004), Chini *et al.* (2008), Chini (2010), Van Nguyen *et al.* (2012), Mietz and Raupach (2015), as a current density drop in potentiostatic experiments and accordingly as a potential increase in galvanostatic experiments (Mietz and Raupach, 2015; Poltavtseva *et al.*, 2015). Possible causes could be a loss of conductivity due to degradation of the anode, a contact loss between anode and concrete, an increase of the concrete resistance or a too-small cathode area (Mietz and Raupach, 2015). However, a decrease in the current density can also be seen for the test specimens with MMO-coated titanium anodes (Figure 11).

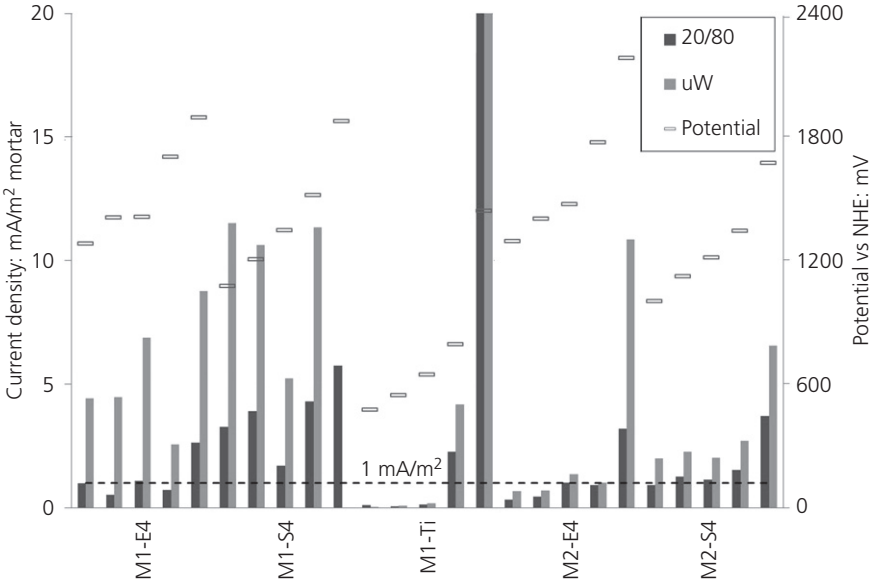


**Figure 12.** Current densities after 240 d for all mortar electrode combinations and both storages at potentials given in Table 3

Figure 12 shows the current densities after 240 d for all mortar electrode combinations and storages. The potentials of the potentiostatic tests are depicted as horizontal bars and – from left to right – indicate the potentials P1 to P5 of Table 3 for each mortar electrode combination. The results will be discussed by means of this bar chart.

## Storage

UW storage results in higher current densities than 20/80 storage with all specimens, due to wetting and ensuing lower electrolyte resistance.

## Material

### Epoxy-impregnated carbon (E4)

Even though P3 is only 3 mV higher in potential than P2, the resulting current density at P3 is considerably higher than the current density at P2 with both mortars and storages. P3 lies in the maximum of the hump, which is shown in Figure 7. Based on the results from Asgharzadeh and Raupach (2018b), it can be said that the existing pores on the surface of the selected epoxy-impregnated carbon become larger and thus more charge can be transported.

By increasing the potential from P3 to P4, the current density decreases with M1. As the potential increases from P4 to P5, the slope changes and propagates, resulting in higher current densities (Figure 7). This phenomenon could have several causes. On the one hand, different electrochemical reactions can take place, which lead to a different charge transfer. On the other hand, the surface of the impregnated carbon can change, and thus more and less charge can be transferred. So far, it has been observed in solution experiments that in E4 the existing pores on the surface become larger with the anodic polarisation. Therefore, one can say that higher applied potentials do not necessarily achieve higher current densities with otherwise identical parameters in long-term polarisation experiments with carbon anodes.

### SBR-impregnated carbon (S4)

With S4, the current density decreases when the potential is increased from P2 to P3, in contrast to E4. This applies to both storages. The reason for this could be the destruction of the SBR-based layer on the carbon surface at this potential, which is apparently different in the mortar than in solution. On the basis of past publications (Asgharzadeh and Raupach, 2018a, 2018b), the destruction of polymer impregnation of CFs under anodic polarisation could be clarified. First of all, different surface oxides form on the CF. The surface oxides are further oxidised under anodic polarisation. In a strongly alkaline environment, carbon could oxidise, and this leads to the formation of carbonates. The reaction products and the kinetics of carbon dissolution are influenced by the electrolyte. Asgharzadeh and Raupach (2018b) have shown that the SBR-based coating with anodic polarisation above a certain potential separated from the investigated carbon. In the solution, the coating could completely detach and fall off. However, in the mortar test, these layers could de-bond but still remain attached to the carbon. These layers may be inhibitory or conductive as a reaction and affect the anodic polarisation.

Generally, S4 specimens deliver more current at lower potential than E4. For instance, 10·64 mA/m$^2$ at 1205 mV against a normal hydrogen electrode (NHE) with M1-S4-UW-P2

compared to 4·42 mA/m$^2$ at 1281 mV against NHE with M1-E4-UW P1. This effect is already known from the investigations in saturated calcium hydroxide solution (Asgharzadeh and Raupach, 2018b). SBR-based coatings can shrink after production and form defects on the carbon surface, allowing better polarisation.

The S4 anodes achieve higher current densities than the E4 anodes at levels P1 to P5. This effect is discussed extensively in Asgharzadeh and Raupach (2018b). They explain that the charge transfer is caused by the defects of the impregnation on the surface. The defects on the surface are probably caused by the shrinkage of SBR-based material during drying. SBR has a greater exposed surface from the outset, which makes charge transfer possible. These layers are destroyed by polarisation after exceeding certain potentials.

The results of this work confirm the conclusions of investigations in calcium hydroxide solution, as shown by Asgharzadeh and Raupach (2018b) regarding the destruction of impregnation at anodic polarisation above a certain potential. The results in mortar specimens especially for specimens embedded in M2 show that the current density at P5 is significantly higher than other potentiostatic polarisation points. This could be due to the destruction of the impregnation, which allows more charges to be transported. This potential, where the impregnation begins to be destroyed, is to be determined by a potentiodynamic measurement and can be recognised by a hump at about 1400 mV against NHE in the investigated materials. Asgharzadeh and Raupach (2018b) have shown that the carbon filaments remain intact under impregnation at current densities below 20 mA/m$^2$.

### MMO-coated titanium

The curves of current density plotted against time with MMO-coated titanium anodes are decreasing with both storages (Figure 11). It is interesting to see that, in contrast to carbon anodes, the current densities with titanium anodes with storage 20/80 exceed those with storage UW. However, the curves get closer, and at 240 d both current densities are almost equal at about 58 mA/m$^2$. At P5 (1440 mV) the current density (about 58 mA/m$^2$) is much higher than that of the carbon anodes at similar potentials. The MMO-coated titanium anodes thus deliver significantly higher current densities than the anodes made of carbon at a potential of about 1440 mV. However, at 240 d the current densities of the tested carbon textiles are still sufficient for typical CP applications and there is no indication of further decrease, in contrast to the MMO-coated titanium anodes (see Figures 10 and 11).

## Mortar

In the following, comparison of the current densities after 240 d obtained with different mortars – the anode material being equal – is based on almost matching potentials. With E4 and storage UW, current densities are much lower with M2 (at P1 to P4) as compared to M1 (at P1 to P5). With M2 (at P1 to P4), current densities differ only slightly with storage, in contrast to M1, where the storage UW always leads to much higher current densities compared to storage 20/80. Only at P5 is an influence of storage also visible with M2. Hence, the electrolyte resistivity of M1 is much more affected by wetting.

Table 5. Electrical resistivity of mortars

| | Resistivity: Ωm |
|---|---|
| Specimens from UW storage: mV | Anode versus cathode |
| M1-E4-P1-1281 | 330 |
| M1-E4-P2-1408 | 310 |
| M1-E4-P3-1411 | 360 |
| M1-E4-P4-1701 | 397 |
| M1-E4-P5-1891 | 313 |
| M1-S4-P1-1075 | 291 |
| M1-S4-P2-1205 | 250 |
| M1-S4-P3-1345 | 260 |
| M1-S4-P4-1515 | 270 |
| M1-S4-P5-1875 | 255 |
| M2-E4-P1-1292 | 721 |
| M2-E4-P2-1402 | 748 |
| M2-E4-P3-1472 | 805 |
| M2-E4-P4-1772 | 789 |
| M2-E4-P5-2181 | 745 |
| M2-S4-P1-1002 | 690 |
| M2-S4-P2-1122 | 685 |
| M2-S4-P3-1212 | 695 |
| M2-S4-P4-1342 | 670 |
| M2-S4-P5-1672 | 667 |

With S4, current densities with M1 are generally much higher at almost matching potentials compared to M2 for both storages. Again, M1 is more sensitive to wetting. In summary, M1 provides better mortar conductivity in dry condition. The conductivity of M1 can be improved much more by wetting compared to M2. This result is supported by independent measurements of electrical resistivity of mortar specimens made of M1 and M2 using an LCR measurement device at a frequency of 100 Hz (Table 5).

## Changes of mortars and carbon textiles over polarisation time

Visible changes or damage due to polarisation have not yet been observed for any of the 50 mortar specimens. In the range of the critical potentials observed in previous works (Asgharzadeh and Raupach, 2018b), a degradation of the anodes can be assumed for all test specimens with carbon anodes. Further, it is assumed that the destruction of SBR-based coating and epoxy impregnation will occur. It is to be expected that the critical potentials in mortar are different because the electrolyte affects the electrochemical reactions. The results of the solution experiments also indicate that the degradation leads to a long-term decrease in the current densities.

A loss of contact of anode and mortar or destruction of the mortar by acidification due to oxygen evolution at current densities between 1 and 20 mA/m$^2$ can be ruled out, as several years' use of MMO-coated titanium as the CP anode at the same current densities does not cause damage in normal cases.

### Results of instant-off measurements

To determine the IR-drop and the compensated anode potentials, instant-off measurements were carried out. The results of the measurements are listed in Table 6.

Table 6. Results of the instant-off measurements

| | Instant-off potential: mV vs NHE (storing 20/80) | | Instant-off potential: mV vs NHE (storing UW) | |
|---|---|---|---|---|
| Specimen: mV | Day 57 | Day 240 | Day 57 | Day 240 |
| M1-E4-P1-1281 | 1261 | 1262 | 1233 | 1207 |
| M1-E4-P2-1408 | 1388 | 1387 | 1350 | 1350 |
| M1-E4-P3-1411 | 1391 | 1394 | 1355 | 1352 |
| M1-E4-P4-1701 | 1640 | 1637 | 1625 | 1581 |
| M1-E4-P5-1891 | 1734 | 1733 | 1686 | 1571 |
| M1-S4-P1-1075 | 1023 | 1019 | 995 | 976 |
| M1-S4-P2-1205 | 1103 | 1095 | 1102 | 1102 |
| M1-S4-P3-1345 | 1275 | 1283 | 1140 | 1114 |
| M1-S4-P4-1515 | 1318 | 1313 | 1186 | 1192 |
| M1-S4-P5-1875 | 1552 | 1452 | 1558 | 1609 |
| M1-Ti-P1-475 | 474 | 474 | 475 | 443 |
| M1-Ti-P2-545 | 544 | 545 | 544 | 544 |
| M1-Ti-P3-645 | 644 | 644 | 644 | 618 |
| M1-Ti-P4-793 | 782 | 782 | 774 | 754 |
| M1-Ti-P5-1440 | 993 | 995 | 989 | 972 |
| M2-E4-P1-1292 | 1271 | 1272 | 1255 | 1244 |
| M2-E4-P2-1402 | 1373 | 1375 | 1372 | 1318 |
| M2-E4-P3-1472 | 1452 | 1454 | 1422 | 1439 |
| M2-E4-P4-1772 | 1653 | 1652 | 1647 | 1530 |
| M2-E4-P5-2181 | 1893 | 1890 | 1773 | 1604 |
| M2-S4-P1-1002 | 987 | 985 | 982 | 967 |
| M2-S4-P2-1122 | 1085 | 1092 | 1084 | 1089 |
| M2-S4-P3-1212 | 1170 | 1179 | 1174 | 1182 |
| M2-S4-P4-1342 | 1295 | 1296 | 1288 | 1281 |
| M2-S4-P5-1672 | 1527 | 1483 | 1460 | 1446 |

The instant-off potentials at 57 d and 240 d show the same grading as the on-potentials that are set.

### Visual analysis of the sawn specimen

The sawn specimen was visually examined for significant changes in the mortar or carbon. These changes could be visible in the form of colour changes in mortar. If the carbon had been destroyed, the mortar should have looked black. No changes of the kind reported by Zhang *et al.* (2016) could be detected (Figure 13).

## Conclusions and outlook

In this work, experiments on carbon anodes in mortar specimens were carried out, and new insights into the state of the durability of carbon fabric under anodic polarisation were obtained.

Although permanent polarisation generally leads to decreasing current densities and thus to a loss of performance in the CP anodes, the current densities after 240 d are still sufficient for typical CP in practice and further decrease does not seem to occur. The decreasing current densities were found for carbon anodes with epoxy resin and SBR-based coating as well as for titanium anodes. For this reason, the decreasing current densities are not exclusively caused by a degradation of the carbon anodes.

In summary, the following provisional statements may be made:

(*a*) CP with the investigated carbon anodes is possible. The carbon anodes can provide sufficient protection current densities at relevant current densities for the CP.
(*b*) The investigated impregnations are de-coated from the carbon from a certain potential, which should be considered for the simultaneous use of the carbon textiles as CP anodes and reinforcement of the component (strengthening). This potential is to be determined after the potentiodynamic test and is shown by a hump at about 1400 mV against NHE.

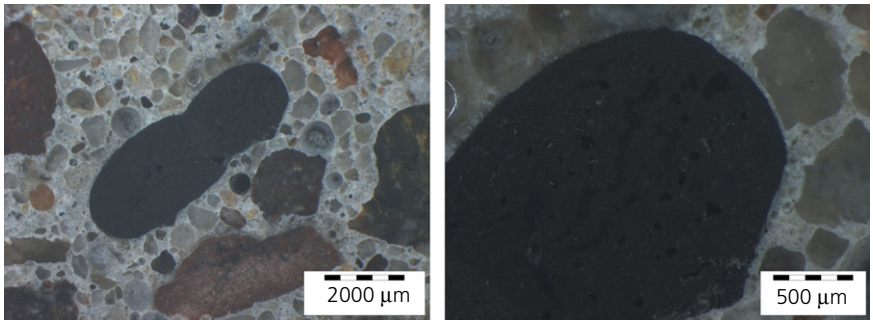


Figure 13. Optical microscope images of S4 carbon embedded in M1 mortar

(*c*) The carbon filaments within the carbon textiles used as CP anodes have not been destroyed with the protective current densities below 20 mA/m$^2$.
(*d*) Destruction of the mortar due to acidification in the CP with carbon textiles due to current densities below 20 mA/m$^2$ can be excluded, since experience has shown that using MMO-coated titanium with the same protective current densities does not lead to decoupling of the anodes and destruction of the mortar.
(*e*) The current density of CP systems can be strongly influenced by temperature and humidity changes. For anodes made of carbon coated with SBR-based material, the impact is greater than for epoxy-impregnated carbon and MMO-coated titanium with the same mortar.
(*f*) Carbon coated with SBR-based material allows for higher current densities than epoxy-impregnated carbon when used as an anode in mortar. In comparison with MMO-coated titanium anodes, however, the current densities at the same potential are significantly smaller.

The reasons for the decreasing current densities must be examined in more detail after completion of the permanent polarisation by microstructural investigations. This requires appropriate sampling from the specimens. It would be desirable to examine the surface of the carbon by SEM before and after polarisation in mortar specimens. On the basis of the results, a model should be developed for the estimation of the service life.

The destruction of the impregnation above a certain potential should be checked by tensile strength tests or bending tensile tests.

## REFERENCES

Anwar MS, Sujitha B and Vedalakshmi R (2014) Light-weight cementitious conductive anode for impressed current cathodic protection of steel reinforced concrete application. *Construction and Building Materials* **71**: 167–180.

Asgharzadeh A and Raupach M (2018a) Development of a test method for the durability of carbon textiles under anodic polarisation. In *Service life and durability of reinforced concrete structures (RILEM bookseries)*. Springer International Publishing, Basel, Switzerland, pp. 143–158.

Asgharzadeh A and Raupach M (2018b) Durability behavior of polymer impregnated carbon textiles in alkaline solution as CP anode. *Materials and Corrosion* **70(2)**: 345–356.

Bertolini L, Bolzoni F, Pastore T and Pedeferri P (2004) Effectiveness of a conductive cementitious mortar anode for cathodic protection of steel in concrete. *Cement and Concrete Research* **43(4)**: 681–694.

Chini M (2010) *Pan-based carbon fiber as anode material in cathodic protection systems for concrete structures*. Doctoral thesis, Norwegian University of Science and Technology, Trondheim, Norway.

Chini M, Antonsen R, Vennesland O, Mork JH and Arntsen B (2008) Polarization behavior of carbon fiber as an anodic material in cathodic protection. In *Proceedings of the 11th DBMC Conference on Durability of Building Materials and Components* (Türkeri AN and Sengül Ö (eds)). Istanbul Technical University, Istanbul, Turkey, pp. 897–903.

Mietz J and Raupach M (2015) Untersuchungen zur anwendbarkeit leitfähiger beschichtungen auf karbonbasis für den einsatz als fremdstromanode im kathodischen korrosionsschutz von stahlbetonbauteilen. Technical Report of AiF research project 17076 N/1. Bundesanstalt für Materialforschung und–prüfung (BAM) Berlin and Institut für Bauforschung (ibac) der RWTH Aachen, Aachen, Germany.

Poltavtseva M, Ebell G and Mietz J (2015) Electrochemical investigations of carbon-based conductive coatings for application as anodes in ICCP systems of reinforced concrete structures. *Materials and Corrosion* **66(7)**: 627–634.

Van Nguyen C, Lambert P, Mangat P, O'Flaherty F and Jones G (2012) The performance of carbon fibre composites as ICCP anodes for reinforced concrete structures. *ISRN Corrosion* **2012**: 814923, http://dx.doi.org/10.5402/2012/814923.

Vennesland O, Haug R and Mork JH (2006) Cathodic protection of reinforced concrete – a system with woven carbon mesh. In *Concrete Repair, Rehabilitation and Retrofitting* (Alexander M, Beushausen H-D, Dehn F *et al.* (eds)). Taylor and Francis Group, London, UK, pp. 811–815.

Zhang EQ and Tang L (2014) A novel anode material for cathodic prevention of steel reinforced concrete structures with hybrid functions. In *Proceedings of XXII Nordic Concrete Research Symposium* (Bager DH (ed.)). Nordic Concrete Federation, Oslo, Norway, pp. 435–438.

Zhang EQ, Tang L and Zack T (2016) Carbon fiber as anode material for cathodic prevention in cementitious materials. In *Proceedings of the 5th International Conference on Durability of Concrete Structures, Shenzhen, China* (Xing F and Zhu JH (eds)). Purdue Scholarly Publishing Services, Lafayette, USA, pp. 308.

applied sciences

MDPI

*Article*

# Damage Mechanisms of Polymer Impregnated Carbon Textiles Used as Anode Material for Cathodic Protection

**Amir Asgharzadeh *, Michael Raupach**

Institute of Building Materials Research at RWTH Aachen University; raupach@ibac.rwth-aachen.de

* Correspondence: zadeh@ibac.rwth-aachen.de, Tel.: +49 241 8095140

Received: 25 November 2018; Accepted: 25 December 2018; Published: 29 December 2018

**Featured Application: Conventional cathodic corrosion protection (CP) systems usually use MMO-coated titanium as anode material. Carbon textiles as anode material provide sufficient current densities for CP as well as strength for structural reinforcement. Therefore, durability is an important issue for both the structure and the CP view. This work should show the border potentials where the impregnation and sizing of carbon textiles are destroyed under anodic polarization.**

**Abstract:** Carbon textiles as anode material for cathodic corrosion protection (CP) have been used in several reinforced steel structures. However, experience with durability is limited. To date, various influencing factors have been discovered and systematic tests on different carbon textiles with different impregnation materials in various environmental media have been carried out and considered the degradation of the impregnation materials. In this work the boundary potentials are determined at which the impregnation and sizing is destroyed under anodic polarization and the damage mechanisms are described.

**Keywords:** textile reinforced concrete; cathodic corrosion protection; durability

## 1. Introduction

Carbon textiles consist of thousands of bundled carbon fibres. Before carbon fibres are combined into bundles, their surface needs to be electrochemically activated (by anodic oxidation in an electrolytic solution). Each fibre is then coated by a mixture of various chemicals (sizing) to protect it from mechanical damage during production handling and improve its wetting performance [1–3]. Furthermore sizing leads to an increased chemical reactive site as well as enhanced adhesion between carbon and impregnation material [4,5]. After single carbon fibres are bundled together, the so-called carbon roving is again impregnated to improve adhesion and handling for further application. Usually, epoxy resin or styrene-butadiene rubber (SBR) based polymers are used for impregnation.

The thesis of Wetjen [6] gives an overview of the production and processing of carbon. The following statements are based on this source, unless otherwise indicated. The carbon rovings usually consist of thousands of individual combined carbon fibres, which are also called filaments and have an average thickness of 5–7 microns. Carbon fibres consist of 92% by weight of carbon. They can be produced chemically from different polymers, the most common being the production from polyacrylonitrile (PAN), since the highest strengths with high carbon yield can be achieved at comparatively low price. Graphite consists of hexagonal layers in which each carbon atom is connected to three other carbon atoms with a strong covalent bond. The individual layers are connected only by relatively weak London forces, whereby the distance of the layers in relation to

the distance of the carbon atoms in the hexagons is large and the direction-dependent conductivity of graphite can be explained [6].

Compared to graphite, carbon fibres have a turbostratic structure that results from random spinning, folding, splitting, canting, branching and concatenation of the lattice structure in the manufacturing process. This inhomogeneity explains both the increased strength between the basal planes and the increased reactivity of the carbon fibre surface in comparison. In addition, the structural inhomogeneity increases the spacing between the lattice planes.

After production of the carbon fibre, surface activation of the carbon fibre follows, typically by electrochemical anodic oxidation in an electrolyte. The amount and type of functional groups formed on the surface depends inter alia on the duration of polarization, the electrolyte and the electrical potential. The surface activation is done to obtain a good wettability of the carbon fibre over a later applied sizing or other impregnating materials by a higher proportion of polar functional groups [6].

Poltavtseva et al. [7] have described the formation of surface oxides in carbons by summarizing relevant literature. The formation of surface oxides is complex because it is not possible to separate the different reactions from each other. It depends on the pH, electrode potential, pressure, temperature and humidity as well as the physical and chemical properties of the carbon compounds. Thus, a different dissolution process results for different carbon-based materials, since materials such as carbon black, graphite and carbon fibres differ in the size and orientation of the graphitic crystalline layers.

Pure graphite consists of hexagonal layers as described above. While graphite has many surface defects, carbon fibres without activation have a high degree of longitudinal orientation with fewer defects. Without these lattice defects, the graphitic crystalline layers behave inertly. The existing lattice defects, pores and edges provide for free valences, which are already functionalized under normal conditions to form surface oxides. Anodic polarization causes the dissolution of water and the generation of further oxygen-containing functional groups on the surface. First, hydroxyl ions are discharged to hydroxyl radicals by the electrolysis of water according to equations (1) and (2).

$$C_{(s)} + H_2O \rightleftharpoons C_{(s)}OH_{ads} + H^+ + e^- \quad (1)$$

$$C_{(s)} + OH^- \rightleftharpoons C_{(s)}OH_{ads} + e^- \quad (2)$$

These radicals immediately react to form hydroxyl, carboxyl, carbonyl or lactone moieties, which are accompanied by an increase in the oxygen content at the carbon surface. The possible functional groups on the graphite surface are shown in Figure 1. Rueffer et al. [8], however, doubt the formation of hydroxyl radicals on the basis of their investigations as an intermediate step and assume a direct incorporation of oxygen into the functionalized groups. The functional groups have different oxidation states and can be further oxidized up to the elimination of carbonates and carbon dioxide [6]. According to Chung [9], these surface oxides have a lower conductivity than non-activated graphitic carbon fibres.

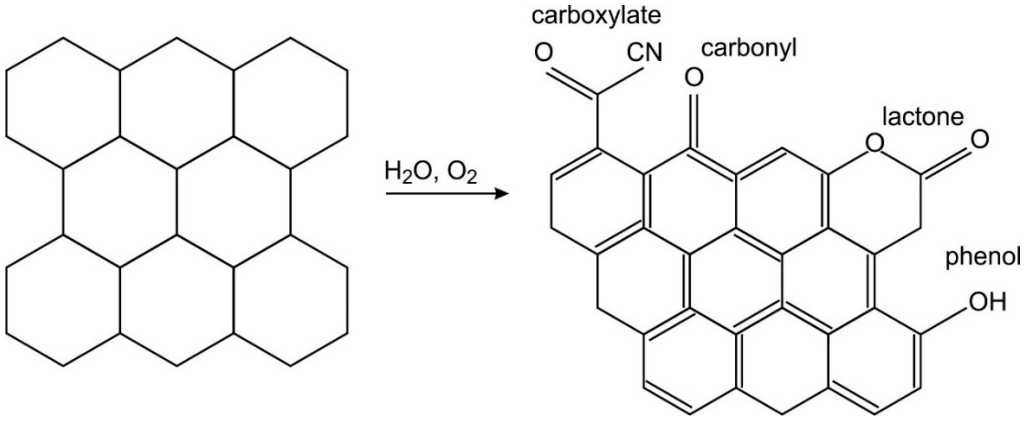


**Figure 1.** Formation of surface oxides in graphite [7].

After activation of the carbon fibre and cleaning of detached carbon fibre fragments, the carbon fibre is always coated in industrial applications [6]. For this, the carbon fibre is passed through a sizing bath filled with a polymer solution or dispersion. However, there are other methods of coating such as electrolytic deposition, electrolytic polymerization and plasma polymerization. As size typically polymer systems are used which have good chemical-physical compatibility for the further use of the carbon fibre. When using epoxy resins, epoxies are used, for example. Other polymer systems include polyhydroxyether, polyphenylene oxides, polysulfones, silanes and cyanamides. The sizing ensures good processability in subsequent processes, good wetting behaviour of the carbon fibre for the impregnation matrix and a strong chemical-physical interaction between these two components for good adhesion. Possible adhesion mechanisms are: mechanical interlocking, secondary bonds, such as London forces and chemical bonds, such as covalent bonds.

In the final processing step, the carbon fibres are combined into rovings and impregnated with materials such as epoxy resin matrix or styrene butadiene rubber matrix (SBR). For a good fibre-matrix interaction, a good mixing of the components carbon fibre, sizing and matrix is essential. During the application of the matrix, with "no release" of the layer, "partial release" or "complete release" of the size, there may be three different interphase formations. In the case of complete release, the sizing thoroughly mixes with the matrix, providing the best mechanical properties. The worst mechanical properties are achieved when there is no intermixing between the size and the matrix, that is no detachment.

Earlier research [10–12] has shown that carbon textile is a suitable anode-material for corrosion protection (CP). Various experiments were conducted in order to investigate the behaviour of carbon textiles under anodic polarization. Carbon textiles were tested both in saturated calcium hydroxide solution and in mortar test specimens. It has been found, that the structure of carbon textiles itself is not affected by anodic polarization. However, sizing and impregnation materials suffer considerable destruction in some cases.

Asgharzadeh et al. [12] investigated the durability of impregnated carbon textile under permanent anodic polarization while stored in saturated calcium hydroxide solution. Carbon textile was potentiodynamically polarized in saturated calcium hydroxide solution. Starting with the open circuit potential, the applied potential was increased at a constant rate of 2 mV per minute until an overall potential shift of 2200 mV in anodic direction was achieved. Based on the obtained current-density versus (compensated) potential curves, three potentials were selected, which indicate changes in the carbon textiles' electrochemical properties. Potentiostatic tests were performed with the identified potentials. After the polarization tests were completed, the test solution was collected. In order to draw conclusions about a possible decomposition of the carbon textile, the carbon content of the solution was analysed. It was found, that the solutions in which polarization of the carbon textile occurred had higher carbon contents than solutions in which unpolarized carbon textiles were stored as reference solution. Furthermore, the carbon content increases with increasing potential of potentiostatic polarization. However, the additional carbon could originate from several sources, such as the carbon textile itself, the impregnation material or the surrounding air. In order to further identify the carbon source, the experiments were repeated with unimpregnated carbon textile. In this case, the carbon content of the solution corresponded to the carbon content of the reference solution. It is therefore assumed, that the additional carbon, which was found in the solution in which polarization tests of impregnated carbon textiles were conducted, originates either from the impregnation material or the surrounding air.

Although SEM images showed a destruction of the impregnating material after polarization, the information at which potentials they are destroyed is missing, which are to be investigated in this paper. Furthermore, based on these results, the influence of polarization on various impregnation materials for carbon textiles is investigated in more detail by additional tests.

## 2. Materials

As an anode material, the styrene-butadiene rubber (SBR) impregnated textile S4 was selected because this material achieved the highest current densities and thus best polarization behaviour in

former experiments [12]. For reasons of comparability, the epoxy impregnated textile E4 was taken which has the same mesh size as S4. In addition, carbon rovings without impregnation but with sizing (UC, see Table 1) were used to determine the destruction of the sizing under anodic polarization. For comparison purposes, carbon rovings without impregnation and without sizing (UC_WS, see Table 1) were also used. This confirmed the actual destruction of the sizing.

**Table 1.** Details of carbon textiles used in the investigations.

| | Specimen Specification | Sizing | Impregnation Material | Mesh Size [mm/mm] 0°/90° |
|---|---|---|---|---|
| impregnated carbon | E4 | yes | Epoxy | 38/38 |
| textile | S4 | yes | SBR | 38/38 |
| unimpregnated carbon | UC | yes | - | - |
| textile | UC_WS | no | - | - |

## 3. Investigations

### *3.1. Specimen Preparation*

The carbon rovings and the counter electrode made of MMO-coated titanium mesh were attached to PVC spacers with cable ties. A reference electrode $MnO_2$ was attached to the spacer between the working electrode and the counter electrode and care was taken to ensure that there is no short-circuit between the reference electrode and any protruding carbon fibres.

The specimens were placed in a container with saturated calcium hydroxide solution.

### *3.2. Potentiodynamic Polarization*

Potentiodynamic tests are used to obtain current density potential curves that allow conclusions to be made about the material behaviour.

The potential was increased from OCP to 2200 mV. The duration of the potentiodynamic test was approximately 18 hours.

### *3.3. Potentiostatic Polarization*

In order to perform the potentiostatic measurements, the potentiodynamic measurements had to be evaluated and the potential points for the tests had to be selected. The different panel areas and especially the change of the slope of the curves in Section 4.1 could be attributed to different electrochemical processes. In order to verify this, it was decided to carry out tests in these three areas, which are hereinafter referred to as potentiostatic tests.

The potentials of the potentiostatic tests are listed in Table 1. They are referred to below as levels 1, 2 and 3.

**Table 1.** Potentiostatic potentials on level 1, 2 and 3.

| Material | Level 1 | Level 2 [mV] vs. NHE | Level 3 |
|---|---|---|---|
| E4 | 940 | 1490 | 1940 |
| S4 | 490 | 1490 | 1840 |
| UC | 690 | 1300 | 1940 |
| UC_WS | 690 | 1300 | 1940 |

For the potentiostatic tests, specimens with the carbon fabrics E4, S4, UC and UC_WS were chosen as working electrode. Counter and reference electrode were produced as already described. The specimen setup for E4 and S4 can be seen in Figure 2. In these tests, the anodes of E4 and S4 consisted of two superimposed parts, each with one connection. The larger element had dimensions

of 12 × 12 cm and the smaller element 10 × 10 cm. The test specimens with unimpregnated carbon fibres corresponded exactly to the test specimens in the presented potentiodynamic tests. Saturated calcium hydroxide solution was used as electrolyte and the test specimens were stored in the solution again 24 hours before the start of the test. Before and after the test, the pH value and the resting potential (OCP) were measured.

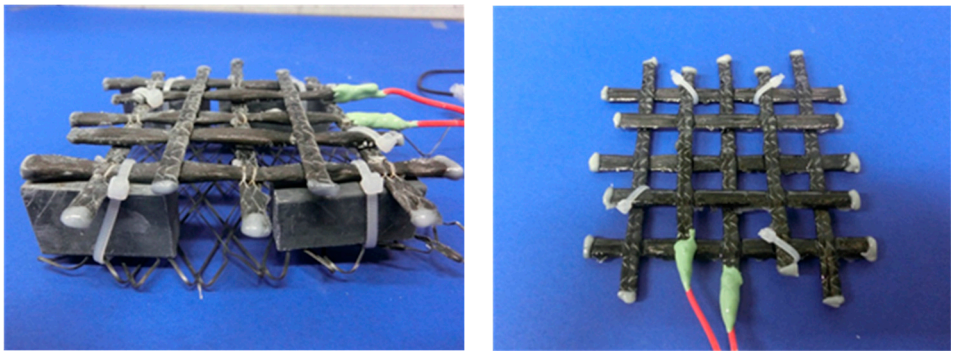

(**a**) (**b**)

**Figure 2.** Specimen with S4 anode, spacers and titanium electrode (**a**) and an E4 anode (**b**).

It should be figured out whether and how the carbon surfaces change on the different levels. In addition, the time factor for destruction can be evaluated, since the holding times are higher than those of the pure potentiodynamic tests. The potentiostatic polarization was maintained for over 72 hours. The polarization was started at the potential of the reference electrode, since a shift of the OCP by the polarization was to be expected.

## 4. Results and Discussion

### *4.1. Potentiodynamic Tests*

The results of the potentiodynamic tests on carbon textiles are shown in Figure 3 as a current-potential curve in logarithmic scaling. The potential labels P1 to P3 indicate the potentials for the potentiostatic tests, see Section 3.3.

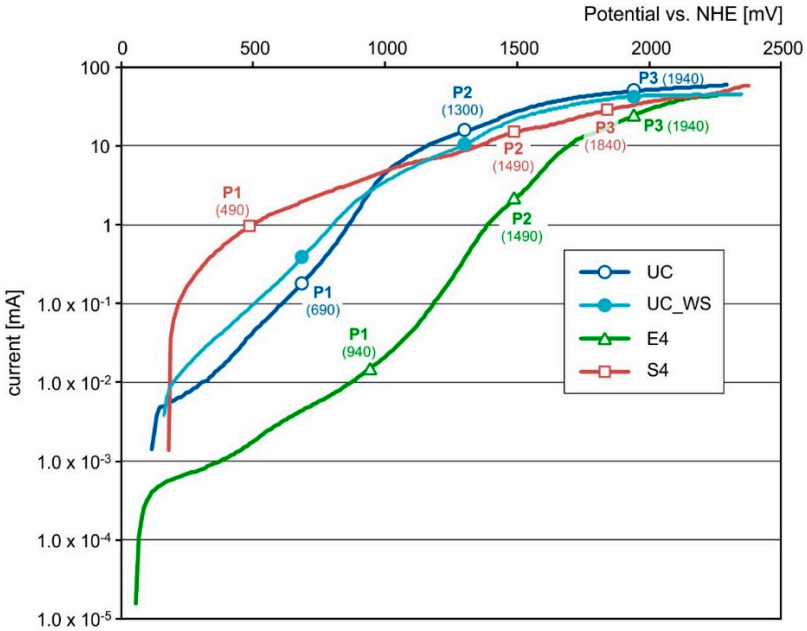


**Figure 3.** Current-potential curve for all materials.

Note, that current and not current density is plotted in Figure 3. This is due to the fact that the exact calculation of the anode surface of rovings without impregnation is complicated: the exact number of fibres in contact with the solution is undefined.

From Figure 3 it is seen that the polarizability of carbon impregnated with SBR-based material until 1000 mV versus NHE is better and thus delivers the highest current, while E4 achieves the lowest current. From 1100 mV versus NHE UC delivers more current than carbon impregnated with SBR-based material. The curve of the test with UC_WS is similar to UC with the difference that UC_WS can deliver more current up to 900 mV versus NHE and after that potential less current than UC.

The OCP of the non-impregnated carbon fibres amounts to about 100 mV versus NHE and is between the OCPs of E4 (60 mV versus NHE) and S4 (180 mV versus NHE). Panel area 1 is between 200 and 900 mV versus NHE for the non-impregnated carbon fibres. The transition section is small, the panel area 2 is between 950 and about 1100 mV versus NHE. For S4, panel area 1 is between about 300 and 1150 mV and panel area 2 between 1225 and 1300 mV. The transition section of E4 is not clearly defined, it could be between 950 and 1150 mV. The transition sections of all experiments are characterized by a brief reduction in the slope of current density followed by a renewed and steeper increase in current density.

The images of carbon samples UC before and after polarization are exemplarily displayed in Figure 4. Strong deposits can be seen on the polarized sample, which will be discussed later in this paper.

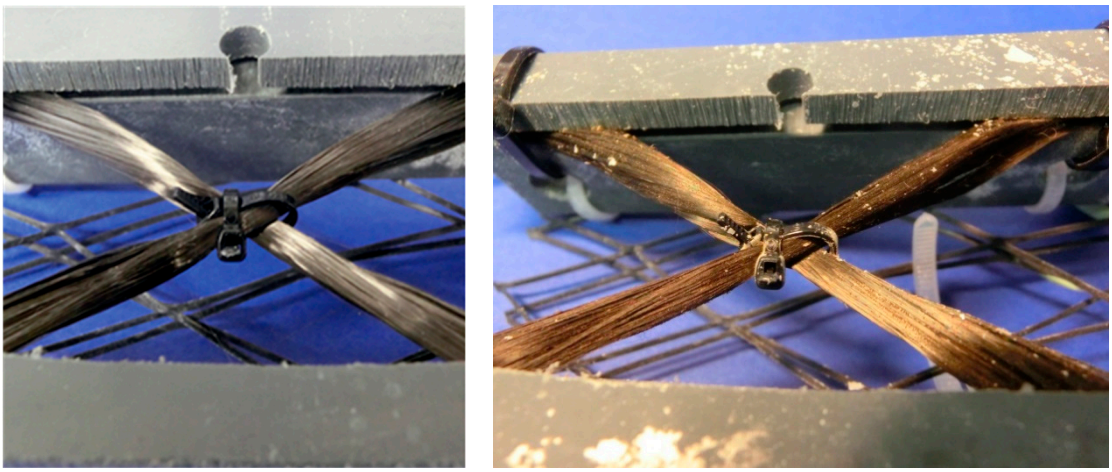

(**a**) (**b**)

**Figure 4.** Unimpregnated carbon fibres before the test (**a**) and after (**b**).

A discoloration of the calcium hydroxide solution could not be observed for the potentiodynamic experiments on all experiments.

The SEM investigations of S4 and E4 before and after polarization in Asgharzadeh et al. [12] showed a destruction of the impregnation material. There was not investigated, whether the sizing under the impregnation was affected or not. To this end, the UC sample is examined in the present study. Figure 5(a) shows the unpolarized carbon fibre. On the right the polarized carbon fibre is shown (Figure 5(b)). The carbon fibres are round and have slight longitudinal grooves. This shows cracks in the sizing both in the longitudinal and in the radial direction at regular distances. The carbon fibre underneath seems to be intact. Such a clear destruction of the sizing was observed at several carbon fibres. It is concluded that the sizing deteriorates and the carbon fibre remains intact.

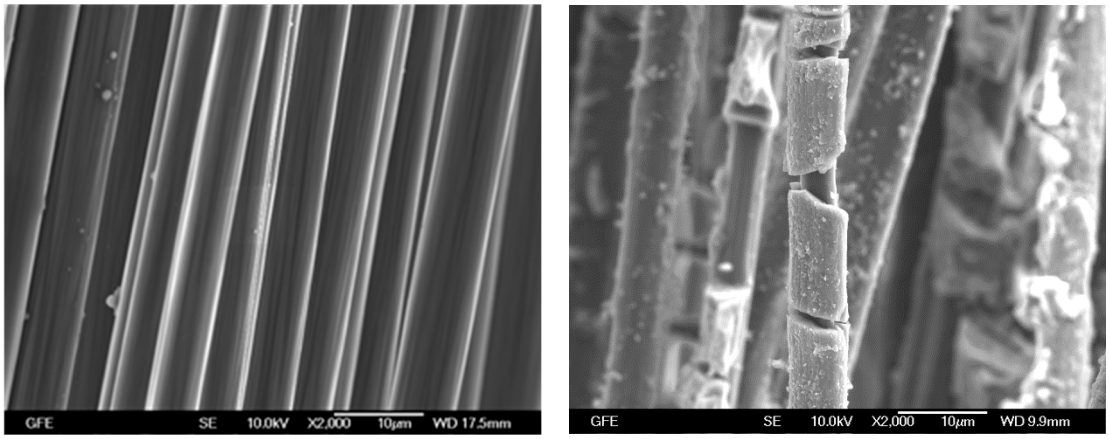


(**a**) (**b**)

**Figure 5.** SEM images of unpolarized carbon fibres (**a**) and a polarized carbon fibre (**b**).

An energy dispersive X-ray spectroscopy (EDX) of the polarized sample probing the deposition shows the presence of calcium, carbon and oxygen (Figure 6).

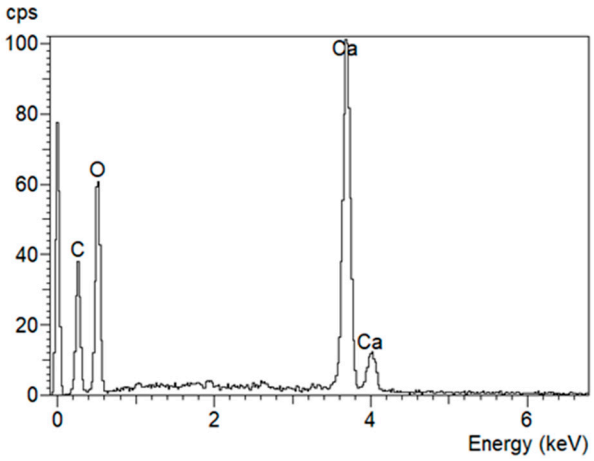


**Figure 6.** EDX analysis of the deposited film.

### *4.2. Potentiostatic Tests*

#### 4.2.1. Epoxy Impregnated Carbon (E4)

No optical changes could be detected on the carbon textile E4 after the potentiostatic polarization at level 1. The epoxy resin impregnation remained even, smooth and shiny. The specimen of level 2 shows isolated areas on which the surface is mat and rough and the structure of the carbon textile is recognizable as well as white deposits indicating the chemical bonds between carbon, calcium and oxygen. These deposits become more significant with increasing polarization, which can be seen at Figure 7 right at level 3 of potentiostatic polarization.

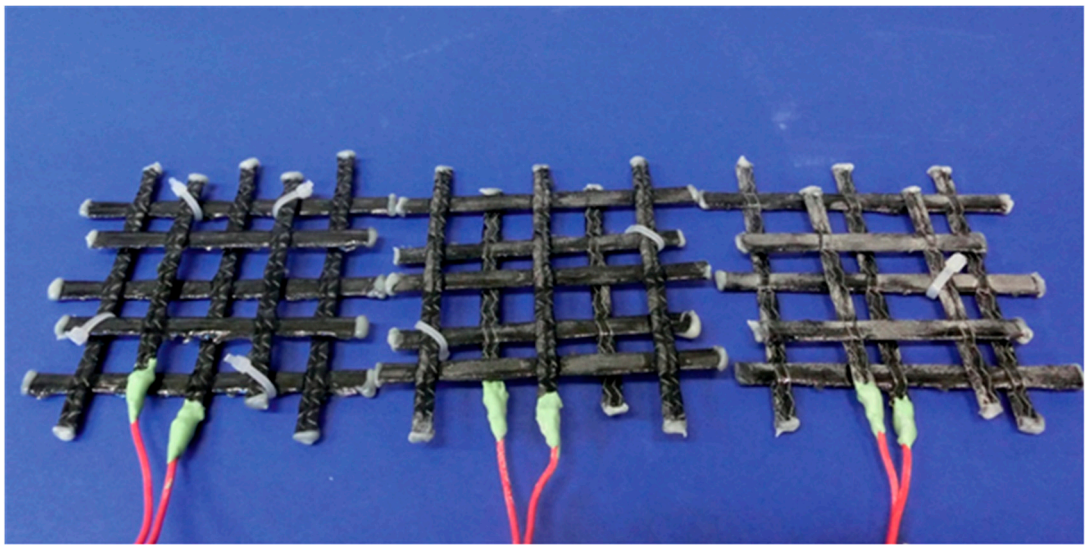

**Figure 7.** From left to right: Anodes E4 of levels 1 to 3 after polarization.

Figure 8 shows the SEM images of the carbon fibre E4 without polarization and after the polarization. No pores can be seen on the entire reference specimen (Figure 8(a)) in contrast to previous findings [12]. There were only a few of them, as well as defects. Apart from impurities and a mechanical crack, the surface is smooth due to the sample preparation. In some places the carbon fibres shine through the impregnation. The epoxy resin layer does not appear to be uniformly thick. Epoxy resin was used in various test series to interrupt conductivity [10,13–16]. Van Nguyen et al. [17] have found that the embedding of carbon anodes with epoxy resin was not successful due to insufficient conductivity.

Due to the pores, defects and the different thickness of the impregnation, it can be explained why the epoxy resin-impregnated carbon fibres are polarizable at all. The potentiostatic test at level 1 did not cause any change in the surface (Figure 8(b)). The image of the specimen polarized at level 2 (Figure 8(c)) shows grooves next to two mechanical cracks and is covered approximately in half with a crystalline deposited film. Calcium, oxygen and carbon could be detected in the coating by EDX analysis. The grooves run along the carbon fibres over which the epoxy resin impregnation is probably thinnest and are due to the destruction of the impregnation. Pores have occasionally formed in the epoxy resin unlike the accumulation of pores in Asgharzadeh et al. [12]. As with the unimpregnated carbon fibres, for the carbon fibres with epoxy resin impregnation destruction in panel area 2 is used, whereas no destruction was observed in panel area 1. Thus, the start of the destruction of the epoxy resin matrix could again be in the transition range between about 1050 and 1150 mV.

The specimen of the polarization at level 3 (Figure 8(d)) is almost completely covered with the crystalline deposited film. There are undamaged areas that are not covered with deposited film. This and individual damages between the film indicate that most damages are obstructed by the film. Hence, it can be assumed that the damage is more pronounced than at level 2.

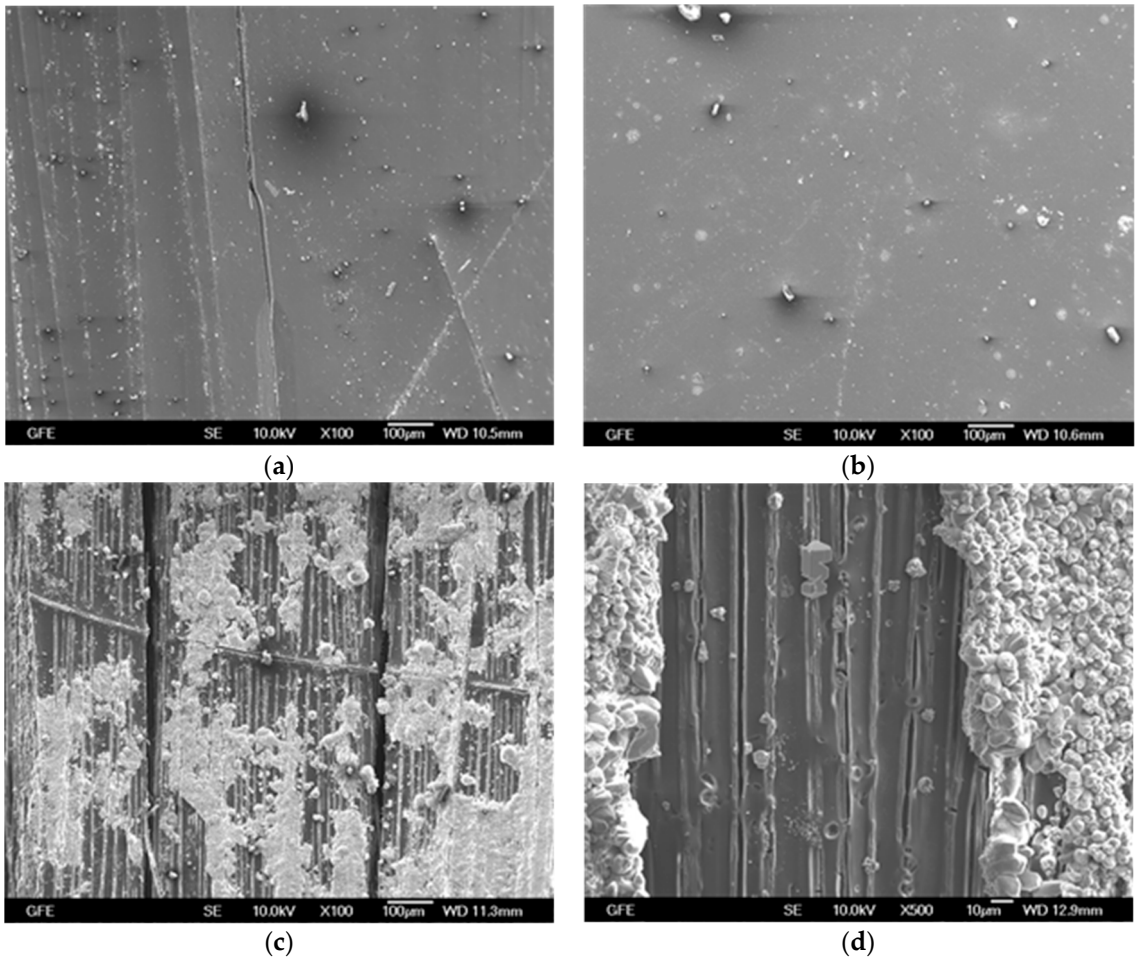


**Figure 8.** SEM images of E4: unpolarized reference (**a**), after polarization at level 1 (**b**), level 2 (**c**) and level 3 (**d**).

#### 4.2.2. Carbon Coated with SBR-based Material (S4)

The SBR-impregnated carbon S4 has a smooth and glossy surface before polarization. Overall, the surface remains glossy but is no longer smooth but rough. The specimens of levels 2 and 3 are mostly mat and rough, there are only a few glossy surfaces left. In addition, an increased resolution of the impregnation in the area of the intersection points can be observed (Figure 9).

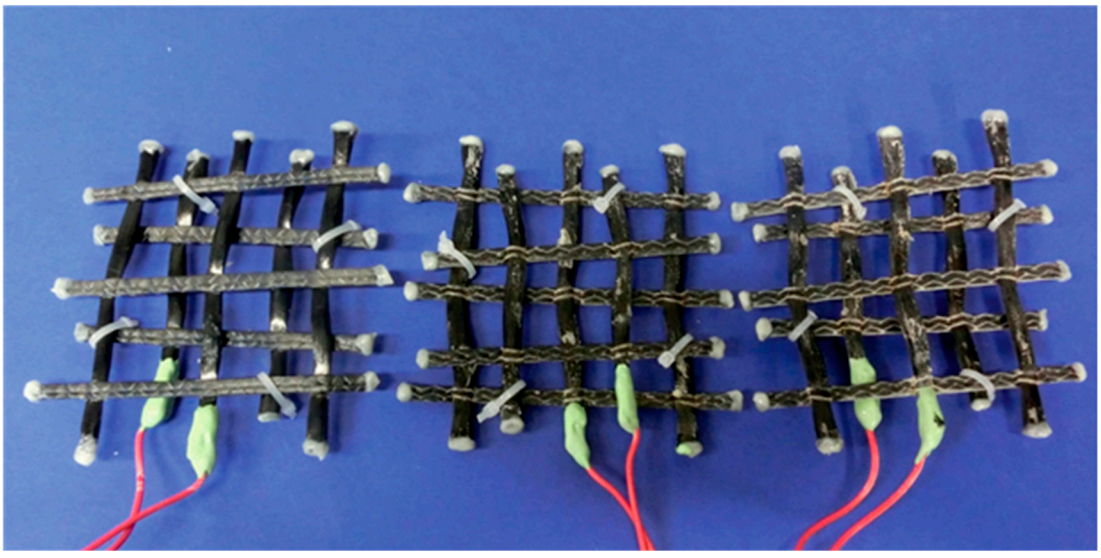

**Figure 9.** From left to right: S4 anodes of stages 1 to 3 after polarization.

Figure 10 shows the SEM images of the SBR-impregnated carbon fibre S4, the surface of the reference (Figure 10(a)) is mostly smooth apart from impurities. Sometimes the carbon fibres shine through; there are randomly arranged pores of different sizes. In the reference specimen, there are also imperfections of different sizes from 20 µm, at which the carbon fibres are exposed. Rubber is known to be non-conductive. The pores and imperfections in the impregnations as well as the poor adhesion between SBR impregnation and carbon fibre explain why the SBR-impregnated carbon fabric also shows polarizability. After the polarization at level 1, destructions are already visible at isolated points where carbon fibres are exposed (Figure 10(b)). Around these areas is a white coating that looks different. According to EDX analysis, this consists mainly of carbon and oxygen and low intensities of calcium and silicon can also be detected. Overall, significantly more carbon fibres are visible due to the impregnation, which suggests that the impregnation dissolves over a large area. A destruction of the SBR impregnation therefore already occurs in panel area 1.

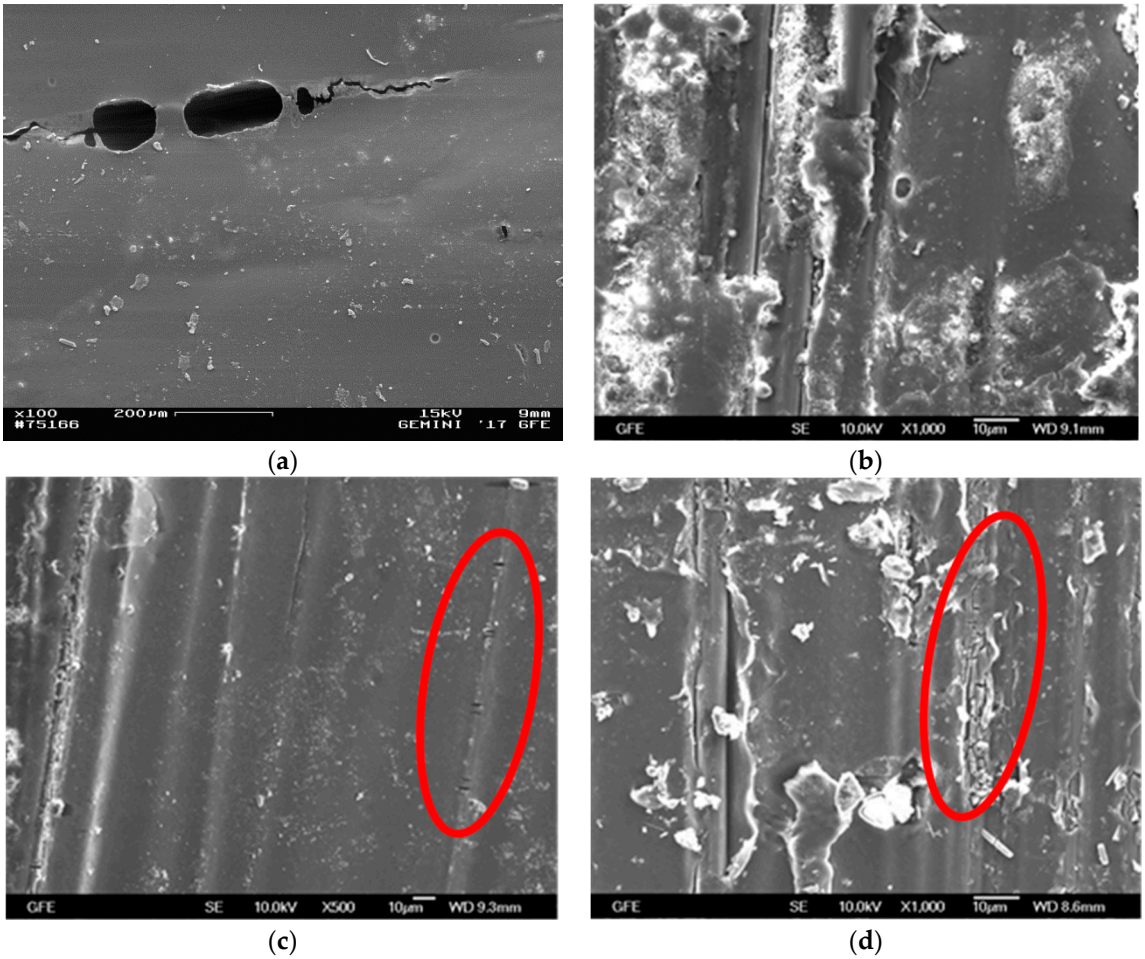


**Figure 10.** SEM images of S4: unpolarized reference (**a**), after polarization at level 1 (**b**), level 2 (**c**) and level 3 (**d**).

With increasing polarization both, the amount of deposited material and the removed surface of the impregnation increase. The impregnations already show imperfections and pores before polarization, so that a liquid electrolyte can enter the roving. Due to the poor adhesion between SBR and carbon fibre, this is particularly pronounced for the SBR-impregnated material and explains its good polarizability compared to carbon with epoxy resin impregnation. By destruction the impregnations, underlying carbon fibres come into contact with the electrolyte and increase the effective surface area with increasing dissolution. In Figure 10(c) a filament can be seen, which has become free and transverse cracks are recognizable, which can be either in impregnation or in carbon

fibre. Figure 10(d) also shows a filament, which is free of impregnation. On the basis of this picture one can say exactly that with anodic polarization this filament is attacked here and cracks developed, which do not come from the production.

Dissolution of the carbon fibres could not be achieved by the potentiostatic tests. Before the carbon fibres are dissolved, the impregnations and the sizing are first destroyed. This can be explained by the fact that the carbon fibre consists of mainly covalent carbon compounds in contrast to the impregnations and the size and the covalent bond has a higher bonding energy. Since no optical changes have occurred with E4 and S4 despite significant decomposition of the impregnation materials, destruction of the impregnation materials to carbon dioxide and calcium carbonates can be assumed. Visible decomposition particles have only formed as a result of the decomposition of the sizing of the unimpregnated carbon fibres. However, the exact composition of these particles could not be determined, since the freeze-dried residual solution consisted mainly of calcium carbonate. Calcium carbonate is formed by the reaction of calcium hydroxide with carbon dioxide:

$$Ca(OH)_2 + CO_2 \longrightarrow CaCO_3 + H_2O \quad (3)$$

However, the carbon dioxide can be a product of carbon from the dissolution reactions as well as from the air.

#### 4.2.3. Unimpregnated Carbon with Sizing (UC)

On most specimens, optical changes could already be detected after polarization. Photos of all specimens from the potentiostatic tests with unimpregnated carbon fibres are shown in Figure 11. The unimpregnated carbon fibres were glossy and soft, comparable to a brush before the test was carried out. After polarization at level 1, the carbon fibre is still soft but less shiny. This could be explained by the deposits of calcium carbonate. The solution of the tests at levels 1 and 2 showed no difference. The solution of the experiment at level 3, on the other hand, was discoloured brown and small black particles floated in the solution. The particles deposited on the ground after a few days. These sediments were freeze-dried with a small remainder of the solution and identified as calcium carbonate by Fourier transform infrared spectroscopy. Since the substance, unlike pure calcium carbonate, was not white but grey, further components must be present. However, these could not be detected by infrared spectroscopy.

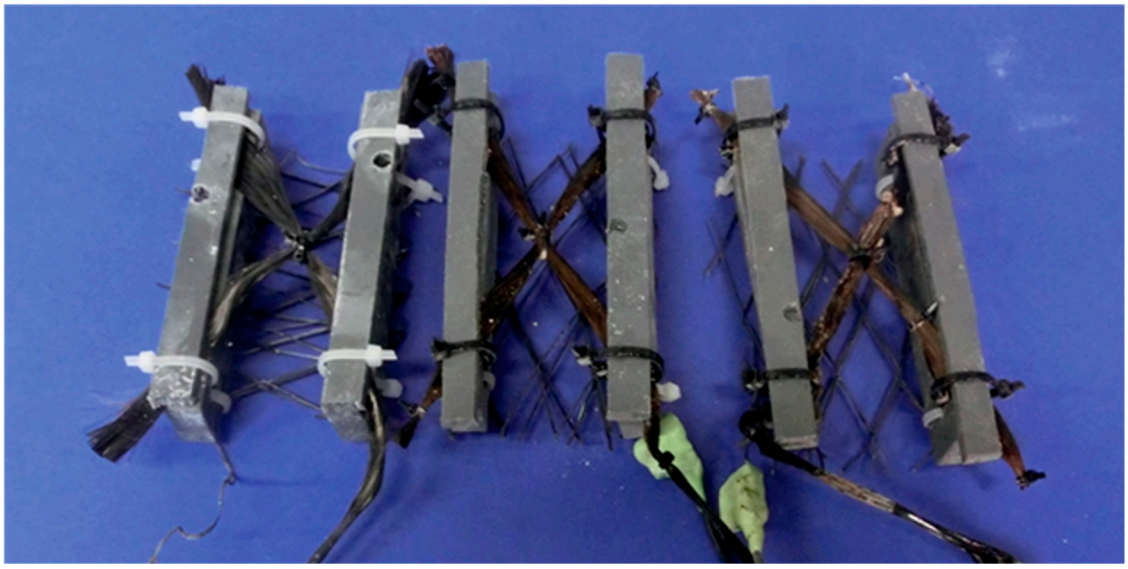

**Figure 11.** From left to right: specimen P1 of levels 1 to 3 after polarization.

Figure 12 shows the SEM images of UC specimens. The unimpregnated carbon fibres show no damage after polarization at level 1 (Figure 12(b)). Slight longitudinal grooves can already be observed at the reference (Figure 12(a)) and no consequence of polarization. Differences in contrast, especially in bright white areas, are caused by charges from the electron ray with insufficient surface

conductivity. After polarization at level 2, the sizing of many fibres is decomposed (Figure 12(c)). This can be seen in most fibres through the formation of deep but narrow longitudinal furrows. Cracks in the radial direction also occur in some fibres, as they have already been detected in the potentiostatic tests. This means that an anodic polarization on level 2 decomposes the size of unimpregnated carbon fibres. On level 1 no destruction of the coating was observed. The change in the slope in the current potential diagram in the phase of the transition range at approximately 900 mV versus NHE is therefore probably due to the reaction that sets in. The sizing of most carbon fibres polarized at level 3 shows very clear destruction phenomena in the form of radial cracks (Figure 12(d)). The decomposition of the sizing of the unimpregnated carbon fibres also took place inside the roving. It can therefore be assumed that all carbon fibres conduct electricity and are in direct contact with the electrolyte. The effective surface area of the unimpregnated carbon fibres should raise after destruction of the sizing.

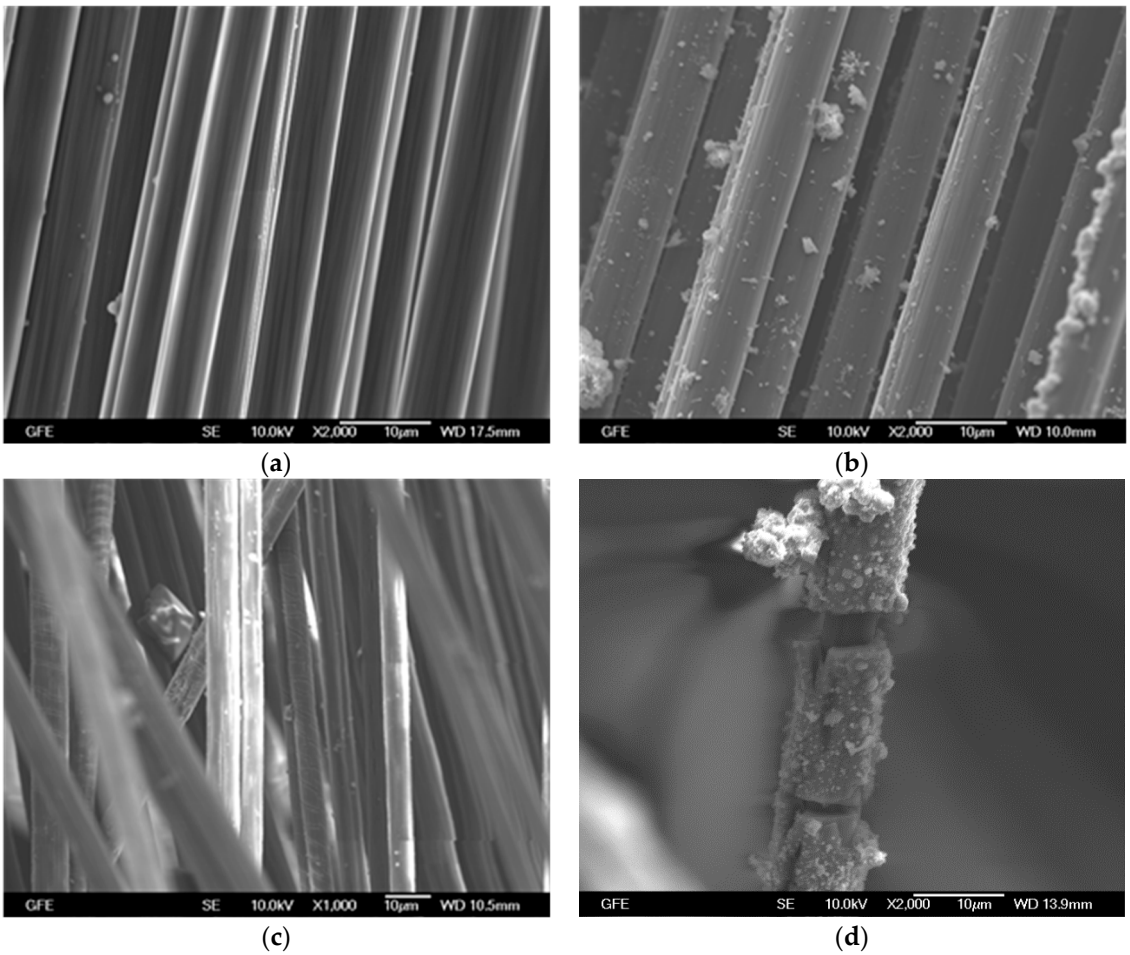


**Figure 12:** SEM images of UC: unpolarized reference (**a**), after polarization at level 1 (**b**), level 2 (**c**) and level 3 (**d**).

In Figure 12(d) it is questionable, whether this destruction is in carbon or in sizing. Because the damaged layer looks thick and the residual cross section of carbon small, this question had to be examined more closely. Three further methods were used to investigate it in more detail.

1) Examination of the average diameter of fibres in a roving

The examination of the diameter of unimpregnated carbon showed that the fibres have a diameter between 5 and 10 µm. Figure 12(d) shows that the diameter of carbon, under the deposited film around the fibre, is 6 µm and therefore in the range of diameters of unpolarized samples. Hence, no destruction of the carbon fibre is observed. This has been confirmed with several samples.

2) EDX examination of the deposited film

EDX analysis was performed on an unimpregnated carbon (UC), in a region, where the deposited film was partly flaked off. So both sides of the film could be analysed.

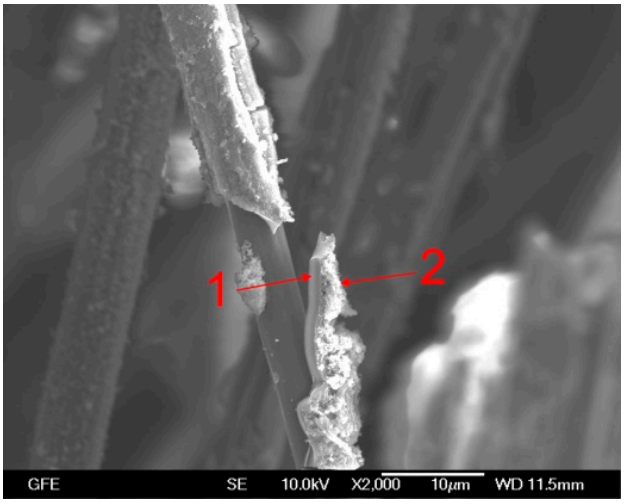


**Figure 13.** SEM image of unimpregnated carbon. 1 and 2 EDX analysis in the marked area.

Figure 13 and Figure 14 show that the inner part of the destroyed layer consists mainly of carbon, which could be part of the sizing. The outer layer indicates the presence of calcium, carbon and oxygen. These are the deposits formed due to chemical reaction between calcium of the solution and carbon from the sizing. These deposits can be found more strongly on the surface of the carbon as the polarization potential increases.

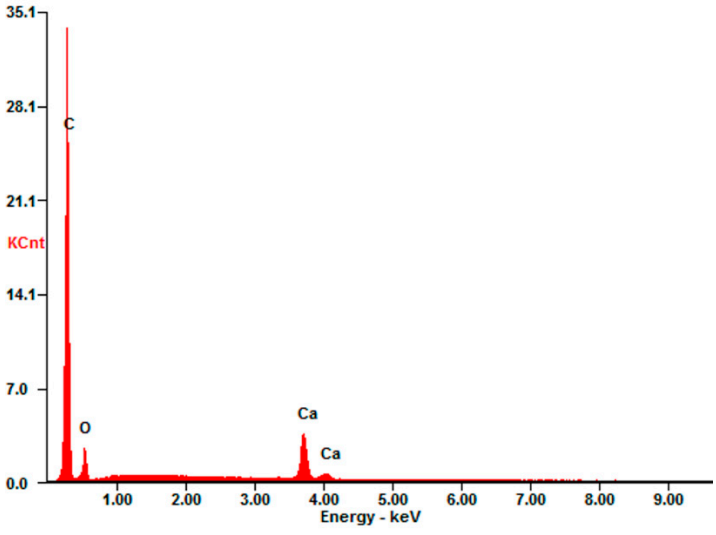


(**a**)

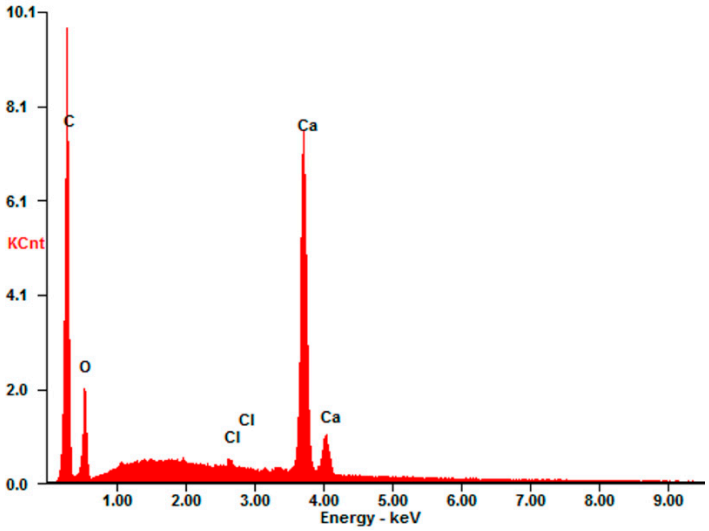


(**b**)

**Figure 14:** EDX analysis in the marked area 1 (**a**) and EDX analysis in the marked area 2 (**b**).

3) Investigation of an unimpregnated carbon without sizing (UC_WS)

Thermal gravimetric analysis (TGA)

First, TGA measurements were performed to be sure that the two unimpregnated samples with and without sizing were different and to identify whether the sample UC really has a sizing. Since the differences cannot be seen from the SEM, TGA measurements were performed to see if the weight changes with increasing temperature. From the Figure 15 it can be seen that the sample UC_WS, which has no sizing, shows no change in mass at elevated temperature. The curve of UC shows that at 300 °C the weight decreases. This indicates that the sizing begins to dissolve. The comparison of the two curves shows that the sizing has about 1 wt% of the total weight of the carbon filament. After 450 °C, it stabilizes to 600 °C and then the curve drops again. From there the carbon textiles could start to decompose. It can be assumed that the examined UC samples with sizing really have a sizing and that the destroyed layer in Figure 12(d) is the sizing including deposited film.

The decrease in the weight of sample UC-WS up to 600 °C could be due to the combustion of impurities and dirt.

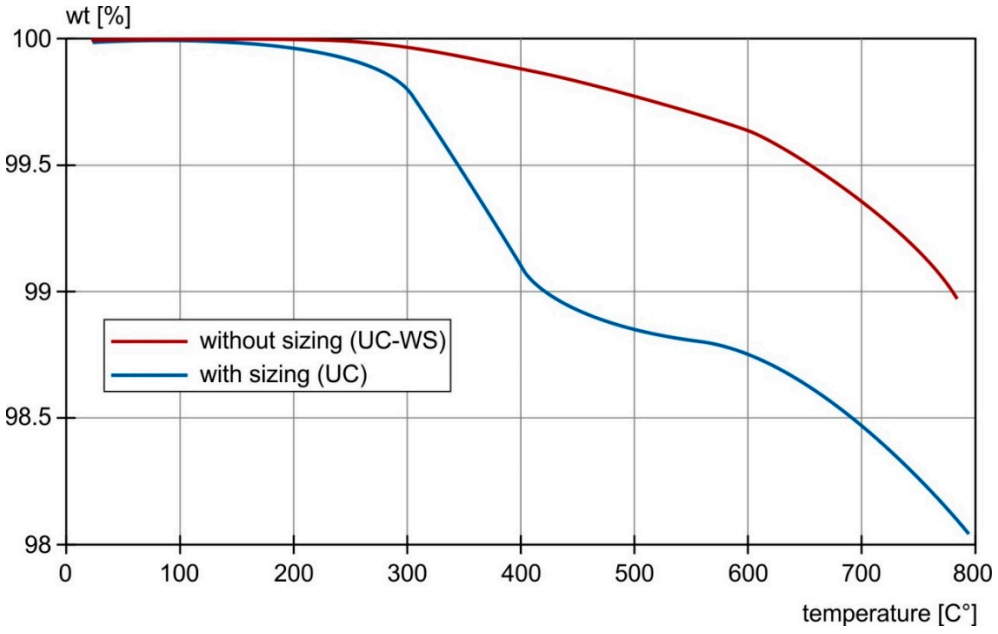


**Figure 15.** TGA measurement of both unimpregnated Carbons.

4.2.4. Unimpregnated Carbon without Sizing (UC_WS)

For comparison purposes, potentiostatic measurements were also carried out on unimpregnated carbon without sizing at the same potentiostatic potentials.

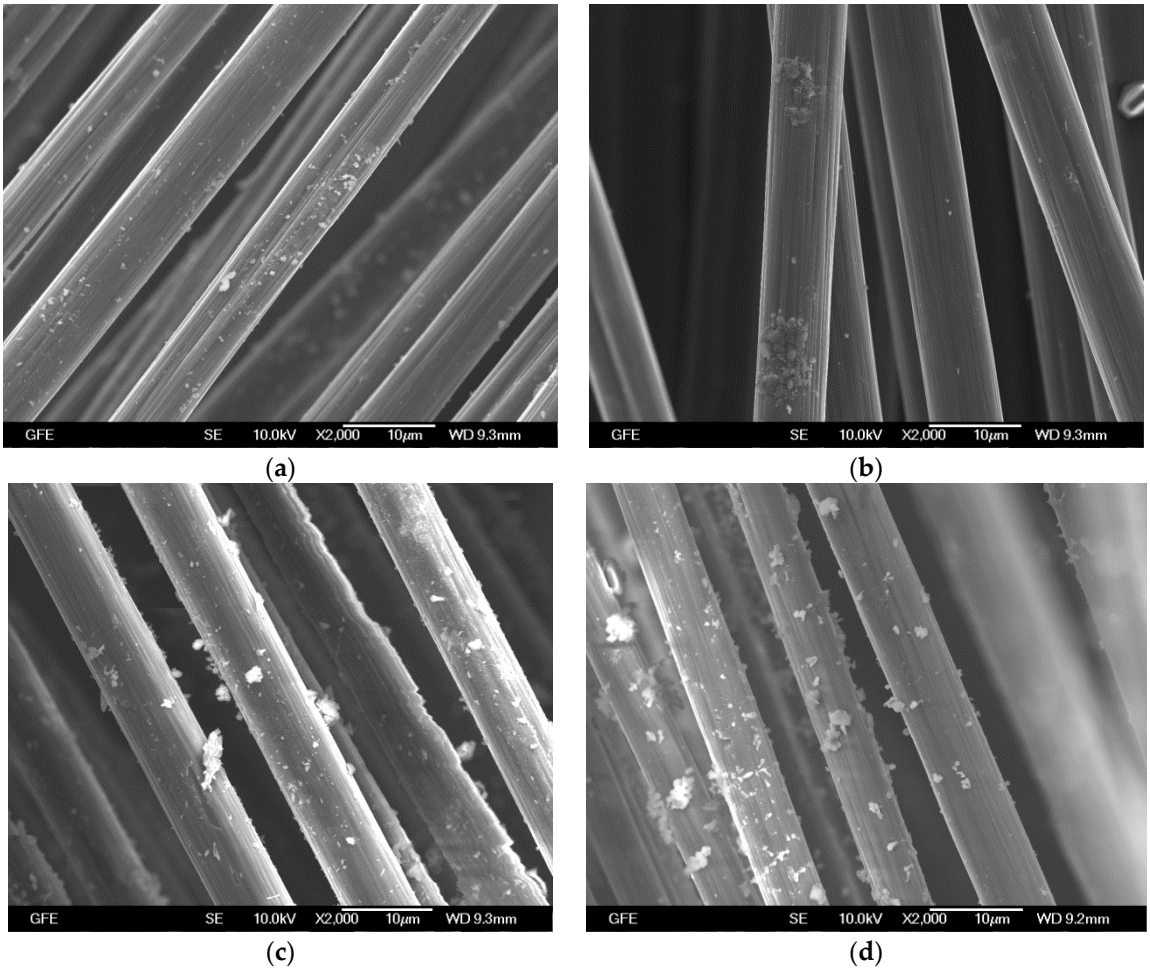


**Figure 16.** SEM images of UC_WS: unpolarized reference (**a**), after polarization at level 1 (**b**), level 2 (**c**) and level 3 (**d**).

The SEM pictures in the Figure 16 confirm the statement that the pictures in Figure 12 show the destruction of the sizing. The unimpregnated carbon fibres without sizing show no damage after polarization at level 1 to 3. Slight longitudinal grooves can already be observed on all samples and are not a consequence of polarization. Differences in contrast, especially bright white areas, are caused by charges from the electron beam with insufficient surface conductivity. After polarization at level 2 (Figure 16(c)), the deposition can be seen on the surface, which is slightly increased at level 3 (Figure 16(d)). But, the deposition is not as strong as with the samples with sizing. It can therefore be concluded that the deposit adheres better to sizing material than carbon. No cracks or damage can be seen on any fibres. This means that anodic polarization does not destroy carbon.

There are no other test results available in the literature, therefore the test results cannot be compared.

## 5. Conclusions and Outlooks

Until now, it was unclear up to which potentials the impregnation materials and the sizing remain undamaged by anodic polarization. The results contribute to the clarification of these questions for the investigated materials.

The results show that the operation of CP with carbon textiles as anode material leads to deterioration of the polymer impregnations and sizing. Since impregnation and sizing are available

to increase the strength capacity of carbon textiles, the deterioration of these materials is very interesting. With epoxy impregnated carbon it is possible to use carbon textiles as CP anode without destroying the epoxy and sizing up to the mentioned potentials.

With the increasing polarization, the strength of the deposited film on the sizing increases.

The conclusion of this work can be summarized as follows:

1. The investigations in solution have shown that CP with investigated carbon anodes up to 2200 mV versus NHE is possible
2. The Carbon filaments within the Carbon textiles as CP anode have not been destroyed up to the investigated potentials up to 2200 mV versus NHE.
3. With SBR impregnated samples, the impregnation is destroyed right from the start during polarization.
4. The sizing is destroyed at a potential of about 900 mV versus NHE.
5. Epoxy impregnation started to destroy between 1050 and 1150 mV versus NHE.

Further tests must be carried out to investigate the bond between polymer impregnated carbon textiles and mortar. It must be observed whether the destruction of the impregnation or sizing has a negative influence on the bond or durability.

**Author Contributions:** Conceptualization, A.A. and M.R.; Methodology, A.A.; Software, A.A.; Validation, A.A.; Formal Analysis, A.A.; Investigation, A.A.; Resources, A.A. and M.R.; Data Curation, A.A.; Writing-Original Draft Preparation, A.A.; Writing-Review & Editing, A.A. and M.R.; Visualization, A.A.; Supervision, M.R.

**Funding:** This research received no external funding

**Conflicts of Interest:** The authors declare no conflict of interest.

## References

1. Gao, S.L.; Mäder, E.; Plonka, R. Nanostructured coatings of glass fibres: improvement of alkali resistance and mechanical properties. *Acta Mater.* **2007**, *55*, 1043–1052.
2. Zhang, R.L.; Huang, Y.D.; Liu, L.; Tang, Y.R.; Su, D.; Xu, L.W. Effect of emulsifier content of sizing agent on the surface of carbon fibres and interface of its composites. *Appl. Surf. Sci.* **2011**, *257*, 3519–3523.
3. Lesko, J.J.; Swain, R.E.; Cartwright, J.W.; Chin, J.W.; Reifsnider, K.L.; Dillard, D.A.; Wightman, J.P. Interphases developed from fibre sizings and their chemical-structural relationship to composite performance. *J. Adhes.* **1994**, *45*, 43–57.
4. Xu, L. Interfacial Engineering of the Interphase between Carbon Fibers and Vinyl Ester Resin. Ph.D. Thesis, Michigan State University, Department of Chemical Engineering and Materials Science, East Lansing, MI, USA, 2003.
5. Broyles, N.S.; Verghese, K.N.E.; Davis, S.V.; Li, H.; Davis, R.M.; Lesko, J.J.; Riffle, J.S. Fatigue performance of carbon fibre/vinyl ester composites: the effect of two dissimilar polymeric sizing agents. *Polymer* **1998**, *39*, 3417–3424.
6. Wetjen, D. Wechselwirkung von Carbonfasern, Schlichte und Epoxidbasierter Polymerer Matrix in Carbonfaserverstärkten Kunststoffen. Ph.D. Thesis, Universität Augsburg, Mathematisch-Naturwissenschaftlich-Technische Fakultät, Augsburg, Germany, 2016.
7. Poltavtseva, M.; Ebell, G.; Mietz, J. Electrochemical investigations of carbon-based conductive coatings for application as anodes in ICCP systems of reinforced concrete structures. *Mater. Corros.* **2015**, *66*, 627–634.
8. Rueffer, M.; Bejan, D.; Bunce, N.J. Graphite. An active or an inactive anode? *Electrochim. Acta* **2011**, *56*, 2246–2253.
9. Chung, D.D.L. Review Graphite. *J. Mater. Sci.* **2002**, *37*, 1475–1489.
10. Asgharzadeh, A.; Raupach, M.; Koch, D. Investigations on the Suitability of Technical Textiles for Cathodic Corrosion Protection. In Proceedings of the 4th International Conference on Concrete Repair, Rehabilitation and Retrofitting (ICCRRR), Leipzig, Germany, 5–7 October 2015.
11. Asgharzadeh, A.; Raupach, M. Development of a test Method for the Durability of Carbon Textiles under Anodic Polarisation. In *Service Life and Durability of Reinforced Concrete Structures (RILEM Book Series)*; Springer International Publishing: Basel, Switzerland, 2018; pp. 143–158.
12. Asgharzadeh, A.; Raupach, M. Durability behaviour of polymer impregnated carbon textiles in alkaline solution as CP anode. *Mater. Corros.* **2018**, 1–12, doi:10.1002/maco.201810098.

13. Bertolini, L.; Bolzoni, F.; Pastore, T.; Pedeferri, P. Effectiveness of a conductive cementitious mortar anode for cathodic protection of steel in concrete. *Cem. Concr. Res.* **2004**, *34*, 681–694.
14. Chini, M.; Antonsen, R.; Vennesland, Ø.; Mork, J.H.; Arntsen, B. Polarization Behavior of Carbon Fiber as an Anodic Material in Cathodic Protection. In Proceedings of the 11DBMC International Conference on Durability of Building Materials and Components, Istanbul, Turkey, 11–14 May 2008.
15. Chini, M. Pan-Based Carbon Fiber as Anode Material in Cathodic Protection Systems for Concrete Structures. Avhandling–Norges Teknisk-Naturvitenskapelige Universitet, Trondheim. Ph.D. Thesis, Norwegian University of Science and Technology Faculty of Engineering Science and Technology Department of Structural Engineering, Trondheim, Norway, 2010.
16. Zhang, E.Q.; Tang, L.; Zack, T. Carbon Fiber as Anode Material for Cathodic Prevention in Cementitious Materials. In Proceedings of the 5th International Conference on the Durability of Concrete Structures, 30 June–1 July 2016; Xing, F., Han, N., Zhu, J.-H., Eds.; Shenzhen University: Shenzhen, Guangdong Province, China; Purdue University Press: West Lafayette, IN, USA, 2016.
17. Van Nguyen, C.; Lambert, P.; Mangat, P.; O'Flaherty, F.; Jones, G. The Performance of Carbon Fibre Composites as ICCP Anodes for Reinforced Concrete Structures. *ISRN Corros.* **2012**, *2012*, 1–9.

*Concrete Repair, Rehabilitation and Retrofitting IV – Dehn et al. (Eds)*
*© 2016 Taylor & Francis Group, London, ISBN 978-1-138-02843-2*

# Investigations on the suitability of technical textiles for cathodic corrosion protection

Amir Asgharzadeh & Michael Raupach
*Institute of Building Materials Research, RWTH-Aachen University, Germany*

Detlef Koch
*Koch GmbH, Kreuztal, Germany*

ABSTRACT: Cathodic Protection (CP) is a widely used method to protect steel reinforcements against corrosion. In the course of the last half century, it has been established as a proven system for repairing corrosion-affected reinforced concrete structures, which have mainly been damaged by chloride-induced corrosion. The impressed current anode system for the protection of steel in concrete is latest state of technology. The CP anodes can be embedded in mortar, as coating or distinct anode on the repair structure surface and exposed to external current. In this way, the potential of carbon steel is shifted in cathodic direction and the anodic dissolution of carbon steel is suppressed. The current densities on the surface of the reinforcement play a key role in the shifting of the potential in cathodic direction. Nowadays, Mixed Metal Oxide coated Titanium (MMO) is used as an anode material for CP due to its high durability under anodic polarization. Also other materials such as carbon fibers are being studied. Carbon textiles in combination with mortar, which provide high mechanical properties and are also conductive, have not been studied systematically so far. In this paper investigations are described, which have been carried out in order to evaluate the capabilities of different carbon-textile anodes and different mortar mixtures for the cathodic protection of steel in concrete. In order to evaluate the polarization behavior of carbon-textile in mortar, galvanostatic experiments were performed. Based on these experiments, current density-potential-curves were derived.

## 1 INTRODUCTION

In order to protect constructions in aggressive environment and restrict the cross-sectional reduction of the reinforcement, repair actions are required. Raupach (2001) To achieve this objective, it is necessary to inhibit one of the two partial reactions (anodic/cathodic) of the corrosion process. Cathodic Protection (CP) is allocated to the process, which suppresses the anodic partial reaction. An advantage of CP is that chloride contaminated concrete does not have to be removed and almost non-destructive repair is still possible. Raupach (1992).

Figure 1 illustrates the principle of CP as follows: By embedding an inert anode, the reinforcement is applied selectively via a DC source with an impressed current. Raupach (1992) This current causes an excess of electrons in the reinforcement which makes the reinforcement act as a cathode. Thereby, the corrosion processes are reduced to an acceptable level.

To prevent the anodic dissolution of iron, a CP system for uncoated steel in concrete buildings is typically operated at current densities between 2 mA/m$^2$ to 20 mA/m$^2$. DIN EN ISO 12696 (2012).

If the component, however, is continuously saturated with water or for preventive CP, a current density of 0.2 mA/m$^2$ to 2 mA/m$^2$ can be considered.

### 1.1 *Textile reinforced concrete*

Textile reinforced concrete is a composite system of cement based concrete with glass or carbon

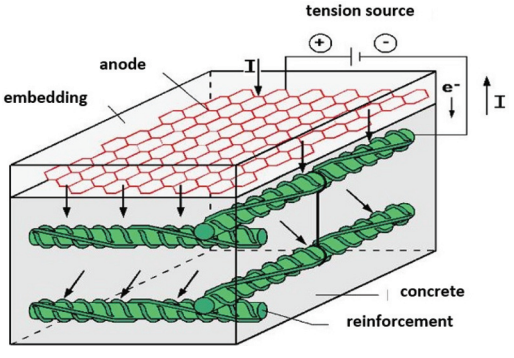


Figure 1. Concept of cathodic protection with an inert external-current-anode according to Boehni (1990).

fiber meshes as a reinforcing material. By using this material, it is possible to achieve low component thicknesses. This is due to the durability of textile reinforced concrete, as no thick concrete cover in the range of 2–5 cm such as for reinforced concrete is necessary.

Conventional CP systems located on the market function with MMO coated titanium as anode material. However, the use of technical textiles as anode material would have advantages to this material. Compared to traditional repair measures, the use of Textile Concrete is considered to be more environmentally friendly and the repair of a corrosion-damaged component could be more resource-efficient and cost-effective. Furthermore, textile reinforced concrete has several considerable advantages regarding serviceability and durability compared to traditional steel reinforced concrete.

## 2 EXPERIMENT SETUP AND TEST PROCEDURE

The test setup presented in Figure 2 was selected to simulate a component surface. The undermost layer of concrete containing reinforcement (here: MMO coated titanium), while the subsequent layer of concrete simulates the concrete cover. To simulate the reinforcement the MMO coated titanium was used, because this material can produce a homogeneous electric field due to its chemical inertness and reticular structure. Carbon Textile is applied onto the component surface by means of a specially developed mortar. Thus, a renovation of a corrosion-damaged concrete component is simulated. For the measurements suitable reference electrodes were required. Electrolyte bridges were placed in the specimens to be able to connect external reference electrodes to the specimen (Fig. 3). This electrolyte bridge was filled for a later connection with silver-silver chloride solution.

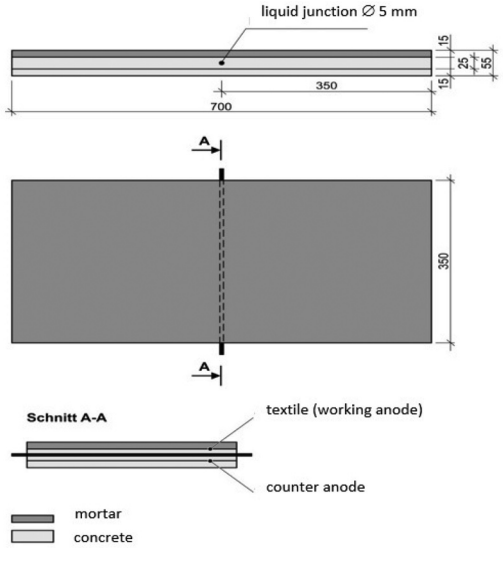


Figure 2. Detailed drawing of the specimen—dimension [mm] according to Henkel (2014).

The following chart, (Table 1), provides an overview of the textile meshes, and the following images show the textiles in detail and their installation into the specimen.

After the Textile anodes were applied to the concrete base, the test specimens were cast with the special mortar. This mortar layer had a thickness of 15 mm and formed finely to the surface of the test specimens (see Fig. 2). Three different mortars were tested. In combination with the four anode materials a total of 12 specimens were made. The following chart, (Table 2), gives an overview of the mortar properties.

When the specimens had matured, they were connected to a potentiostat. The carbon textiles act as a working electrode, while the MMO coated titanium was connected as a counter electrode (see Fig. 8). Galvanostatic tests with stepwise increased applied electrical currents were carried out. Here, the potentials of the working electrode were measured against the reference electrode. The current densities

Figure 3. Installed liquid junction (left), concrete base plate (right) according to Henkel (2014).

Table 1. Properties of the textiles.

| Textile | Material/ structure | Coating | Mesh width (0°/90°) (mm) |
|---|---|---|---|
| 1 | Carbon/single mesh | Styrene-butadiene-rubber | 14/8 |
| 2 | Carbon/single mesh | Epoxy | 20/20 |
| 3 | Carbon/double mesh | Styrene-butadiene-rubber | 15/15 |
| 4 | Carbon/single mesh | Styrene-butadiene-rubber | 14/13 |

Table 2. Overview of the mortar properties.

| Mixture | Mortar mixture | Water | Water-reducing admixture | Special aggregate | Compressive strength [N/mm²] | Density [kg/dm³] |
|---|---|---|---|---|---|---|
| B | X | X | No. 1 | X | 110.3 | 2.37 |
| C | X | X | – | – | 77.6 | 2.26 |
| D | X | X | No. 2 | X | 118.2 | 2.40 |

Figure 4. Textile 1 according to Henkel (2014).

Figure 5. Textile 2 according to Henkel (2014).

Figure 6. Textile 3 according to Henkel (2014).

Figure 7. Textile 4 according to Henkel (2014).

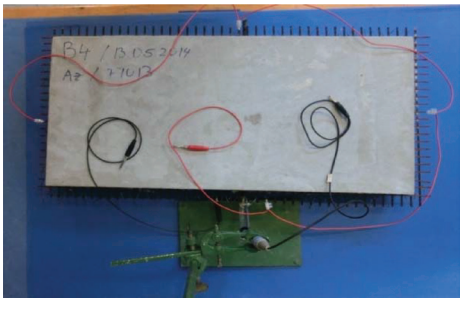

Figure 8. Complete test specimen according to Henkel (2014).

in detail, were 0 mA/m² (open circuit potential); 1 mA/m²; 3.2 mA/m²; 10 mA/m² und 20 mA/m².

Following each stage, instant-off potential measurements were performed. This procedure ensured that IR drop compensated potentials were measured, and that the actual polarization of the anode material is not overrated. Following the last instant-off measurements, the depolarization was determined. The duration of the intervals were chosen sufficiently large (12 h), so that the recorded potentials began to approach a limit where almost no changes were detected.

## 3 RESULTS

Figure 9 shows an exemplary curve of the galvanostatic stages experiment of the specimen B1.

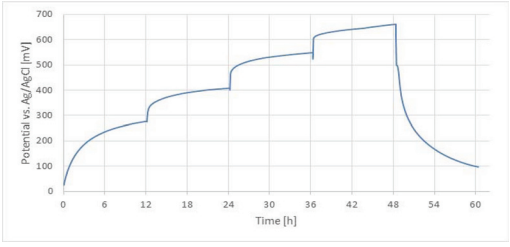


Figure 9. Galvanostatic test by progressive current densities—specimen B1 according to Henkel (2014).

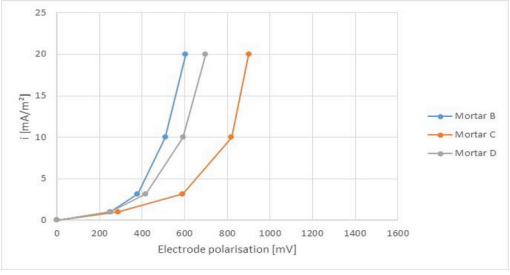


Figure 10. Current density-potential-curve textile 1 Henkel (2014).

The four stages in the various current densities can be clearly seen, and that the potential values stabilize after 12-hour depolarization's measurement. The IR drop can also be seen in the graph. After 36 hours, the galvanostatic test is completed with 10 mA/m$^2$ related to concrete surface.

To evaluate the galvanostatic stage testing with relation to the CP, current density versus potential curves were generated, as the following four Figures 10–13 show for the different embedding mortars and textiles. It can be seen, from the comparison of the curves, which combination of mortar and carbon textile requires the lowest voltage to achieve a current-density of 10 mA/m$^2$.

On the basis of the measurements for textile 1, mortar B is the most appropriate. In textile 3 and 4, mortars B and D have almost identical results. In textile 4, the difference of polarization of textiles in mortars C, B, and D is still less than 100 mV, and in textile 3 several hundred millivolts. The significantly deviating course of the measurement curves of textile 2 can be explained to the epoxy coating. This represents an increased resistance compared to Styrene-Butadiene (SBR) coating, so the conductivity of the textile decreases.

The evaluation with respect to the three tested mortar mixtures has shown that mortars B and D, with each textile, have almost identical polarization properties. Accordingly, they have the lowest

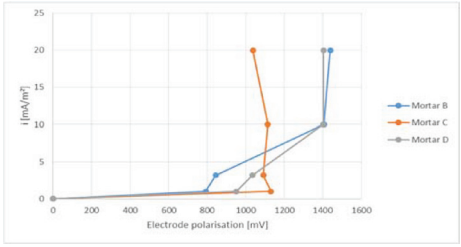


Figure 11. Current density-potential-curve textile 2 Henkel (2014).

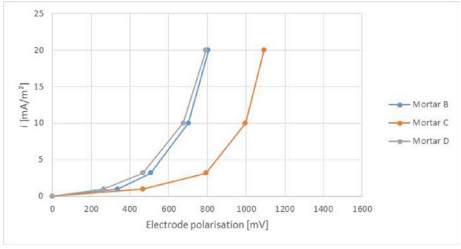


Figure 12. Current density-potential-curve textile 3 Henkel (2014).

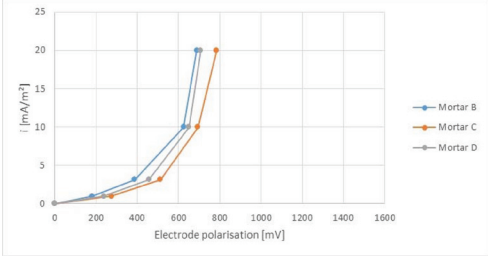


Figure 13. Current density-potential-curve textile 4 Henkel (2014).

voltages needed to achieve the same protective current density.

The lowest values in absolute terms are among the systems B1, B4 and D4.

In this work, these combinations were favored for further investigation. Benefits can result due to the different properties of the anode materials in practice. While textile 1 is on rolls, the textile 4 is supplied in mats.

## 4 CONCLUSIONS

The results of the experiments carried out within this study led to the following conclusions.

Carbon textiles are suitable as an anode material for the CP.

The SBR-impregnated materials revealed a significantly better polarization behavior compared to the EP-impregnated textiles.

The double mesh textile structure of the textile type 3 has been found to not be as advantageous compared to the single mesh structures of the textile types 1 and 4.

All investigated mortars can be used as embedding material for CP. The conductive hard aggregate used in B and D takes considerable benefits for the conductivity and compressive strength of the mortar.

## 5 OUTLOOK

This study has shown, that carbon textiles are generally suitable to be used as anodes for CP. Based on these results further investigations are required to shows the durability of carbon textiles.

## ACKNOWLEDGMENT

The investigations have been carried out at the RWTH-Aachen University in cooperation with Koch GmbH for the project “cathodic corrosion protection with textile concrete”, supported within from AiF ZIM (Central Innovation Programme) initiated by Federal Ministry for Economic Affairs and Energy. We would like to thank to AiF for the support of this interesting project.

## REFERENCES

Baeckmann, W. v. 1999. Historische Entwicklung des elektrochemischen Korrosionsschutzes. In W. v. Baeckmann, W., *Handbuch des kathodischen Korrosionsschutze*: 1–14. Weinheim: Wiley-VCH.

Boehni, H. 1990. Grundlagen der Korrosion und des elektrochemischen Korrosionsschutzes. *Korrosion und Korrosionsschutz*. Schweizerischer Ingenieur- und Architektenverein.

Deutsches Institut für Normung e.V. 2012. DIN EN ISO 12696 Kathodischer Korrosionsschutz von Stahl in Beton. Berlin: Beuth Verlag GmbH.

Henkel, P. 2014. Bachelorthesis. Untersuchung zur Bestimmung der Eignung technischer Textilien für den kathodischen Korrosionsschutz. Aachen: Institute of Building Materials Research of RWTH-Aachen University

Raupach, M. 1992. Kathodischer Korrosionsschutz im Stahlbetonbau: Instandhaltungsverfahren fuer Spezialfaelle. *Beton* 42: 674–676.

Raupach, M. 2001. Korrosionsschutzverfahren fuer Stahlbetonbauwerke: Entwicklung und Tendenzen. Restoration of Buildings and Monuments, 25. Aachener Baustofftag.